Design of Orbital Construction Cubesat Using 3D Printing

a project presented to
The Faculty of the Department of Aerospace Engineering San José State University

in partial fulfillment of the requirements for the degree
Master of Science in Aerospace Engineering

by

Matthew Gallelo

Fall 2020

approved by

Dr. Maria Chierichetti
Faculty Advisor

ABSTRACT

This report discusses the design and first iteration prototyping of a 6U research cubesat using Fused Deposition Modeling to construct small structures in Low Earth Orbit for potential of future upscaling. The design takes many commercially available off the shelf hardware components and integrates or modifies them for in-situ FDM operation on a 6U cubesat power and mass budget. The printing head of this system will be mounted onto a hardpoint in the structure of the cubesat and will use a Polycarbonate/ASA thermoplastic filament with a carbon fibre core and embedded tungsten microparticles print structures in LEO. Utilizing two 6-axis robotic arms the cubesat will move the build plate/model for the printing operations. The prototype developed will be constructed using FDM and SLA additive manufacturing techniques as well as traditional fabrication methods; and will be used for visual sizing and testing of manufacturing accessibility/feasibility.

Table of Contents

LIST OF TABLES

LIST OF FIGURES

1 Introduction

1.1 Motivation

Traditional methods of habitation in Low Earth Orbit (LEO) require small modules to be launched into orbit individually for later orbital assembly. Using the high material and energy efficiency of additive manufacturing, the core structure of future habitats could instead be manufactured in orbit. The preferred in orbit manufacturing approach is Fused Deposition Modeling (FDM) due to its simplicity. The FDM process requires a printing area and a printing head that extrudes a melted thermoplastic, this allows for modularity. Minor modifications to existing FDM printers allow them to be used with fibre cored thermoplastics to manufacture composite structures, resulting in a great increase in the mechanical properties compared to traditionally non-composite structures. Integrating an additive manufacturing system into a small satellite could greatly increase the size of individual habitats in LEO. With regular shipments of ready to use fibre cored thermoplastics this manufacturing satellite could construct strong and pressurizable structures many times its own size. The objective of this project is the design of a cubesat satellite capable of in orbit manufacturing using the FDM method of additive manufacturing.

1.2 Literature Review

1.2.1 Cubesats

Cubesats are nano satellites that are designed for research and development, they come in arrangements of 10cm x 10cm x 10cm cubes. Each of these cubes is considered 1U each one weighing between 1 and 1.33kg (See Figure 1). Most cubesats range from 1U (10cm x 10cm x 10cm) to 6U (12cm x 24cm x 36cm) however the cubesats can range from .25U (2.5cm x 10cm x 10cm) to 27U (34cm x 35cm x 36cm). The cubesat platform is on the rise in popularity due to the low barrier to entry because of reduced costs compared to traditional satellites[1]. The low cost is attributed to the simplicity of design and the common integration of off-the-shelf parts for internal components. Using cubesats, smaller aerospace companies, universities, and nations with low space research budgets can reliably and affordably get spacecraft into LEO for testing. Cubesats are a great platform for integrating novel systems in order to demonstrate their feasibility for future work.

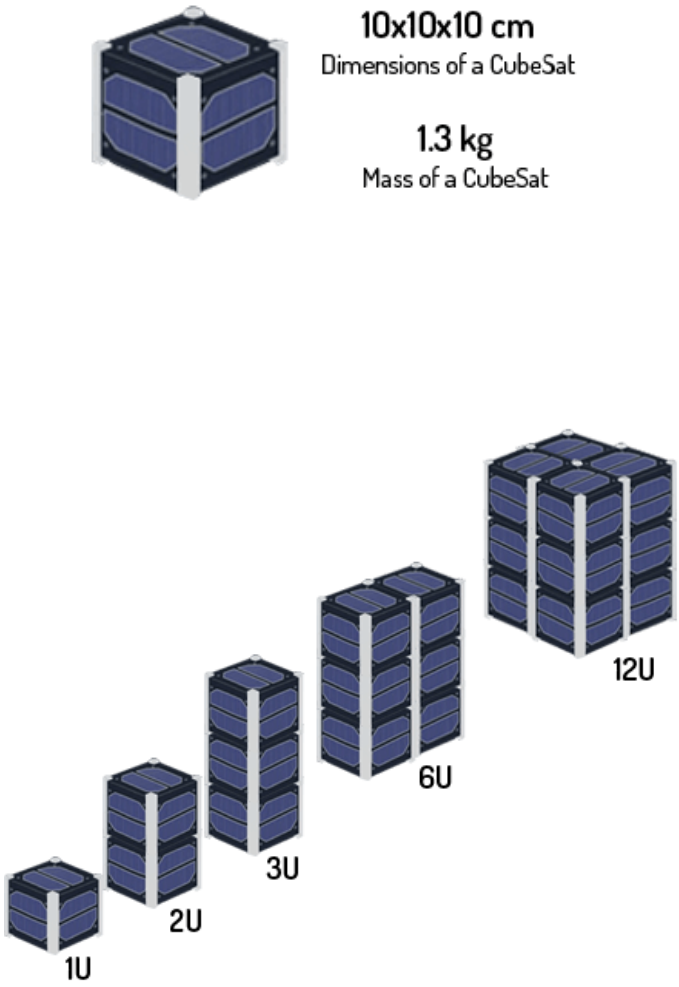

Figure 1. Visualization of a 1U cubesat (left) and some cubesat arrangements (right) [2]

1.2.2 Manufacturing in Space

In Space Manufacturing (ISM) is a NASA program dedicated to developing technologies and processes that will enable manufacturing on demand that has the capacity to support long term space missions [3]. Manufacturing in space can help with the logistics, maintenance and longevity of missions due to its flexibility. The ability to fabricate replacement parts, spare tools, and recycle those same items in mission has measurable cost savings on mission budgets. ISM has tested 3D printing in microgravity on the ISS and concluded that there is no significant impact on the FDM process. The company: “Made In Space” has made huge strides for the space manufacturing initiative like designing and delivering the first 3D printer for the ISS.

1.2.3 Additive Manufacturing

Additive Manufacturing is a method of fabrication that adds material to a structure layer by layer. 3D printed pieces can be made to be more complex while still being cheaper compared to traditional machining methods. There are many methods of additive manufacturing, some of the more common ones are material extrusion, powder bed fusion, and vat photopolymerization[4]. Vat photopolymerization is a process that uses a large vat of photopolymer resin and a UV light source to harden specific parts of the resin, layer by layer to form a final model. This method is impractical for use in this project due to the need for a large printing vat full of photopolymer. Another common method is powder bed fusion; this method is similar to vat photopolymerization as it also needs a bed of workable material, except this bed is filled with a fine metal dust ready to be sintered together layer by layer via high powered laser. This method is also impractical due to the large material bed and power requirements for operation. Material extrusion is where a 3D model is constructed by extruding a material onto a model, layer by layer until the desired structure is complete. In comparison to Vat photopolymerization and powder bed fusion that require large amounts of excess material around the print bed, the only required modules for operation in material extrusion are a printing head and some region for printing. For all of these methods a 3D model will be designed through CAD software and then “sliced” by a slicer program into many 2D layers to path the printing method [5]. The simplicity of material extrusion is it’s strength as well as already being tested to work in microgravity on the ISS [3]. Several material extrusion approaches exist, such as FDM and photopolymer extrusion. FDM printing allows for fast prototyping and precise individual manufacturing at a low cost, but results in significant truncations of small details during the slicing process, as any rounded edges will be removed in the XY plane of the model (See Figure 2). The second method of material extrusion considered was photopolymer extrusion, which is conceptually similar to FDM: it extrudes a liquid photopolymer resin that would harden when exposed to the abundance of UV radiation in LEO. Previous experiments using a UV lamp showed some feasibility[6], however the material properties of the UV resin from that experiment are well below the material properties of most thermoplastics used in FDM printing. This finding as well as the unsuitability of non-material extrusion methods led FDM to be selected as the superior method for this project.

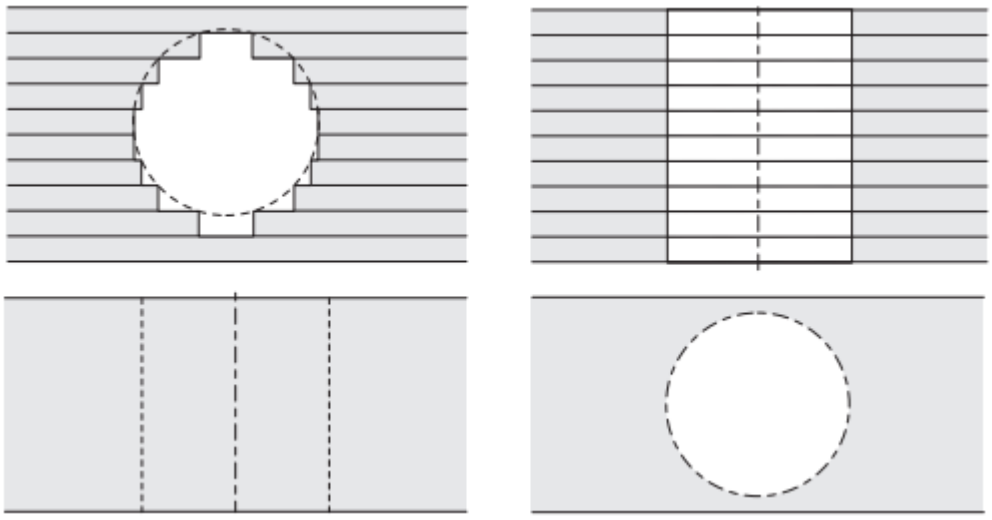

Figure 2. Two slicing examples[5] (Left two images are a rectangular prism with a cylindrical extrusion through the XZ plane, Right two images are a rectangular prism with a cylindrical extrusion through the XY plane)

1.2.4 Materials in Additive Manufacturing

The two most common thermoplastics in FDM printing are Acrylonitrile butadiene styrene (ABS) and Polylactic acid (PLA) due to their effective strengths and ease of use. The greatest advantage of ABS is the ruggedness of the printed part, low cost, and mid temperature requirements of a 230-250 °C nozzle. ABS is normally used by more advanced 3D printing enthusiasts due to its required heated bed. PLA gives up the durability of ABS and provides a slightly cheaper and slightly lower nozzle temperature of 190-225 °C for reliable prints. Without the need of a heated bed, PLA prints have the least requirements to start 3D printing. PLA prints have been tested to have enhanced material properties when embedded with a carbon fiber core [7,8]. Unfortunately both ABS and PLA are highly susceptible to UV weathering and are by no means the strongest or most durable thermoplastics that can be used in FDM 3D printing [9]. Polycarbonate is one of the stronger FDM suitable thermoplastics with its largest downside being it's high printing temperature of 255-300 °C and known weakness to extended UV exposure. In the testing of many printing variations Polycarbonate exceeded ABS in mechanical properties and UV resistance [10,11]. Acting to mitigate the weakness to UV weathering in polycarbonate parts, a filament of Polycarbonate and Acrylonitrile Styrene Acrylate Alloy was selected (PC/ASA). This filament is commercially available and combines the strength of Polycarbonate and UV

resistance of ASA [12]. Further improvements to polycarbonate have been tested in a study that integrated tungsten microparticles into a polycarbonate filament for FDM printing. This introduction of 12um particles at 5% total mass of the filament had a 10% increase in X-ray shielding as well as a minor improvement to mechanical properties[13]. With all these advancements a filament of PC/ASA with 5% embedded tungsten microparticles and a carbon fibre core was selected as an ideal material for in space additive manufacturing. Looking at a simple breakdown of material information relevant to FDM printing (See Table 1) polycarbonate printing comes with some other requirements such as a heated bed, heated enclosure, additional adhesion methods and a reinforced All Metal Hotend. All of these can be mitigated through the project design, for example: in a vacuum printing environment heat dissipation is far less than in atmosphere, negating the need for a heated enclosure.

Material	ABS	PLA	Carbon Fibre Filled	ASA	Polycarbonate
Ultimate Strength	40 MPa	65 MPa	45-48 MPa	55 MPa	72 MPa
Maximum Service Temperature	98°C	52°C	52°C	95°C	121°C
Coefficient of Thermal Expansion	90µm/m-°C	68µm/m-°C	57.5µm/m-°C	98µm/m-°C	69µm/m-°C
Density	1.04g/cm^3	1.24g/cm^3	1.3g/cm^3	1.07g/cm^3	1.2g/cm^3
Price (per kg)	$10 - $40	$10 - $40	$30 - $80	$38 - $40	$40 - $75
Extruder Temperature	220 - 250°C	190 - 220°C	200 - 230°C	235 - 255°C	260 - 310°C
Bed temperature	95 - 110°C	45 - 60°C	45 - 60°C	90 - 110°C	80 - 120°C
Heated Bed	Required	Optional	Optional	Required	Required
Recommended Build Surfaces	Kapton Tape, ABS	Painter's Tape, Glue	Painter's Tape, Glue	Glue Stick, PEI	PEI, Commercial

	Slurry	Stick, Glass Plate, PEI	Stick, Glass Plate, PEI		Adhesive, Glue Stick
Other Hardware Requirements	Heated Bed, Enclosure Recommend	Part Cooling Fan	Part Cooling Fan	Heated Bed	Heated Bed, Enclosure Recommended, All Metal Hotend

Table 1. Differences between thermoplastics used in additive manufacturing [14]
(Note that the "Carbon Fibre Filled" material is a representation of PLA and ABS prints with small carbon fibre strands integrated into the filament randomly, not with a continuous carbon fibre core)

1.3 Project Proposal

The objective of this project is to design and prototype a 6U cubesat for large scale additive manufacturing in LEO. The cubesat will utilize a printing head and two mover arms in order to operate and print on structures larger than itself. Using off the shelf hardware, a commercial FDM printing head will be the basis for the design of a printing head capable of printing using a proposed Polycarbonate/Acrylonitrile Styrene Acrylate Alloy (PC/ASA) filament embedded with tungsten microparticles (12um diameter) up to 5% total mass with carbon fibre core. The prototype this project will produce will not be for testing/launch as the materials and components available for use do not meet requirements for launch. The prototype will be completed to the furthest extent as a demonstration of feasibility and scale.

1.4 Methodology

The first step of design is to do a top level sizing of the cubesat to find the power and thermal budget allotted for each subsystem (See Figure 3 for a visualization of all major subsystems). After preliminary budgets are found, the printing arm and moving arm's individual mass, power and thermal budgets will be determined. Design will now begin on the printing arm with these budgets in mind as the edges of design space. A computer aided design program will be used to model parts and assemblies. Design of the printing arm will also take previous printer head designs into consideration and try to modify off the shelf parts

as much as possible. Prototype construction will be done using additive manufacturing and conventional methods with as many off the shelf parts as is practical.

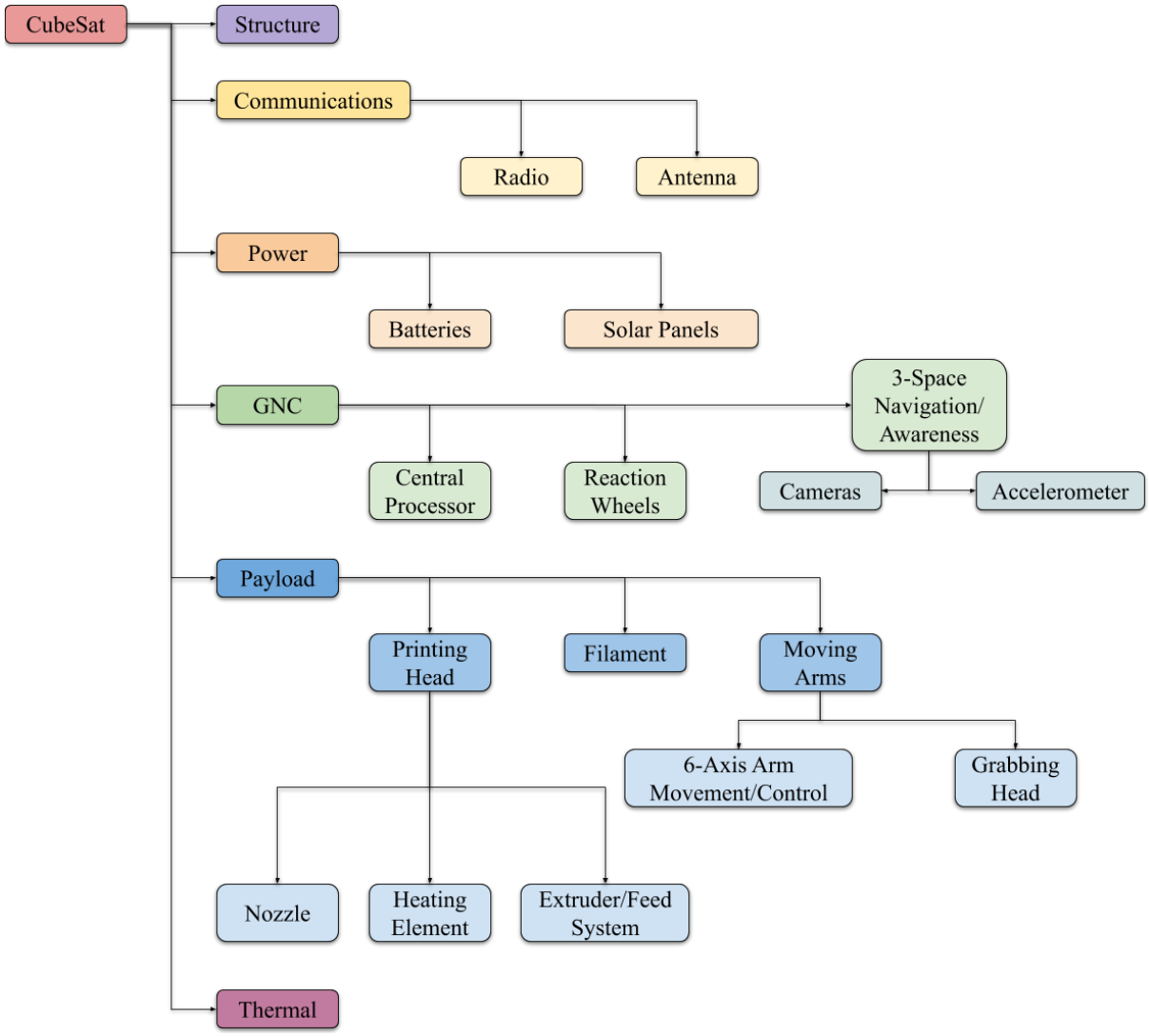

Figure 3. Major Subsystems Breakdown

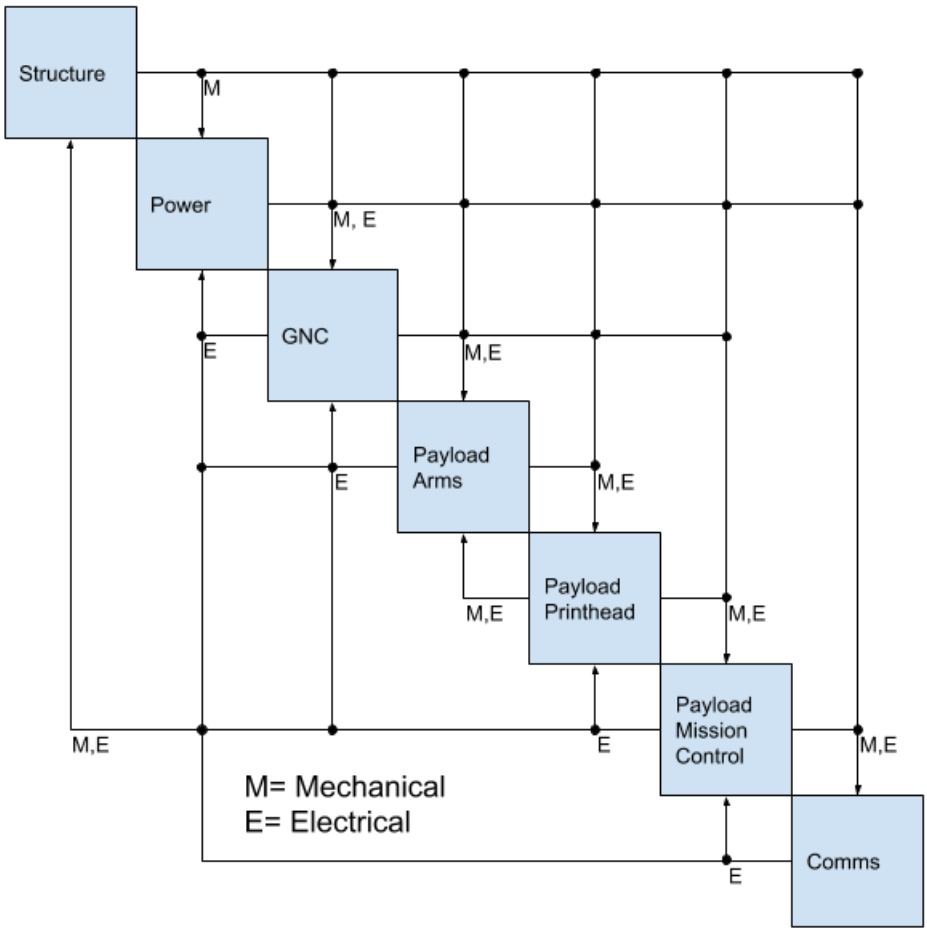

Figure 4. Major Subsystems N2 Diagram

2 Preliminary CubeSat Subsystem Sizing

Preliminary system sizing is required to find a rough mass and power budget for the payload. Top level subsystem analysis and first iteration design process was conducted for each subsystem laid out in Figure 3 except payload to find mass and power budgets for each subsystem. A top level thermal analysis was conducted to check for radiator and cooling requirements. A simple N2 diagram was made for the major electrical and mechanical subsystems (See Figure 4).

2.1 Structure Subsystem

A 6U configuration was selected for its large size and weight allowances that will allow for larger filament mass, power and thermal budgets. Planetary Systems Corporation's Canisterized Satellite Dispenser system (CSD) was selected as a basis for design. CSD's tabs

munting method allows for better force and vibrational modeling as well as simplifying the design [15] in comparison to a traditional rail method. The rail mounting system tends to have some slight vibrational increase when compared to the clamped tabs method. A prototype chassis was designed for visualization purposes in accordance with the specifications for CSD (See Figure 5). This chassis has spaces allocated for the large solar array and thermal subsystem required for the mission.

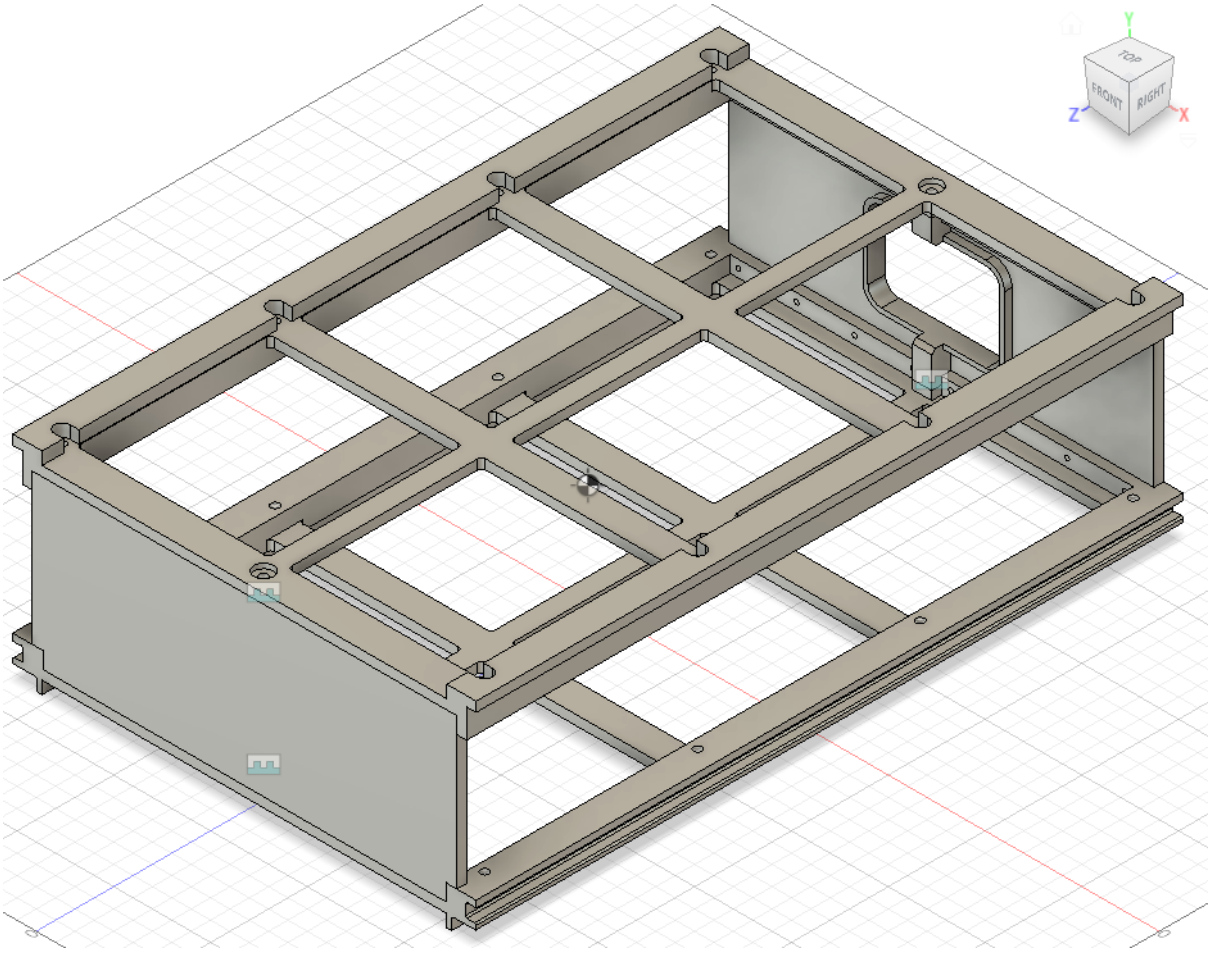

Figure 5. Preliminary Chassis

2.2 Thermal Subsystem

The thermal regulation subsystem is designed considering two thermal loading conditions, the maximum and minimum thermal load on the system from the LEO environment. At maximum thermal load the satellite is positioned between the sun and earth and at minimum thermal load the satellite is in the earth's shadow relative to the sun. Numerical values associated with these states can be seen in table 2 [16].

	Maximum Thermal Load	Minimum Thermal Load
Solar Thermal Radiation	1414 W/m^2	0 W/m^2
Earth Albedo	0.30 +/- .01	0.25
Earth Thermal Radiation	234 +/- 7 W/m^2	220 W/m^2

Table 2. Thermal Load Values

The maximum area facing these thermal loads will be the area of the XY plane once all solar panels are deployed (See section 2.3 for details). This area will have parts with different thermal emissivity based on the material. Calculations for this and total heat energy from the environment can be seen in table 3.

	Max	X planar area	Y planar area	Z planar area
Area [m^2]	Cubesat Body	0.042456	0.087474	0.027724
Area [m^2]	Solar Panels Deployed	0	0	0.25986
Area [m^2]	Arms extended	+10%	+10%	+10%
Area [m^2]	Total	0.042456	0.087474	0.287584
Emissivities	Solar Panel Collect	0.75	0.75	0.75
	Polished Gold	0.025	0.025	0.025
	Aluminum (Chassis)	0.1	0.1	0.1
From Sun	@ 1414W/m^2	45.024588	92.766177	304.982832
From Earth	@ 241 W/m^2	0.2557974	0.52703085	1.7326936
Albedo	0.3 @ 1414 W/m^2	1.80098352	3.71064708	12.19931328
Total [W]		47.08136892	97.00385493	318.9148389

	Min	X	Y	Z
Area [m^2]	Cubesat Body	0.042456	0.087474	0.027724
Area [m^2]	Solar Panels Deployed	0	0	0.25986
Area [m^2]	Total	0.042456	0.087474	0.287584
Emissivities	Solar Panel Collect	0.75	0.75	0.75
	Polished Gold	0.025	0.025	0.025
	Aluminum (Chassis)	0.1	0.1	0.1
Solar constant	0 W/m^2	0	0	0
From Earth	220 W/m^2	0.233508	0.481107	1.581712
Albedo	0.25 @ 0 W/m^2	0	0	0
Total [W]		0.233508	0.481107	1.581712

Table 3. Maximum and Minimum Environmental Energy Absorption

Table 3 shows that the system must have enough radiators to dissipate 320W of thermal energy at maximum environmental thermal load. Combining this with a worst case scenario of perfect conversion of electrical energy to thermal energy, the maximum thermal dissipation required is 380W. Assuming radiators with near perfect emissivity of .95 [ϵ], Stefan-Boltzmann constant 4.670373e^{-8} [σ] and an operating temperature of 300° K [T] we can solve for radiator area from:

$$P = \epsilon \cdot \sigma \cdot A \cdot T^4$$

Equation 2.1

With a final required radiator area of .87 m^2 at peak 380W cooling requirement (this is assuming constant temperature which is not true as the temperature will fluctuate depending on available radiator space). Using louvers and a thermal control system the effective radiator surface area can be modified in real time to fit the need of the system.

2.3 Power Subsystem

The Power subsystem will contain solar panels for power generation and a battery for power regulation. The models for solar panels in preliminary power sizing come from GOMspace NanoPower MSP and are arranged on the 4 largest surface areas to be deployed [17]. See figure 6 for Panel wattage calculation and power production and Figure 7 for visual example.

Solar Panels				Dimensions:				
Side	Product Name	Cells	Mass (g)	Z (mm)	Y (mm)	X (mm)	Power min (W)	Power Max (W)
A1	MSP-A-7-1	7	190	326.5	1.5	82.6	7.9450	8.4
A2	MSP-A-7-1	7	190	326.5	1.5	82.6	7.9450	8.4
B1	MSP-B-8-2	16	438	326.5	209.0	2.5	18.1600	19.2
B2	MSP-B-8-2	16	438	326.5	209.0	2.5	18.1600	19.2
C	MSP-C-5-1	5	132	1.5	221.5	97.5	5.6750	6
D	n/a	n/a	n/a	n/a	n/a	n/a	n/a	n/a
Total		51	1388				57.8850	61.2

Figure 6. Solar Panel data from [17]

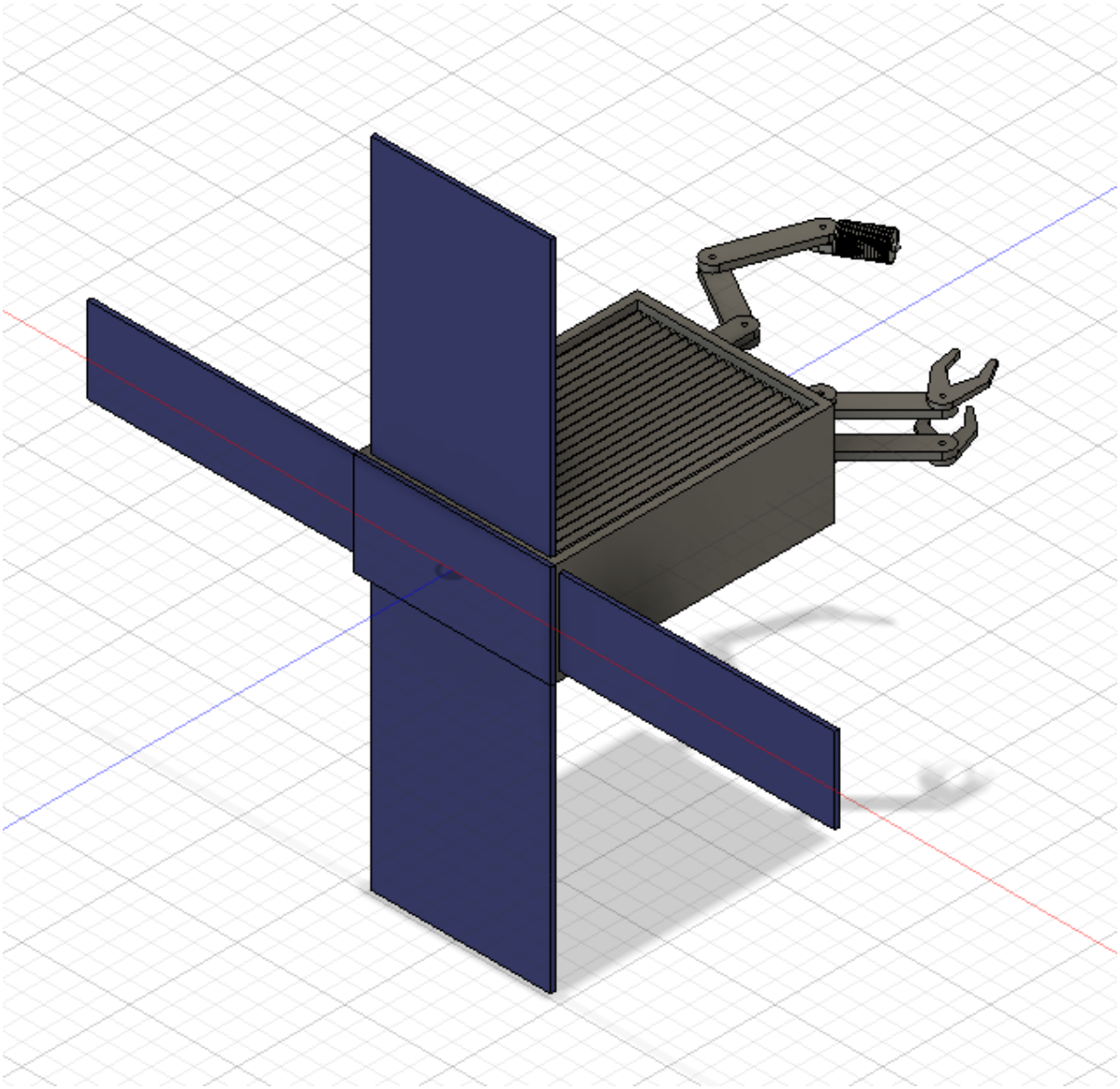

Figure 7. Example of Deployed Solar Panels (not to scale)

Operating solar panels can degrade at up to 1.5% per year making an ideal power budget for systems about 55W for a planned 3 year mission. Assuming a worst case scenario where the cubesat is in LEO with a beta angle of 0 deg, 59% of flight time will be in sunlight, requiring a battery to support almost half of the orbit without solar power. Therefore, the total active system power draws a maximum of 32.45W with the remaining 22.55W dedicated to charging the batteries for use when solar panels are offline. This requires a 28.4 Wh battery to provide the power during solar eclipse from earth assuming a near 100% charging efficiency from the battery. GOMspace again can provide a model for preliminary design in their NanoPower BP4 battery pack. It will provide four 18650 series Lithium-Ion cells with a capacity of 38.5Wh at a mass of 270g [18].

2.4 Additional Mission Hardware

With the goal of the cubesat to move autonomously around on the active 3D print, onboard imaging and image processing is required for positional data and pathing correction. Using commercially available open source hardware, the Raspberry Pi Zero W and Raspberry Pi camera module V2 are great options with their low power draw, small size and low weight. With a combined power draw of less than 2W they are a great option for power efficient computing and control. Teensy 4.0 is another developer board that offers similar features to the Raspberry Pi but with less power draw and a smaller footprint. The performance drop between them is significant but the Teensy 4.0 still has enough computing power to process the required one image per second to ensure positional accuracy. To decrease power draw further a comparison between the BF3710 720p and the Pi camera module V2 was conducted. Both cameras offer 720p quality, but the BF3710 offers single image capture rather than the 30-60fps video that the pi camera module can provide. With one image per second being the required capture rate, the power and size advantages of the BF3710 make it the better choice for the mission. The Teensy 4.0 and BF3710 combination offer a mass and power reduction from 12g at 2W to 4g at .023W compared to the pi zero and pi camera module v2.

To control cubesat movement, CubeSpace has a great system of reaction wheels that will serve as the basis of design. Using three of the medium size CubeWheel, one on every major axis, the cubesat will have full rotational control, and it will use the payload for translational movement via the moving arms[19]. The reaction wheels will be controlled by NanoMind A3200 from GOMspace for acceleration and rotational data collection and processing[20].

Communications play a minor role for this mission, only used to receive print files and send image updates. As such, low data rates are acceptable and low power rates are preferred so a miniaturized transceiver would be ideal. GOMspace has the AX100 NanoCom that would fit great into the design space. With a maximum power consumption of 4W and data rates ranging from .1 kbps to 28.4 kbps it will be paired with a 6u rated antenna also from GOMspace[21-22].

2.5 Preliminary Sizing Summary

The payload will be made up of two moving arms and a printing arm that will work in tandem to continuously print without the need to stop. The final deliverables for this chapter are the payload total mass and power budgets which are 7.8kg and 18.1W respectively. With these budgets payload design can begin with an estimated mass/power breakdown of 2kg at 8W for movement arms, 4kg at 10.6W for printer arm and 1kg @ 0W for filament. Preliminary subsystem sizing will govern the physical and technical requirements for first iteration of arm design seen in chapter 3.

Subsystem	Mass [kg]		V - A	Power [W]
Structure	2	~1800g from cad example +10%		n/a
Power	1.388	Solar Panels		55
	0.27	NanoPower BP4		22.55
GNC	0.45	3x CubeWheel Medium		6.9
	0.003	Teensy 4.0 Development Board	3.3v @ 100mA	0.33
	0.001	BF3710 720p camera		0.14
	0.024	NanoMind A3200		0.9
Communications	0.0245	NanoCom AX100	3.4V @ 1.2A	4.08
	0.09	NanoCom Ant-6f UHF		2
Payload	7.8395	tbd		18.1

Table 4. Preliminary Subsystem sizing

3 Printing Head Design

The printing head contains a nozzle, extruder and hot end that all work similarly to commercial FDM hardware. The nozzle and extruder can be based on off-the-shelf hardware with minor modification, while the heat block, and hot end will require specific design.

3.1 Printing Head

3.1.1 Extruder

There are two main types of FDM extruder, the bowden extruder and the direct drive extruder. In both systems a filament is driven through a system of gears that precisely feeds the hot end and nozzle with a steady supply of filament. The difference between these

methods is in the location of the gear system: in a direct drive extruder the feed system is mounted directly to the hot end, usually through a heat break and cooling system, while in the bowden extruder system the filament is fed from the feed system through a tube to the printer hot end. This makes the printing head lighter at the cost of more powerful motors being required to drive the filament. Due to more powerful motors being required for the bowden system, the direct drive system was selected. The basis for design of the direct drive extruder system is based off of the E3D Titan extruder. This extruder was selected as a base for its simple and effective design. The main modifications to the standard extruder are an increase in the heat dissipation capabilities of the heat break and a change in the material from plastic to aluminum. Minor modifications were done to the structure to make it lower profile for size constraints. The Nema 17-40 standard motor is suggested by E3D for the titan extruder however its large power requirements and large profile make it an inferior option when compared with the Nema 17-20. The motor model 17HS08-1004S has half the motor volume while still keeping the same form factor as well as a power requirement reduction from 4.7W to 3.6W.

3.1.2 Nozzle

The nozzle is the last component that the thermoplastic will travel through for final heating and extrusion. As such it must be hard enough to withstand the wear of the carbon fibre core and tungsten microparticles and it must operate at constant temperatures greater than 250 °C. The E3D Volcano 1.2mm diameter, hot work tool steel nozzle meets all these requirements and was selected as the base of design [23] (See Figure 8). Unlike traditional FDM printing where the filament diameter is usually greater than the nozzle exit diameter, a larger diameter nozzle is required to ensure constant flow diameter. The carbon fibre core requires that the diameter be constant from extruder through the nozzle to ensure steady flow and minimize buildup. The E3D Volcano 1.2mm nozzle will therefore be modified to have a 1.5mm diameter exit in order to reduce the chance of flow inconsistencies.

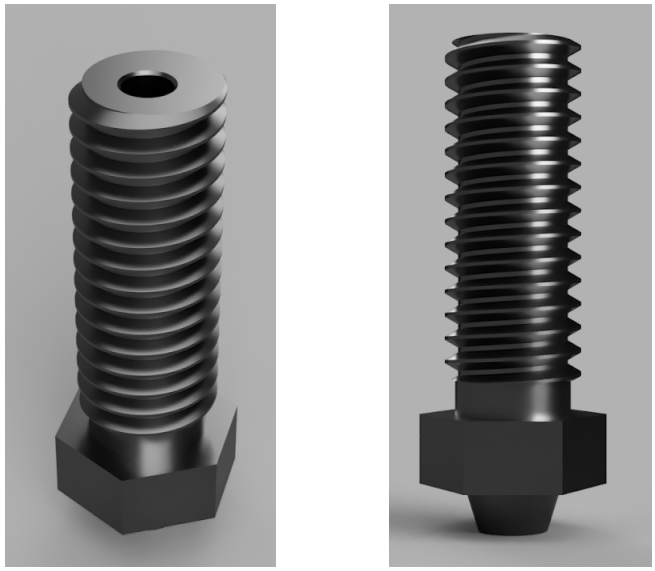

Figure 8. Volcano 1.2mm nozzle

3.1.3 Hotend

The Hotend is the component of the printing head that contains the heating element, temperature sensor and the printer radiator, it also connects the extruder to the nozzle. This piece needs to provide enough heat to keep the nozzle at 540 °K to print the filament, while keeping the extruder cool enough to not preemptively melt the filament or damage internal systems. Therefore all heat produced from the heating element must either go into the filament or be radiated off to ensure system operating temperature of 300 °K. Initial Hotend design begins with the heating block, which is a highly thermally conductive metal block with slots for a heating element, temperature sensor, nozzle and heat break (See figure 9 for example). Integration of two specialized heaters and two thermal sensors was chosen instead of a basic one cartridge heater and one temperature sensor for better temperature accuracy and more reliable heating (See Figure 10). The heaters selected are based on custom cartridge heaters from WATLOW that are specified to have an operational voltage of 12v and power draw of 3w [24]. These needed to be customized because of their low power draw requirements. The temperature sensors modeled are off the shelf PT100 cartridge 3D printer temperature sensors, these were chosen for their reliability and high operating temperature ceiling of 770 °K.

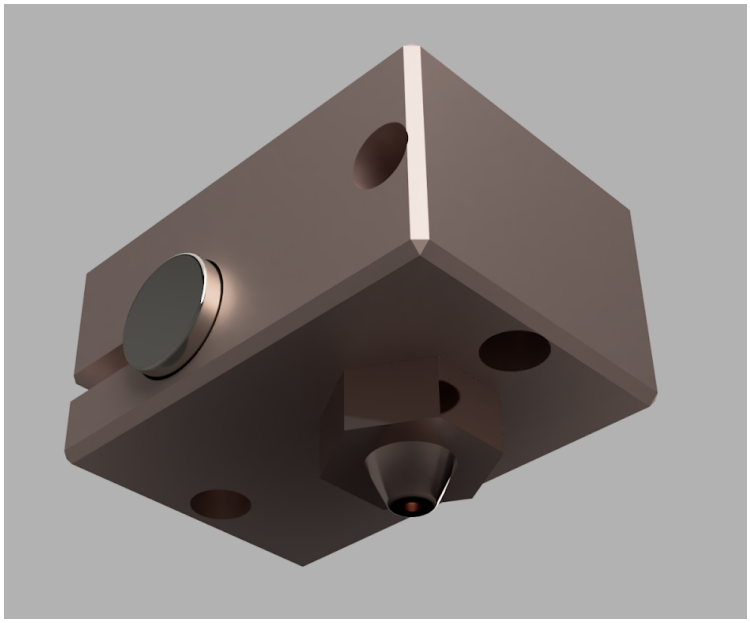

Figure 9. Example of off the Shelf Hot End

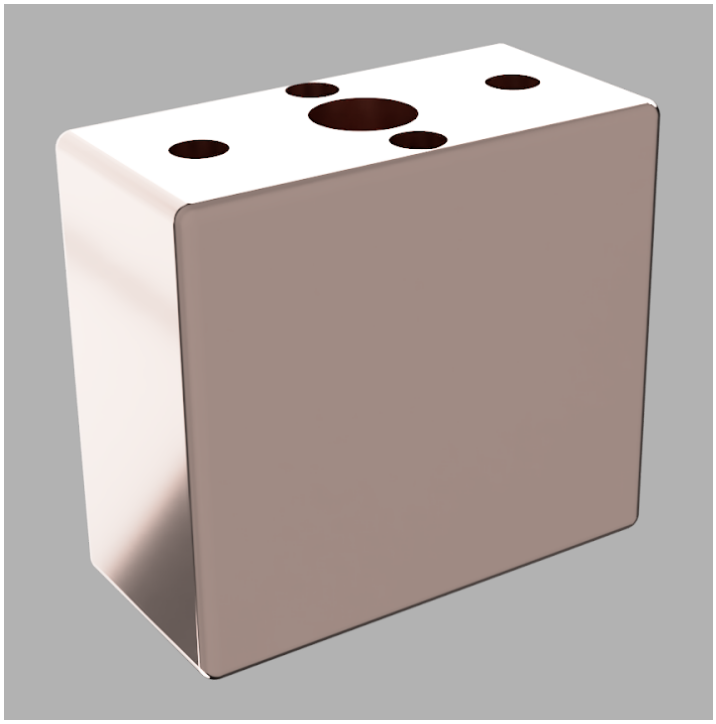

Figure 10. Heat Block

Calculation of the heat energy required for melting 1mm of filament every second was conducted using matlab (See Appendix). The matlab code takes the average density of a 1.5mm diameter polycarbonate/ASA filament with an area of .04mm^2 of carbon fibre in its core and finds the density and specific heat per unit mass. The carbon fibre modeled is the same that was used in reference material. The code then calculates the mass flow rate from

filament feed/extrusion speed and density of filament and area of layer. With this the calculated mass flow rate is 7.62×10^{-7} kg/s and a required heat energy of .2424W. Payload heaters generate a combined 6W of heat energy, after accounting for the heat lost to the thermoplastic for heating, the radiator must radiate at least 5.75W of heat to ensure thermal equilibrium for the hot end. Using the thermal radiation equation (Equation 2.1), and assuming a surface temperature target of 300 °K and anodized aluminum as the radiator material with emissivity of .77, the area required to radiate 5.75W is ~.016m^2. This a radiator is designed with corrugated radiating faces to maximize surface area per m^2 (See Figure 11).

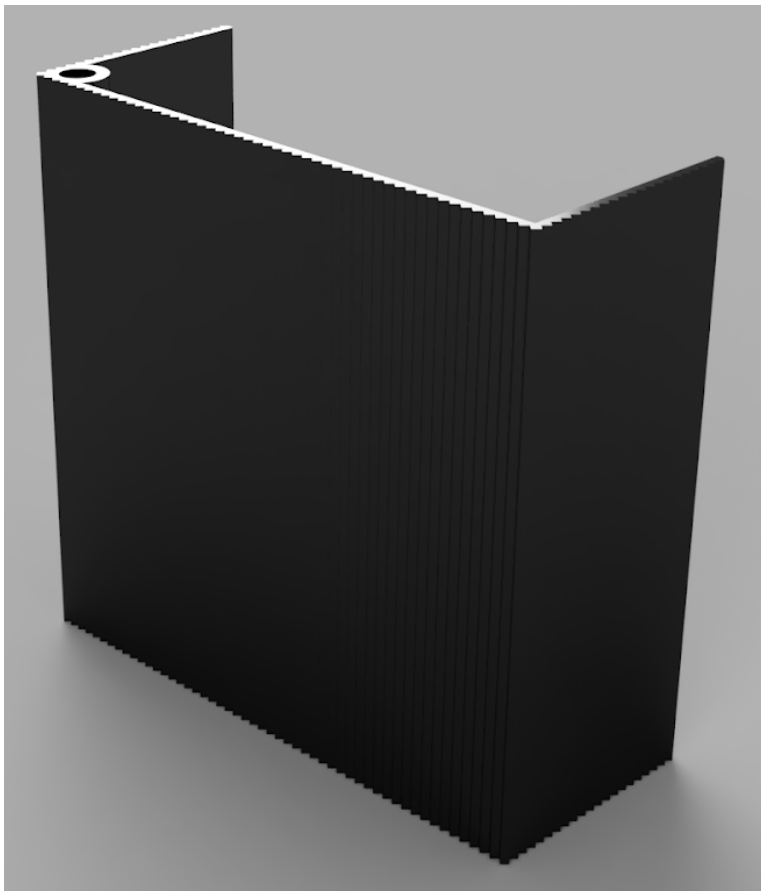

Figure 11. Radiator

Design of the heat break is simple as a threaded and cored titanium rod allows for great thermal resistance and structural support (See Figure 12). Titanium alloy Ti-6Al-4V is selected for its low thermal conductance and strong physical properties up to 400°C. With this threaded base to connect the heat block to the extruder, a heat pipe mount is designed to be placed on the heat break in between the hot end and extruder. This mount would allow for attachment of heat pipes to transfer any excess thermal heat to the radiators. The first version

had a large mass to act as a heat sync (See Figure 13), however this larger mass decreased the maximum temperature to 201°C, far lower than the required 260°C minimum (see Figure 16). The second version was slimmed down (See Figure 13) and had simulated temperatures just above 300°C (See Figure 17). The filament only requires temperatures of 260-280°C but with the model surpassing this, it allows for better thermal control of the system. The second mount was simulated again with a modeled filament, and the maximum temperature increased again allowing for greater thermal control. Final assembly of the hot end can be seen in Figure 14 and 15.

Figure 12. Heat Break

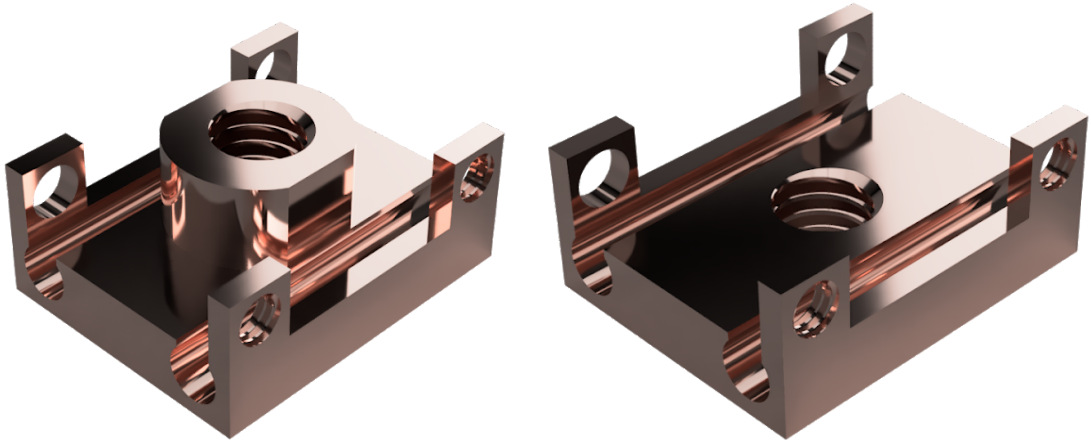

Figure 13. Heat Pipe Mount [Left: Preliminary][Right: Final]

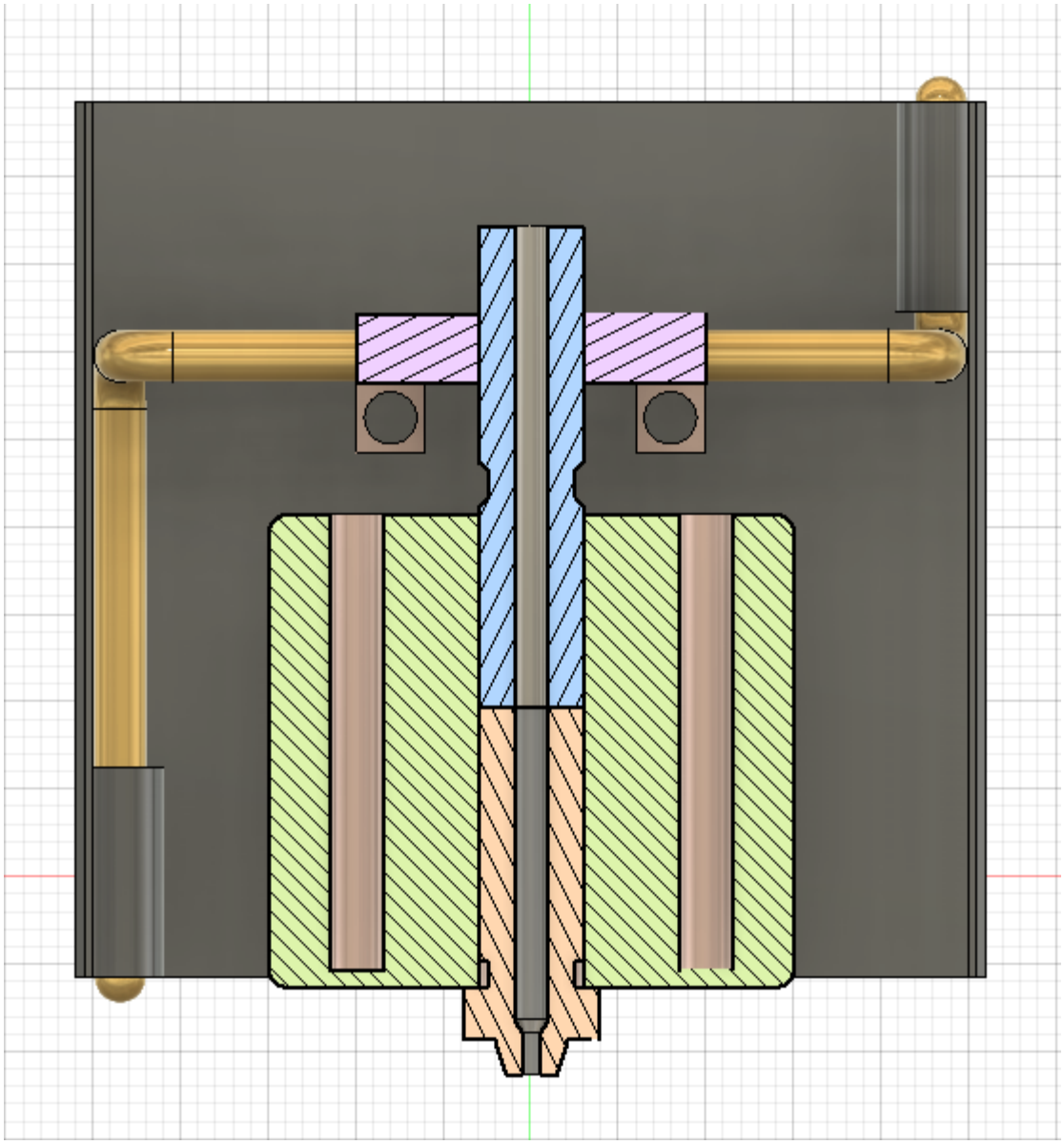

Figure 14. Hot End Assembly Cutaway View

[Green: Heat block][Pink: Heat Pipe Mount][Blue: Heat Break][Orange: Nozzle]

[Brass: Heat Pipe][Grey: Radiator]

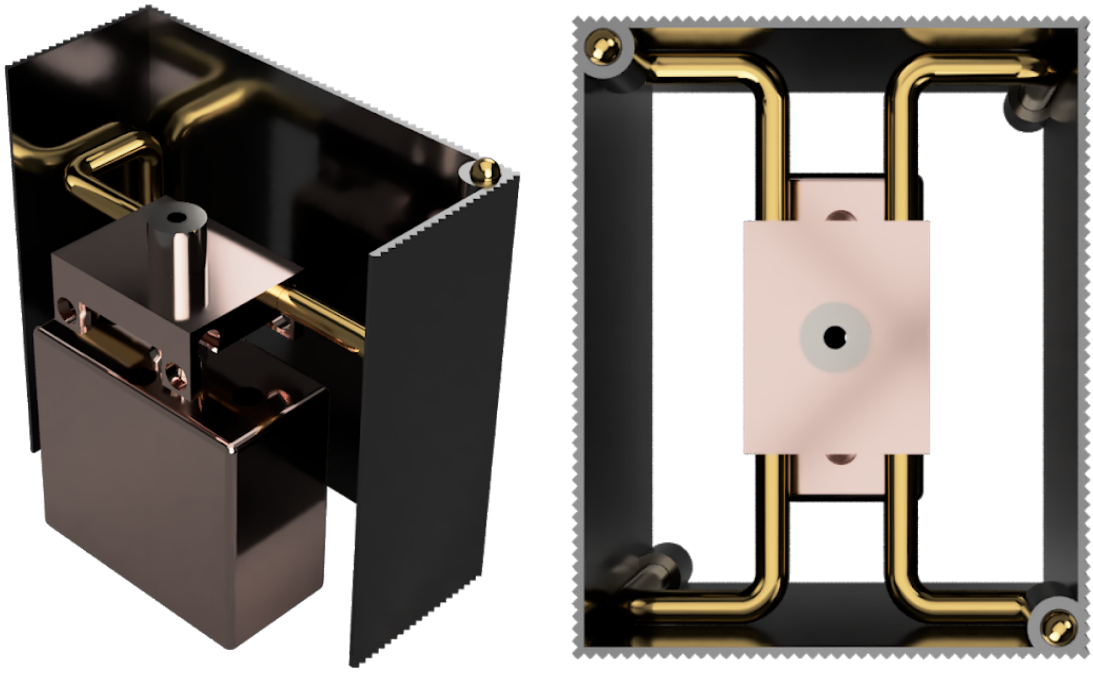

Figure 15. Hot End with one Heat Pipe and Radiator Removed (Left)
and Hot End Top View (Right)

3.1.4 Thermal Simulations

All thermal analysis presented are modeled using Ansys steady state thermal solver 2019 student edition. In the student edition the fidelity of the simulation is limited by the number of mesh nodes and elements to a combined total of 35,000 as such simulating all the required components together was unrealistic. In order to get the detail required for model accuracy the simulation had to be conducted in two parts, one of the heat block, nozzle, heat break, and heat pipe mount, and the other with the radiator alone. For all simulations, the heat block and heat pipe mount were modeled as cast copper, the nozzle as tool steel, the heat break as titanium alloy Ti-6Al-4V and the radiators as aluminum all these material properties were taken from Ansys Engineering Data Materials. The two simulations were linked by the assumption of convective flow between the hot end and radiators via the heat pipe.

For the simulation with one radiator panel the meshing methods used were automatic method and face sizing to reduce nodes and elements to below 35,000 sum threshold. The thermal analysis was conducted with the simulation settings: initial temperature of 30°C, convection through heat pipe mounting locations, and a heat flux of -370 W/m^2 on the corrugated radiator face. These conditions simulate a heat flow of 2.875W though each heat

pipe. The 370W/m^2 heat flux is the calculated heat loss due to radiation (5.75W over 0.0156m^2) and was only applied to the corrugated face because the .77 emissivity value used to calculate radiation only applies to the anodized aluminum on the corrugated section as the rest of the piece will be polished aluminum. This simulation shows that the peak temperature is just over 30°C where the heat pipes mount to the radiator (See Figure 19). The 30°C maximum allows the assumption that a 30°C convective flow can be simulated for the heat pipes in the hot end simulations.

For the simulations with the assembled heat block, nozzle, heat break, and heat pipe mount default meshing method was used with contact sizing on all contacting surfaces. The thermal analysis was conducted with the simulation settings: initial temperature of 30°C, 3W of heat inflow to the surface areas with heaters, convection out through the heat pipe mount on the surface areas to have heat pipes mounted, .25w heat flow out through filament or area in contact with filament, and time frames from time 0s to 100s. The images shown were the steady state met after approximately 3 seconds for both calculations (Figures 3.9-3.11). There were three simulations done with these mesh and thermal analysis settings with the only differences between them being the following differences in geometry:

-Simulation 1: the original heat pipe mount design with mass of 10.15g. (See Figure 16)
-Simulation 2: an updated design for the heat pipe mount with a mass of 8.1g and mounted upside down relative to initial design. (See Figure 17)
-Simulation 3: Simulation 2 with filament modeled in the system as a mass inside the nozzle and heat break. (See Figure 18)

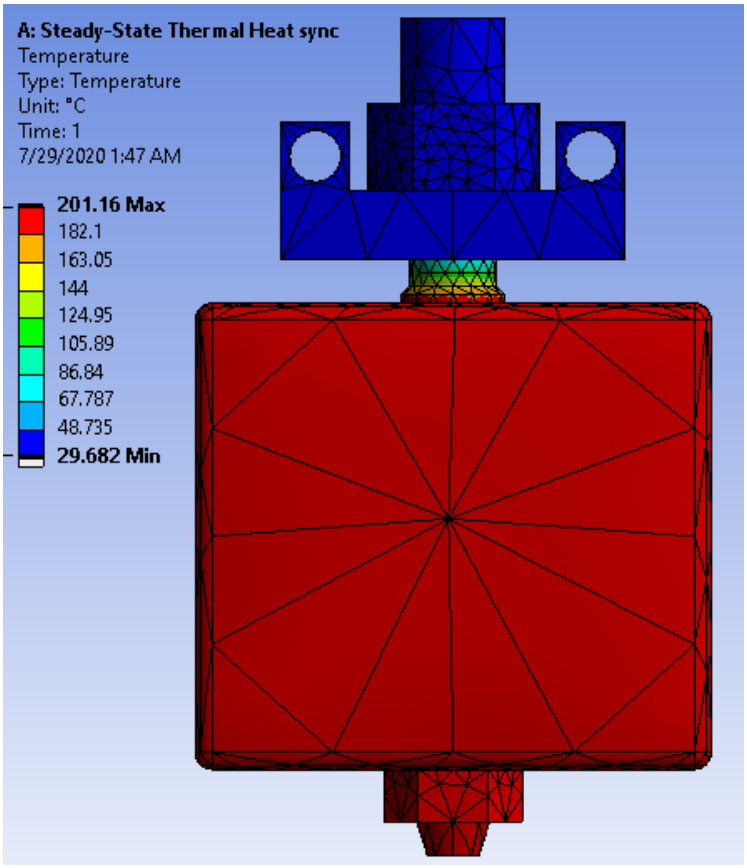

Figure 16. Hot End Simulation 1

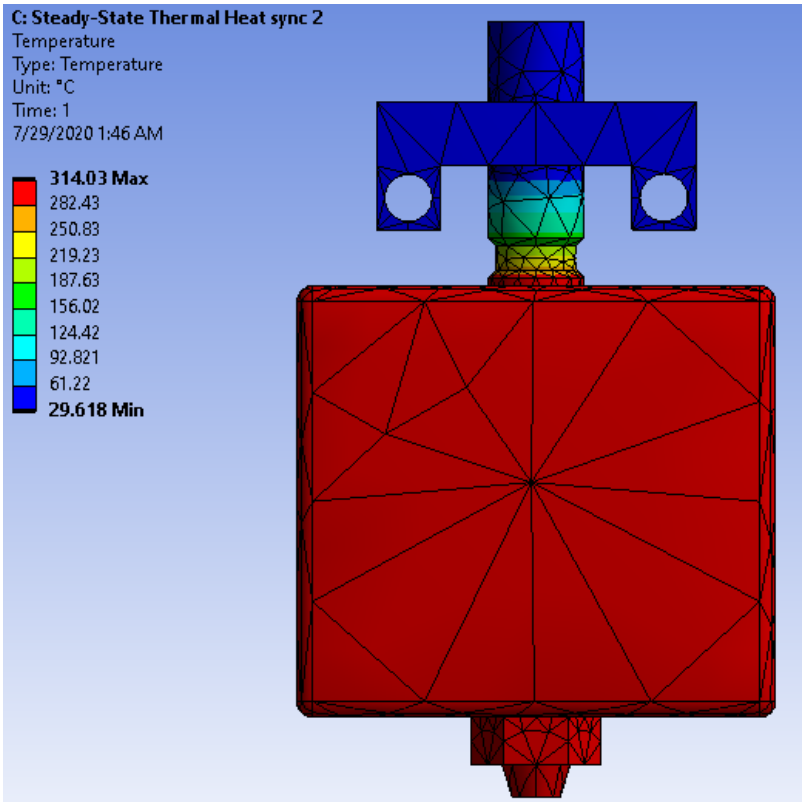

Figure 17. Hot End Simulation 2

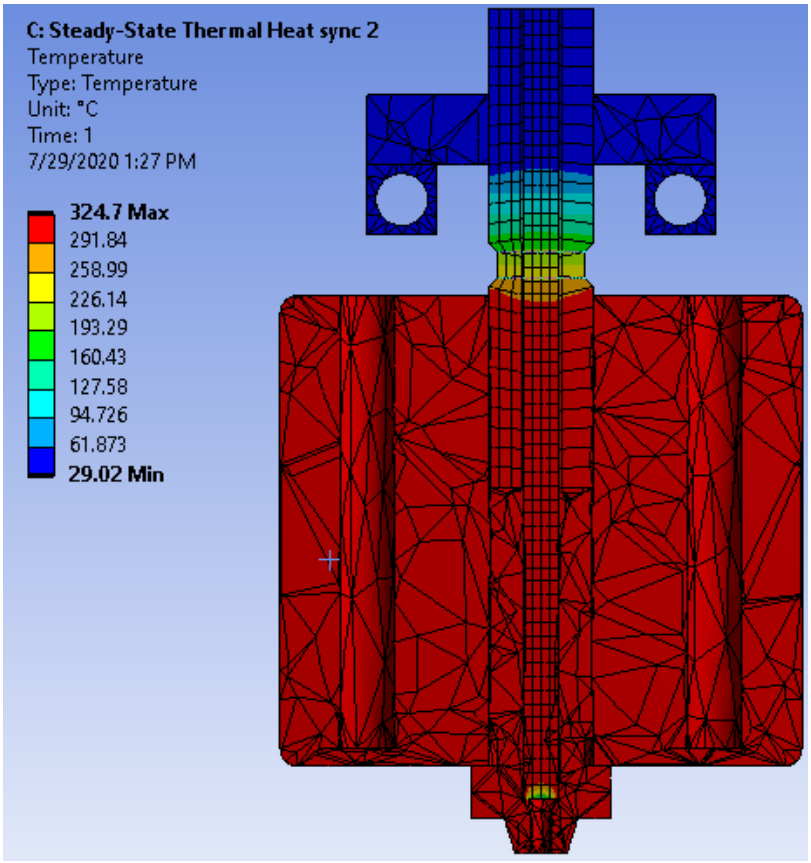

Figure 18. Hot End Simulation 3

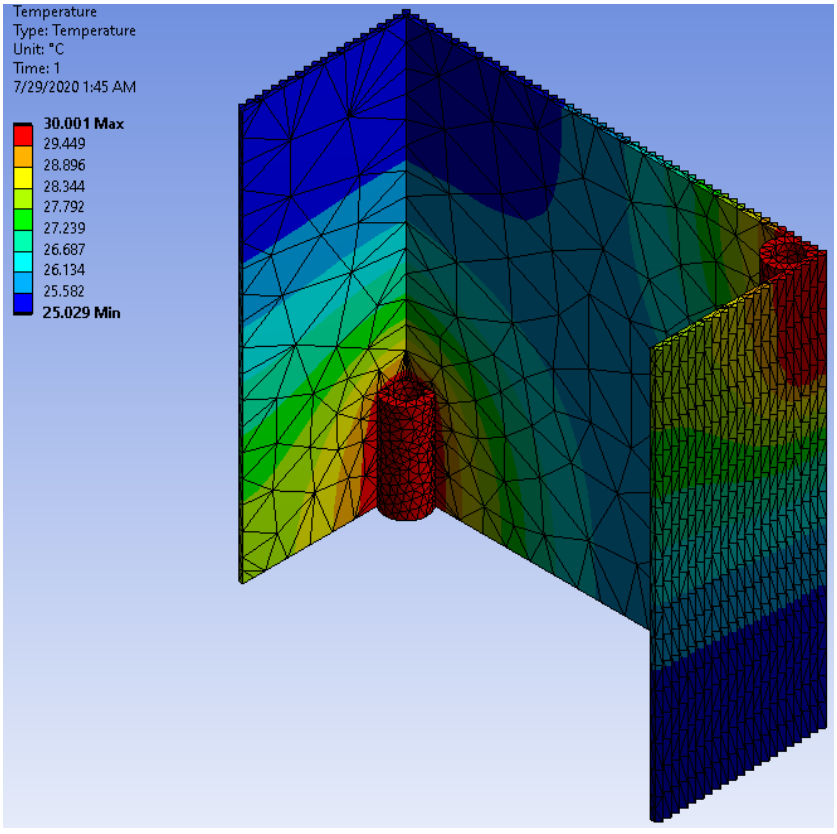

Figure 19. Radiator Simulation

3.2 Assembly

For assembly two mounts were required, one that would mount the hot end to the extruder and one to mount the extruder to the chassis. To connect the extruder to the hot end a simple 6mm threaded piece was designed on the titan hot end mount (See Figure 20). The printer head mount was more involved due to a required deployment mechanism mounted into the chassis. The basis for this mount has holes for M5 all thread to linearly and accurately deploy the printhead. This deployment system will be discussed in detail in chapter 5 Cubesat Subsystem Design.

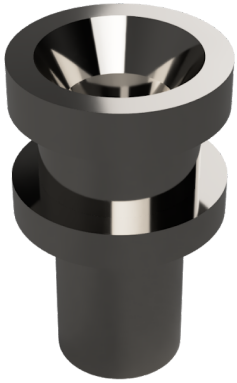

Figure 20. Extruder to Hot end Mount

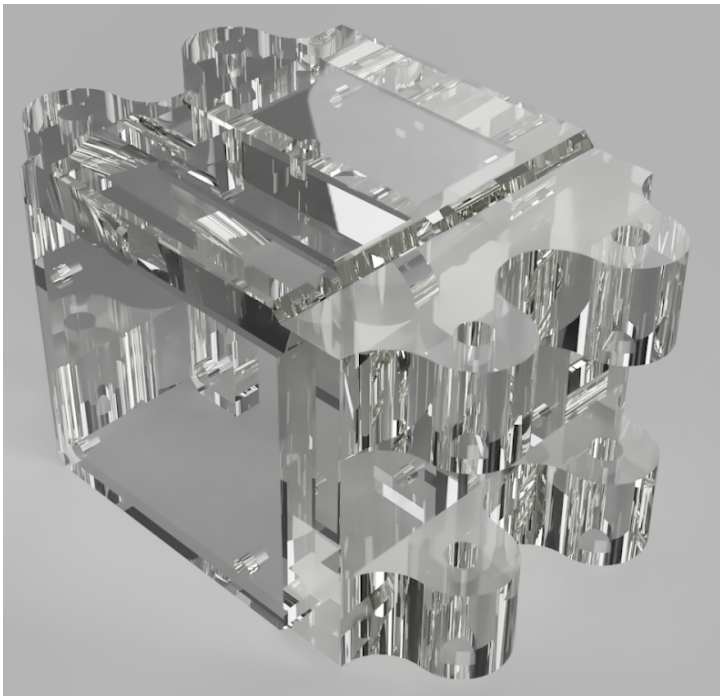

Figure 21. Print Head to Deployer mount

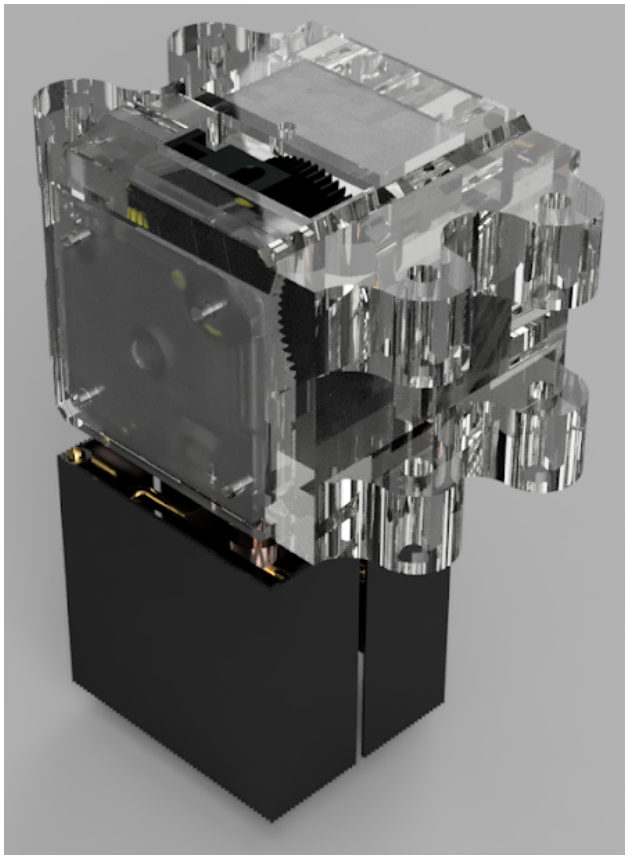

Figure 22. Printhead Assembly

3.3 Printing Arm Budget and Summary

From the Final Mass and Power Budgets, the final design comes in just below budgeted power and far below budgeted mass. This allows for more power to be budgeted to the moving arms and to the onboard computer. The large mass budget savings are helpful for later cubesat designspace.

Printer Head				
	Sections	Component	Mass [G]	Power Est. [W]
	Hot End	Heating Cartridge	3.32	6
		Heat Block	95.281	N/A
		Temperature Sensor	4.6	0.2
		Radiator	19.514	N/A
		Heat Pipes	14.576	N/A
		Heat Break	2.985	N/A
	Nozzle	Nozzle	4.148	N/A
	Extruder	Assembly	26.7	N/A

		Motor: 17Hs08-1004S	150	3.6
	Adapter		9.685	
Printer Arm	Mount		147.26	
	Sum		478.069	9.8
	Budgeted Amount		4000	10.6
	Remaining		3521.931	0.8

Table 5. Mass and Power Budget

4 Moving Arm Design

In conventional FDM style 3D printing, a printing head is moved across a print bed where a model is printed. For prints larger than the printer a moving printer design is required. For the Orbital Construction Cubesat two identical “Mover” arms will transport the chassis and printhead over the active print. Each of these arms was designed for minimum retracted volume as well as stable and accurate movement.

4.1 Axial Rotation Segment

The axial rotation segment hereby referred to as ‘ARS’ went through two iterations of design both are discussed below.

4.1.1 ARS Version 1

The design methodology for the ARS is to design an axial rotation joint with full 360 degree rotation while being as compact as possible. As such ARS V1 was designed around the SRC022A-12 slip ring with a Portescap 08GS61 motor with the internal volume mostly taken up by a gearbox and the slip ring. The slip ring acts both as a way to effectively keep contacts throughout rotation as well as axle about which the mechanism works. It is held in place with an RNA4903 bearing and actuated by an integrated 15:1 step down gearbox. This gearbox used exclusively spur gears, this is not ideal when compared to the locking abilities of worm gears. After being put into the arm assembly V1 with the TRS V1 [See Section 4.2.1] and grabber V1 [See Section 4.3.1] it was test fit into a mock-up chassis. This test fit showed that the current model was too large and needed to be downscaled to fit in a new battery system and new reaction wheel system [See Section 5..]. A cutaway view of ARS V1 can be seen below in Figure 23.

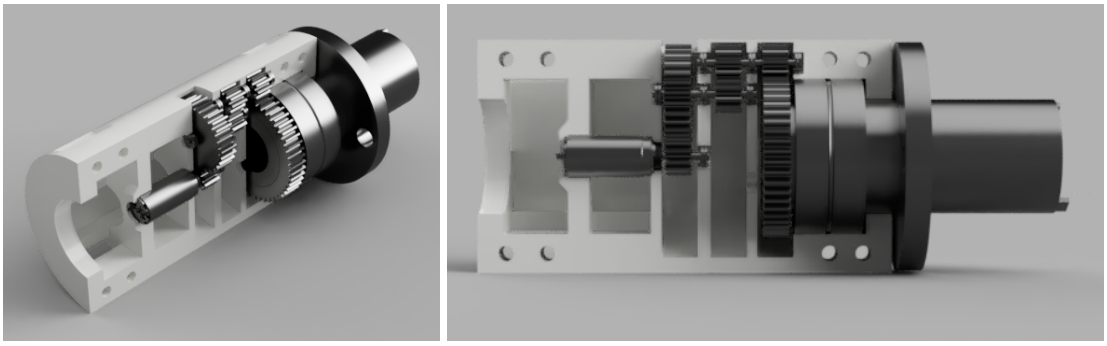

Figure 23. ARS V1

4.1.2 ARS Version 2

ARS V2 was designed around the M155C-24 slip ring with a Faulhaber 0615 003 S motor. The M155C-24 is held in place by three 6703ZZ bearings to help with radial and axial forces applied to the joint. This new slip ring is not only smaller than that of the ARS V1, it also has more channels allowing for a PA2-50 encoder to be mounted to each motor. The decrease in size allows for ARS V2 to take up nearly 66% less volume than ARS V1. The internals are similar to version one as they are made up of a 50:1 step down gearbox, this time incorporating a worm gear. The ability of a worm gear to effectively stop unwanted rotation when the motor is not powered is a great advantage over version one. The ARS V2 was integrated into arm assembly V2 and V3 with no variations between integrations and is the most current version of the ARS. Cutaway views of the ARS V2 are below as well as a size comparison to ARS V1.

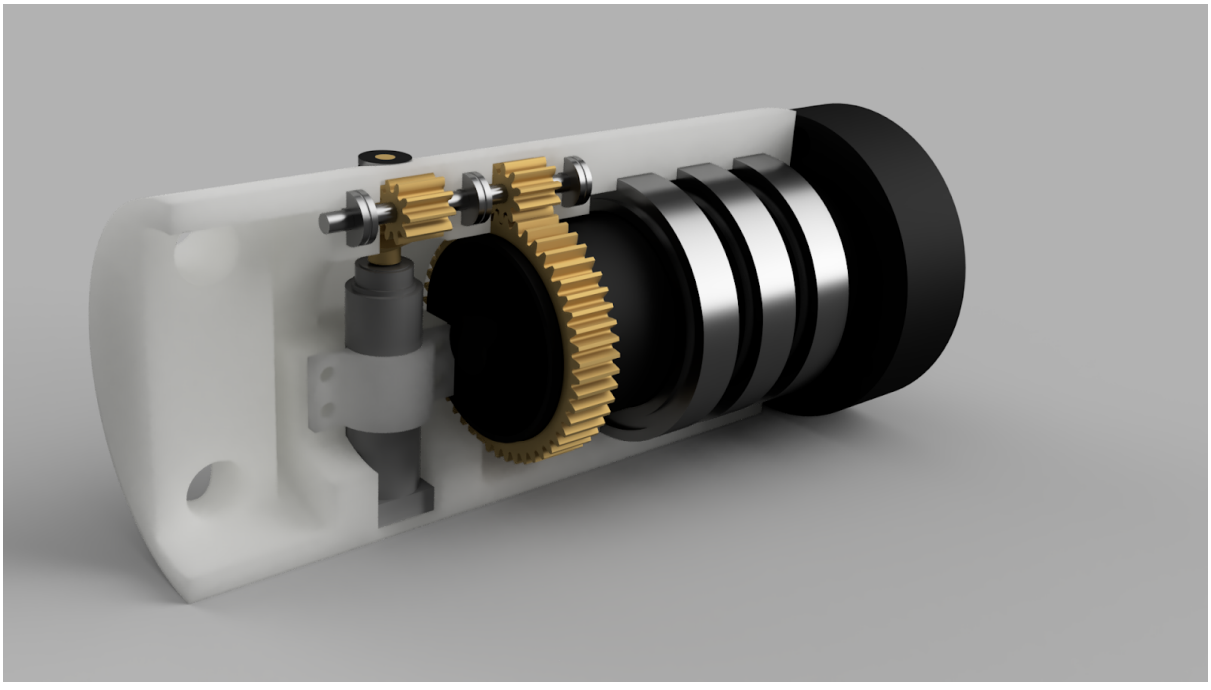

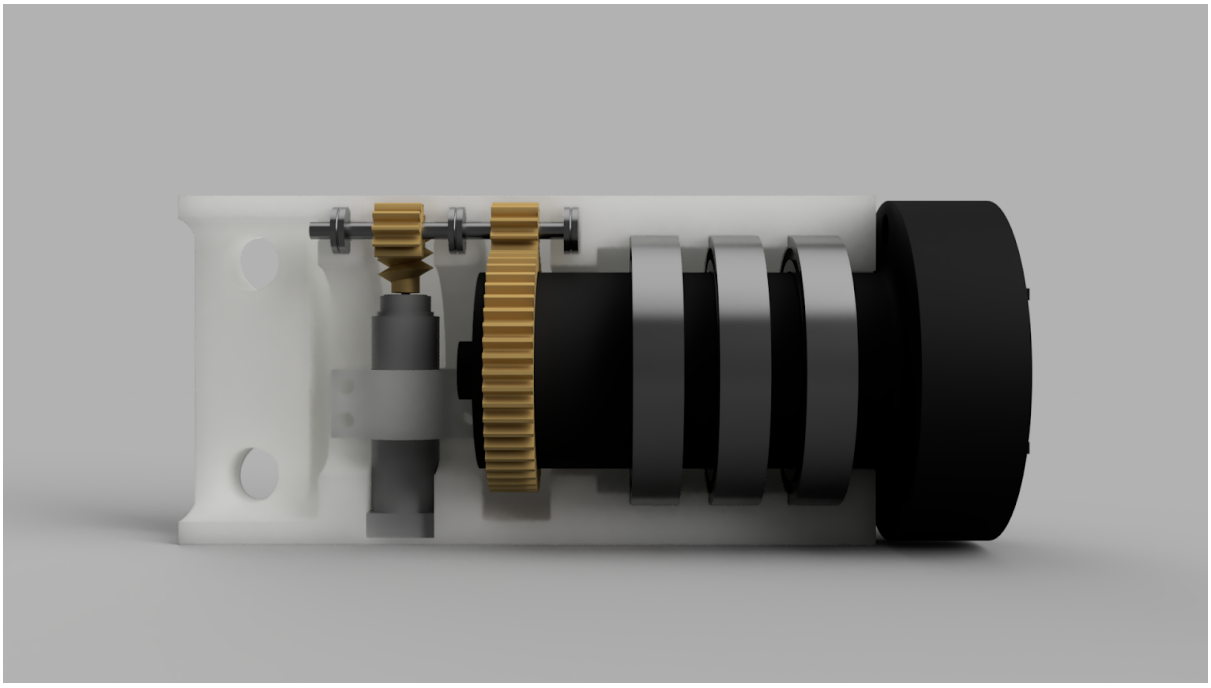

Figure 24. ARS V2

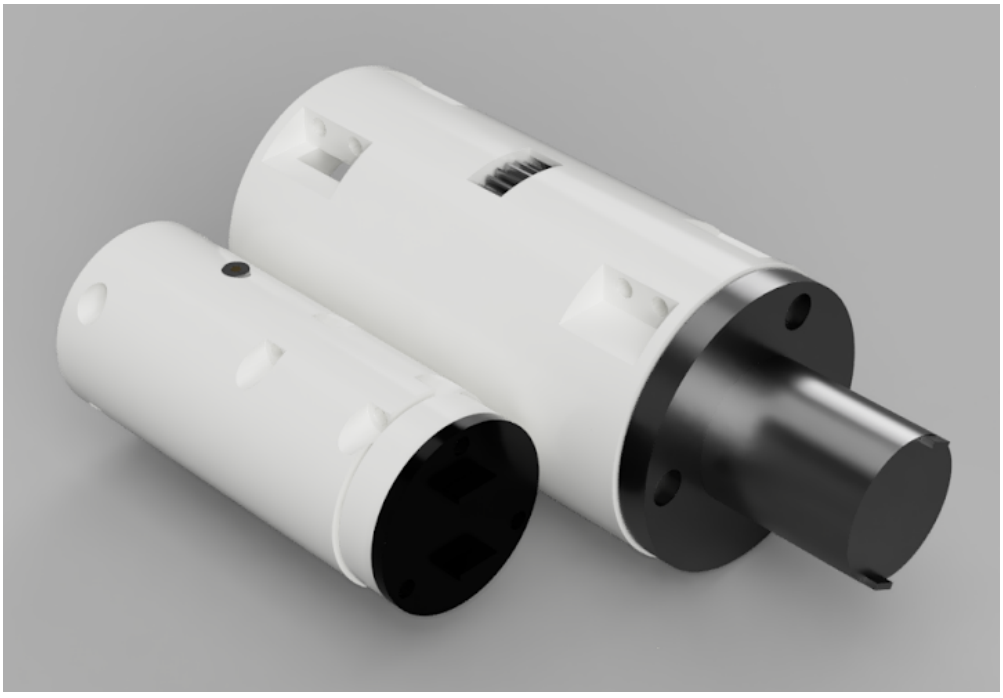

Figure 25. ARS V1 compared to ARS V2

4.2 Tangential Rotation Segment

The tangential rotation segment hereby referred to as ‘TRS’ went through three iterations of design. Unlike the ARS iterations, TRS V1 and TRS V2 are radically different in

approach, and V3 being an easier to fabricate V2. These iterations are discussed in more detail below.

4.2.1 TRS Version 1

TRS V1 was designed similarly to the ARS V1, around the SRC022A-12 slip ring with a Portescap 08GS61 motor. The nature of this joint required a different 200K bearing to be used for gearbox stability. This internal gearbox has a 12.5:1 step down gear ratio incorporating a worm gear for unpowered locking. When integrated into arm assembly V1 TRS V1 was too large for the system and did not have sufficient range of motion to be effective. The range of motion for the TRS V1 joint was designed to be +/-90deg from parallel, this would be improved on in TRS V2. Various views of TRS V1 can be seen below in Figures 4.4 and 4.5.

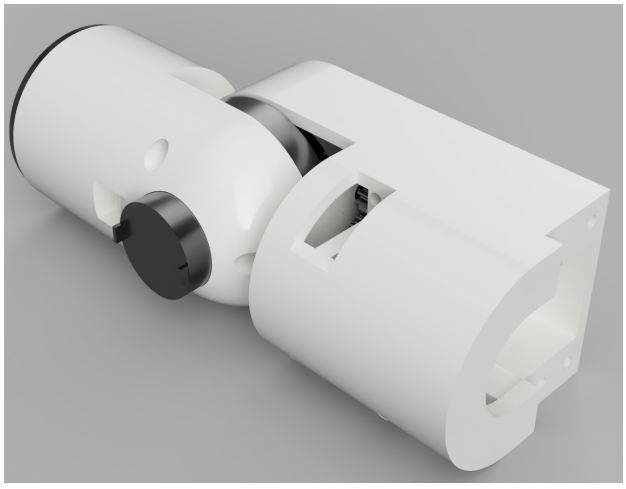

Figure 26. TRS V1

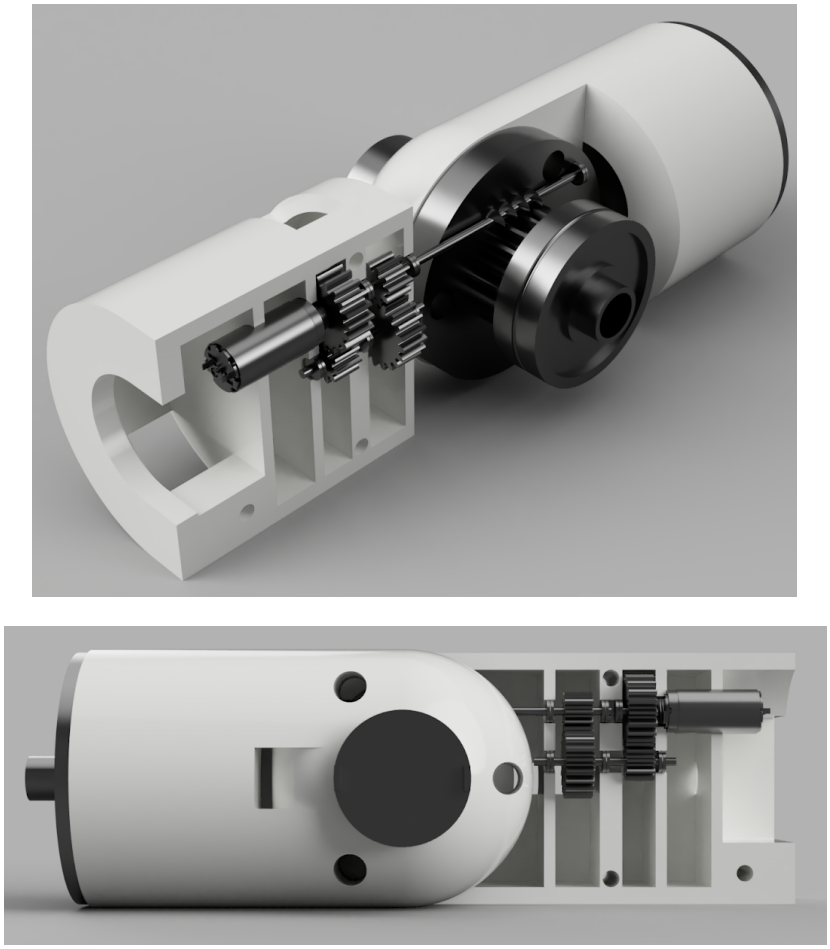

Figure 27. TRS V1 Cuttaway Back (Top) and Front (Bottom)

4.2.2 TRS Version 2

The TRS V2 is a redesigned version of the TRS V1 integrating the M155C-24 slip ring and the Faulhaber 0615 003 S like the ARS V2. The 180 degree range of motion of the TRS V1 was improved to full 360 degree rotation with the change of the joint location. The internal 50:1 step down gearbox utilizes a worm gear directly off the motor for more stability. After integration into arm assembly V2 the TRS met all mechanical and electrical operation goals, but the motor and gearbox were difficult to access during fabrication. The TRS V2 was redesigned into the TRS V3 with an emphasis on streamlined assembly and ease of access to internal components. The TRS V2 can be seen below from various views in figures 4.6/4.7.

Figure 28. TRS V2 Front (left) and Back, with bearing panel removed (right)

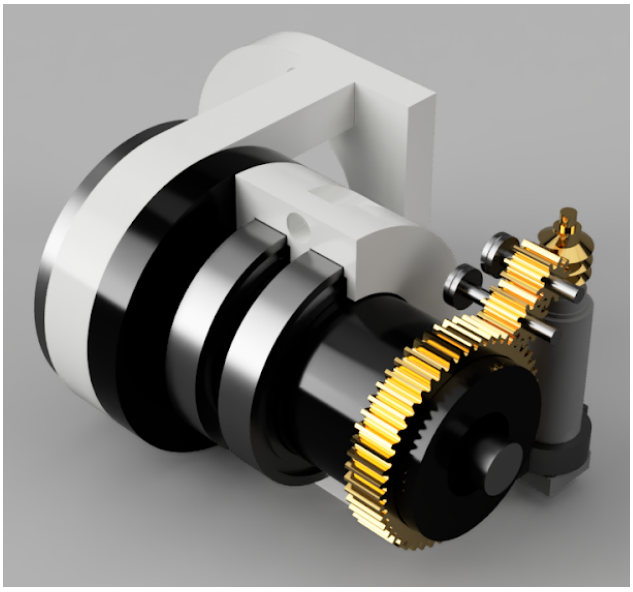

Figure 29. TRS V2 with gearbox shroud removed

4.2.3 TRS Version 3

Taking the basic design from TRS V2 hte TRS V3 was designed to be easy to assemble and access. It uses the same bearings and slip ring as the TRS V2 and the ARS V2 as well as the same worm gear 50:1 step down gear ratio. For accessibility there are panels integrated into the structure that are secured with M3 and M2.5 bolts. The TRS V3 takes up less than one third of the volume compared to the TRS V1. Views of the TRS V3 as well as a comparison of all TRS versions can be found below in Figures 4.8 to 4.10. The TRS V3 is the most current tangential rotation segment in the arm assembly.

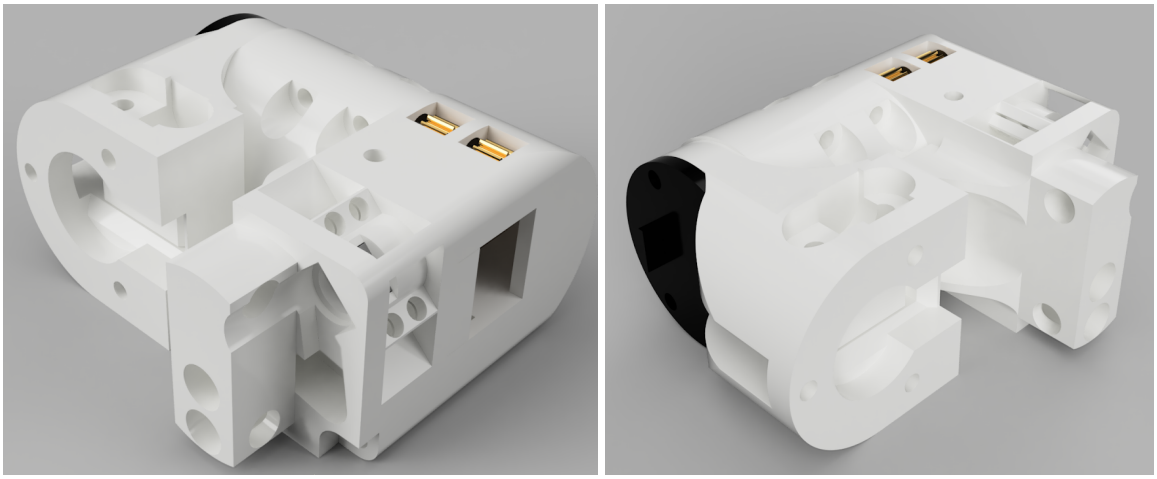

Figure 30. TRS V3 Front (Right) and Side (Left)

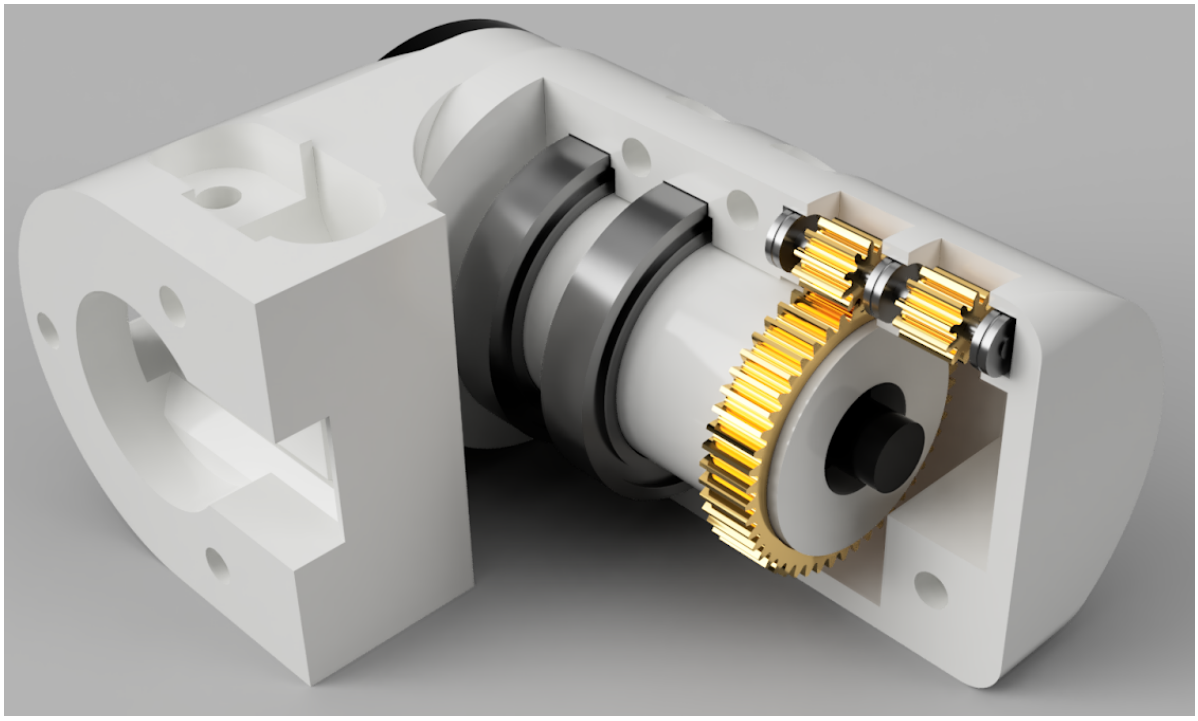

Figure 31. TRS V3 cutaway Motor Mount removed

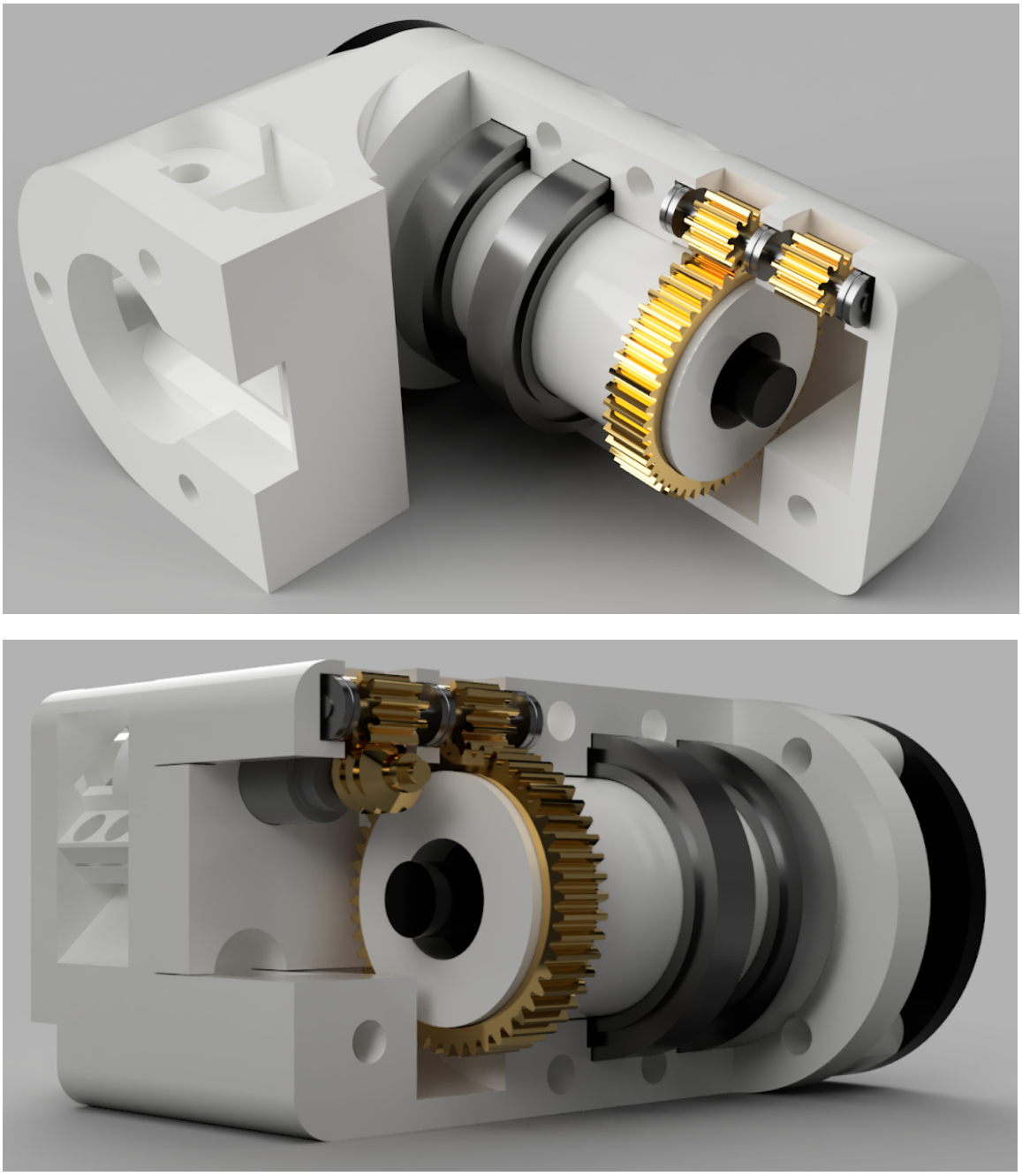

Figure 32. TRS V3 cutaway Back Panel removed

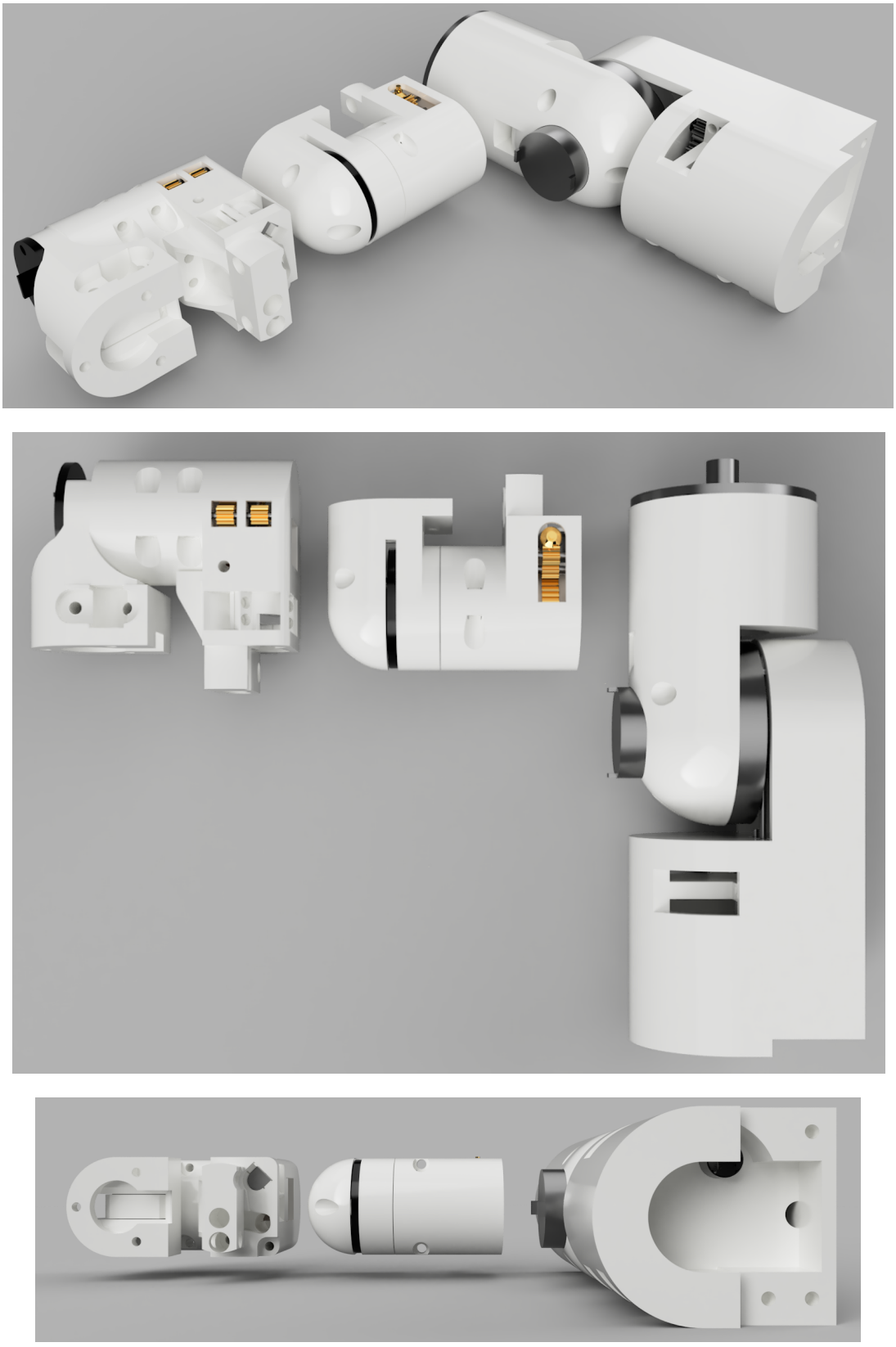

Figure 33. TRS V1, V2 and V3 (Right to Left)

4.3 Grabbing Claw

The Grabbing Claw component is a simple double geared mechanism being driven by a worm gear and motor. There were three design iterations finalizing in the Claw V3 design. The initial design Claw V1 was designed with Portescap 08GS61 motor and large grabbers. This design ended up too large for the system and needed to be scaled down. Claw V2 was designed smaller with the Faulhaber 0615 003 S and much smaller grabbers compared to the body size. The Claw V2 worked well with its mounting mechanism designed for mounting into the TRS V2. When the TRS V3 was designed a modification to the mounting mechanism was required so the Claw V3 was designed. All three versions can be seen below in figures 4.12 to 4.15. The Claw V3 is the most current grabber in the arm assembly.

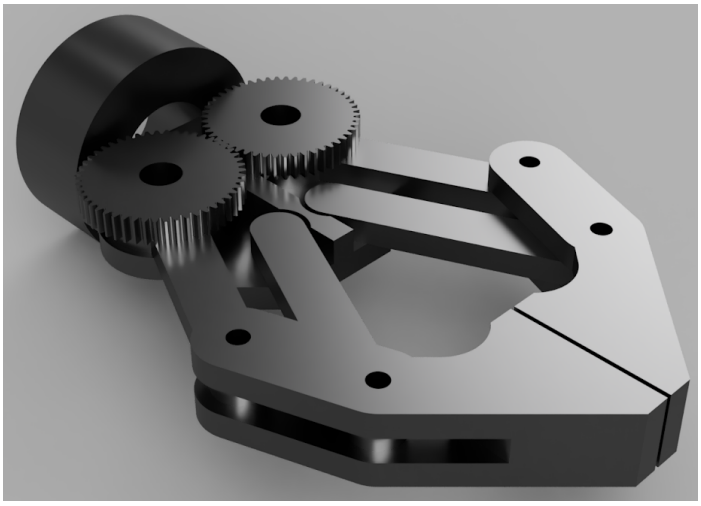

Figure 34. Claw V1

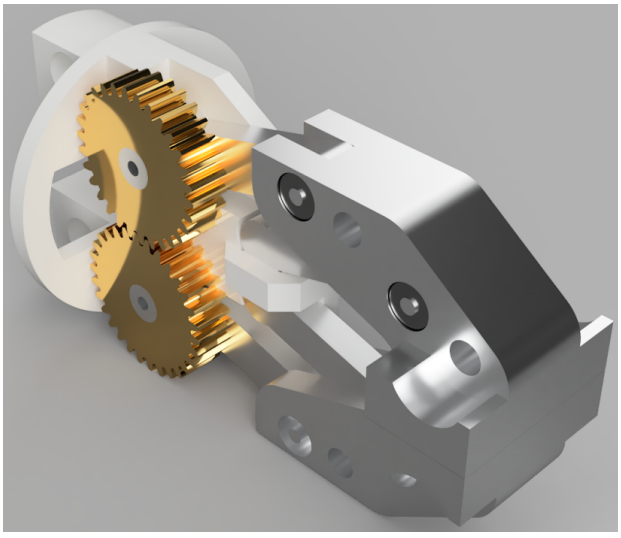

Figure 35. Claw V2

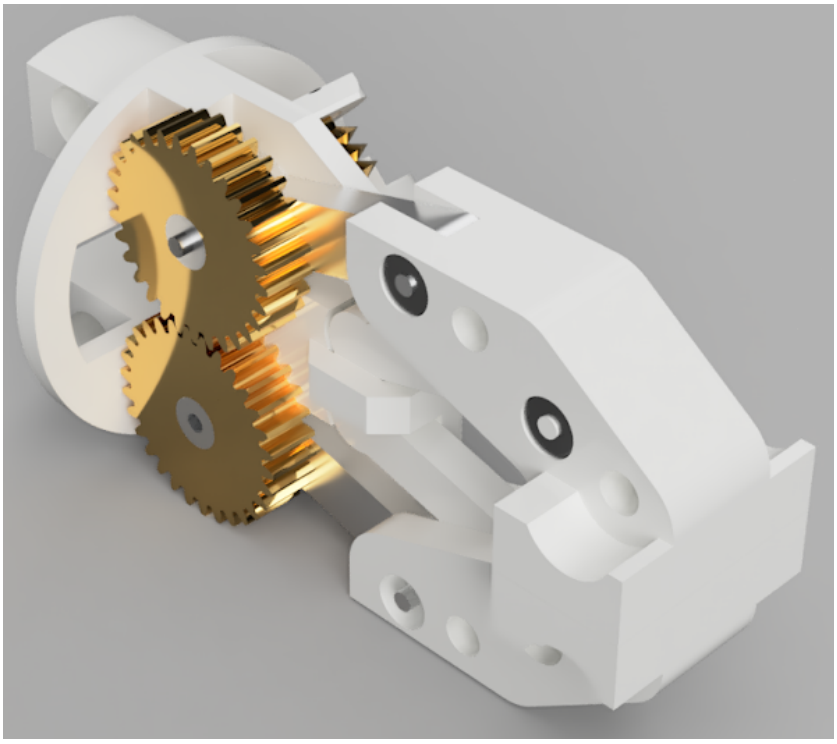

Figure 36. Claw V3

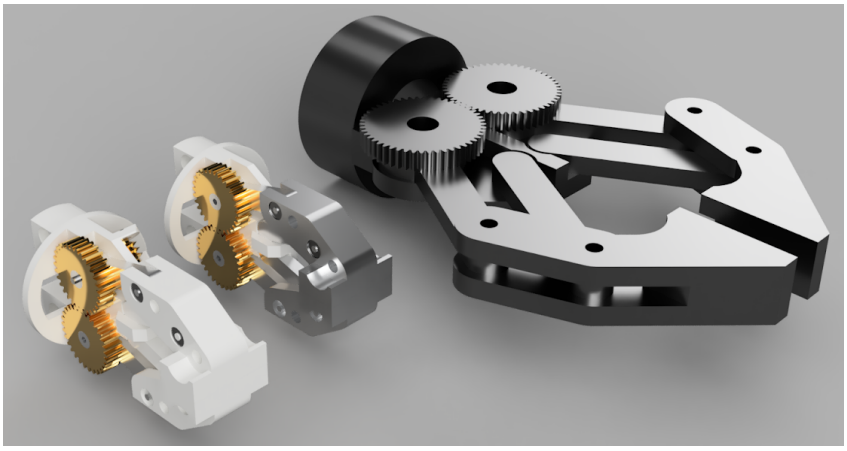

Figure 37. Claw V1-3 size comparison (Versions 3 to 1 from left to right)

4.4 Assembly

Three assemblies were designed with the ARS, VRS and claw components. Arm Assembly V1 with the ARS V1, TRS V1 and Claw V1 was iterated on due to its large size and poor range of motion. Arm assembly V2 from ARS V2, TRS V2 and Claw V2 met operational requirements, but was replaced with arm assembly V3 with the ARS V2, TRS V3 and Claw V3. All arm assemblies had the same basic layout, starting from the chassis mount:

ARS, TRS, ARS, TRS, ARS, TRS, ARS, Claw. This format was chosen to allow for maximum reach of the arm as well as convenient storage options. A model of Arm assemble V3 can be seen in figure 38.

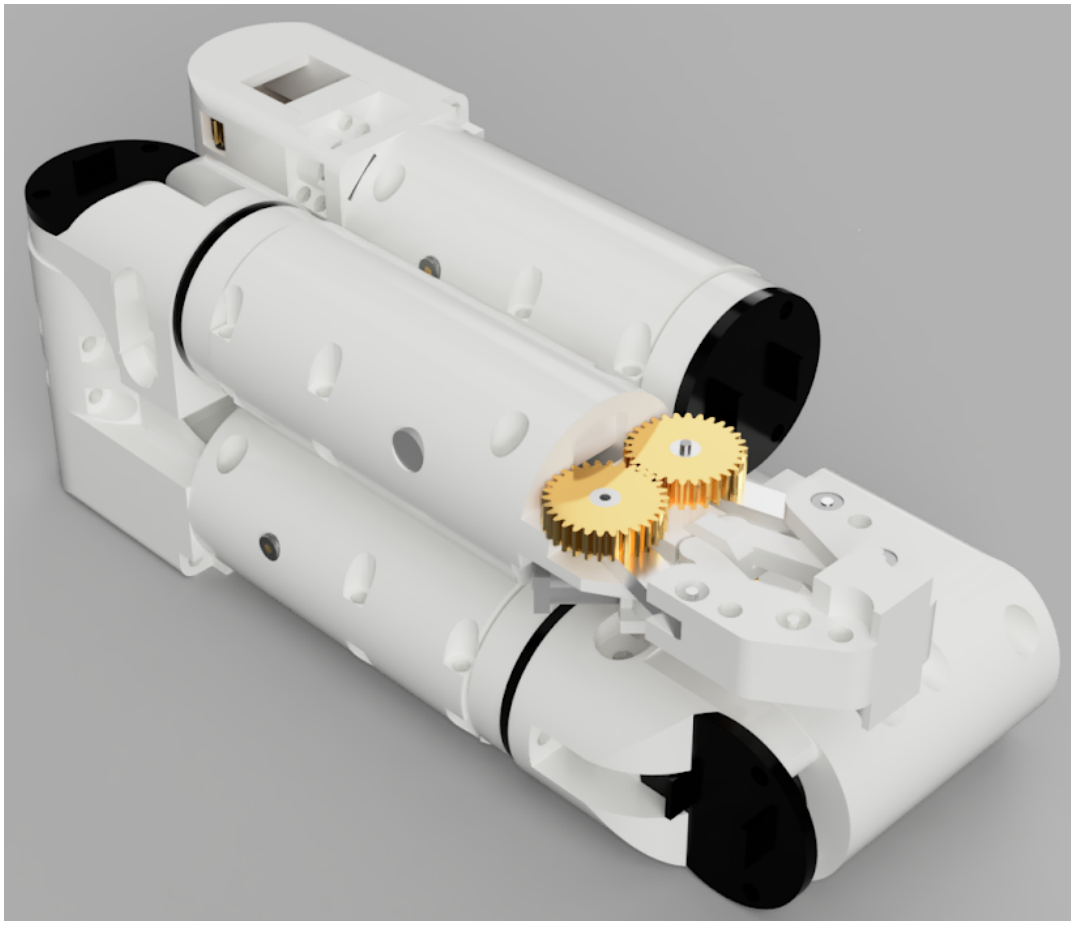

Figure 38. Arm Assembly V3

4.5 Wiring

Wiring for each arm is identical and starts from the P-60 powerdock and CAN bus (See section 5.1.3 for more details) modeled as an 8V supply voltage and . From there the supply voltage and CAN data go into each motor driver and the signal and power go from there to each motor in succession. All encoder power sources and grounds are linked in order to save on wiring as the supply voltage/current should always be constant. Another channel saving measure was taken by dropping one of the channels of the two channel encoder. This will make directional observations impossible but the rotation amount will still be able to be observed and with motor voltage monitoring the direction of rotation can still be found. In the

diagram below the visualization of the writing can be seen, there are 4 inputs from the electrical system into this visualization: +8V, GND, CAN_H, and CAN_L.

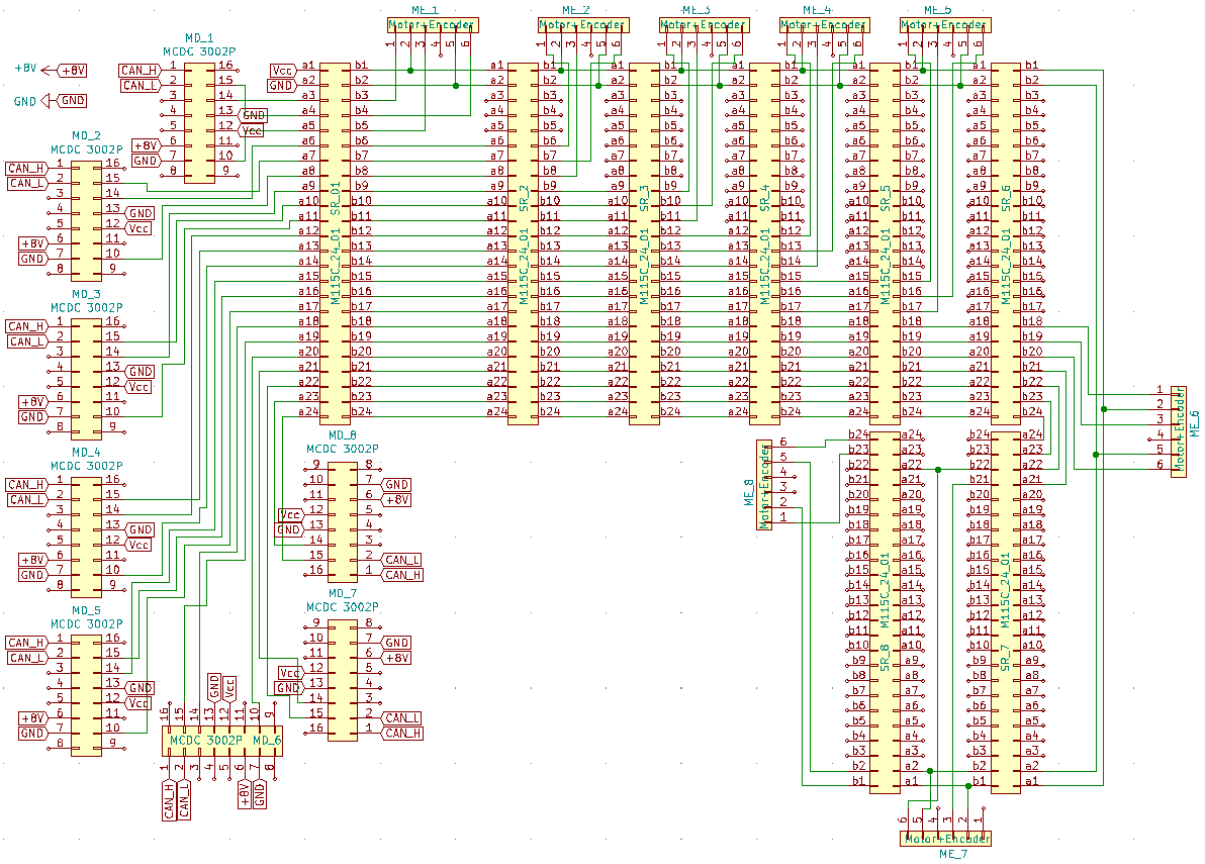

Figure 39. Single Arm Wiring Diagram

5 Cubesat Subsystem Design

This chapter discusses the first design iterations for each major mechanical subsystem of the orbital construction cubesat.

5.1 Electronics

5.1.1 Solar Panels

The preliminary subsystem design Solar Panel Arrays were chosen as the final solar panels for design as they are commercially available and are well documented. As stated in preliminary subsystem design these solar panels will produce a maximum power of 61.2 W and a mission end power of 55W. These solar panels will be mounted to limbs and deployed after cubesat deployment using the solar (more detail can be found in section 5.2). Modeled versions of these solar panels can be seen below in Figure 39 through 41.

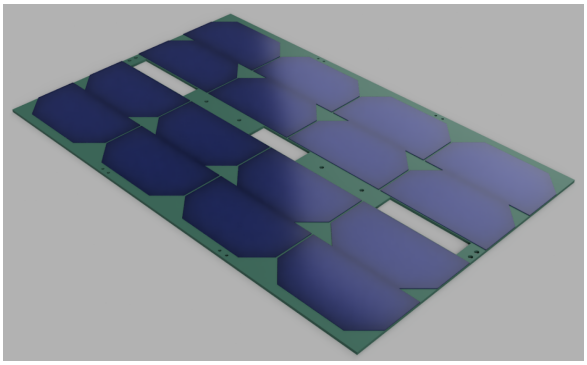

Figure 39. MSP-B-8-2 Solar Array

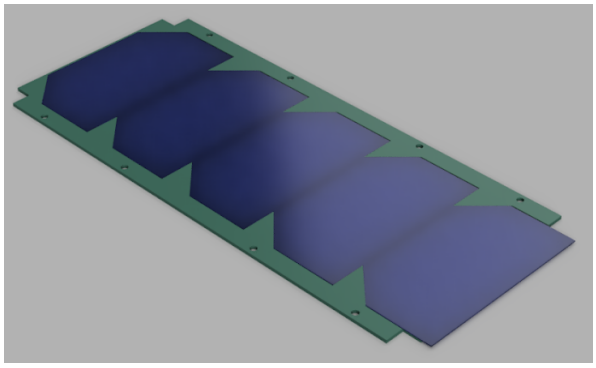

Figure 40. MSP-A-7-1 Solar Array

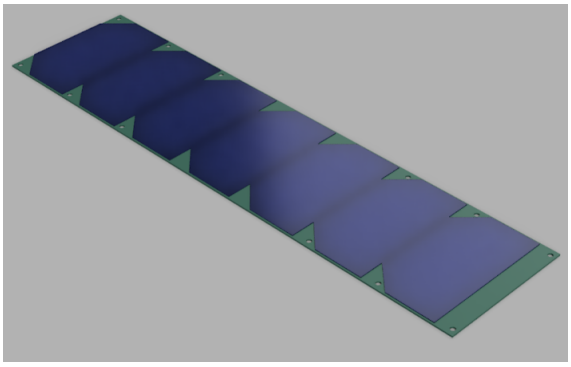

Figure 41. MSP-C-5-1 Solar Array

5.1.2 Battery Bank

The GOMspace BP4 module from preliminary subsystem design was replaced with the GOMspace BPX module, this was done to account for better power delivery. The BPX module hase double the power storage in the form of 8x 18650 lithium ion cells, doubling the power storage capacity of the BP4. These cells will be configured into one set of 8 cells in series, providing 77Wh of capacity at a supply voltage of ~30V. Using the ACU-200 each solar array will go through a boost converter to increase their respective voltages to the battery storage voltage. The ACU-200 has 6 photovoltaic cell array input channels allowing

for each solar array to have an independent input channel. The P-60 will then use the PSU-200 to convert the stored power into 3.3, 5, and 8 volt supplies for the components as necessary. Both the PSU-200 and ACU-200 will have an identical sister board mounted to the P-60 powerdock to allow for effective power storage and delivery as well as component redundancy.

5.1.3 Wiring

Electronic components are connected together via direct solder, free wires and utilization of the PC104 system in conjunction with GOMspace daughterboard docks. See Table 6 for a list of all major electrical components and their uses in respect to their subsystem. This list presents the components with their required power consumption and voltage/amperage tolerances. GOMspace hardware and microcontroller components will communicate via CAN bus though the OpenMV Cam H7 microcontroller and Nanomind A3200. The on camera microcontroller was not initially intended to be the main computing element of this cubesat, however when it is not capturing live video at maximum fidelity and framerate it is by far the most powerful computer on the vehicle. As the camera module was chosen for its functionality, availability and simplicity, the maximum frame capture rate will never be required making it the best choice for computing, so it will handle the video processing and cubesat controls. The Nanomind A3200 will be relegated to GPS data processing, burn wire deployment and power monitoring.

			Voltage [V]			Current [A]			Power [W]			
Subsystem	Component	Part Name/#	Min	Nom	Max	Min	Nom	Max	Min	Nom	Max	Mass [g]
GNC	Controller	NanoMind A3200	3.2	3.3	3.4		0.05	0.27		0.17	0.9	24
	Reaction Wheels	NanoTorque GSW-600	4.9	5	5.1		0.06	0.5		0.3	2.55	940
	GPS	NovAtel GPS		3.3			<.4	0.4			1.32	31
	Component Dock	NanoDock DMC-3	4.3		6	N/A	N/A	N/A	N/A	N/A	N/A	51
Comms	Transceiver	NanoCom AX100	3.3	3.3	3.4	0.045	0.055	0.12		4	4	24.5
	Antena	NanoCom ANT430	N/A	N/A	N/A	N/A	N/A	N/A	N/A	N/A	N/A	30
Power	Battery	NanoPower BPX	N/A	N/A	N/A	N/A	N/A	N/A	N/A	N/A	N/A	500

	Panels to Battery	ACU-200	N/A	N/A	N/A	N/A	N/A	N/A	N/A	N/A	N/A	54
	Battery to System	PDU-200	N/A	N/A	N/A	N/A	N/A	N/A	N/A	N/A	N/A	57
	Power Dock	P-60 Dock	N/A	N/A	N/A	N/A	N/A	N/A	N/A	N/A	N/A	80
Payload	Arm Motors	0615 003 S	3	3	3	.03		0.14	.09		0.42	2
	Motor Encoder	PA2-50		3.3			.009			0.03		1
	Motor Driver	MCDC 3002 P	8	8	30	.04	2	3	.32	1.26	4	7
	Camera/ Cpu	OpenMV Cam H7	3.3	3.3	3.3	.11	0.16	0.17	.36	0.53	0.56	19
	Heater	Custom	3.3	5	8	.75	2	10	0	6	30	3.32
	Extruder Motor	17HS08-1004S		3.6		0	1	2		3.6	7.2	150

Table 6. Electronic Components list

5.2 Structure

5.2.1 Core Structure

The key considerations for the design of the core structure were structural stability, rail incorporation and ease of access. This was done to meet the Planetary Systems Corporation requirements for a 6U Canisterized Satellite Dispenser and for ease of manufacturing [15]. To ensure structural stability Aluminum 7075 alloy is proposed as the main structural material while polycarbonate/asa plastic will be used to construct the mounting structures.

The core structure is made of two models connected via a burn wire deployment mechanism and a center supporting brace (See Figure 42). The burn wire will allow for the bottom of the cubesat to eject once the solar panels are deployed, giving the payload room to deploy and operate. To increase ease of access and manufacturing, the core structure is composed of a skeleton structure onto which different sections will mount. Each section contains either the payload, electronics or solar array, these are discussed in better detail in 5.2.2, 5.2.3 and 5.2.4.

Design began with the rail dimensions from PSC and total allotted volume in the shape of a rectangular prism to visualize the outer limit of the structure. From this, volume was removed for the solar array deployment mount. Looking at existing 6u satellite structures from GOMspace and Pumpkinspace, the outer wall structure thickness ranged from 5mm to

2mm depending on the location. From this the minimum structural wall thickness was set to 4.8mm in order to allow for a +/-.1 mm manufacturing tolerance. Once this outer wall was defined the challenge was to integrate a mounting point for the arms and printhead while keeping the whole system within the volume. This mounting point began as a single supporting piece, however it was modified to become the center supporting brace and the payload mount (this is discussed more in section 5.2.3). Two doors were incorporated on the sides for ease of any electrical component modification during manufacturing. The mass properties of the core structure can be seen in Table 5.19 and are discussed more in section 5.4.

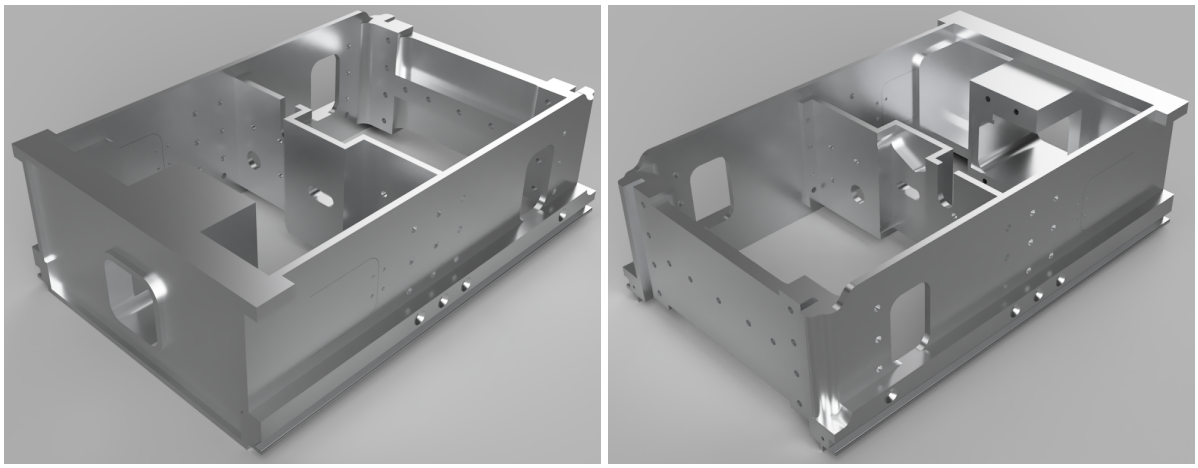

Figure 42. Core Structure with central supporting brace Z- Face (left) and Z+ Face (right)

5.2.2 Solar Array Section

The solar array mounts and deployment section use a fold open design, with 4 limbs and a central piece that will mount onto the cubesat core structure. Aluminum 7075 limbs were designed to reinforce the solar panels with an emphasis on light weight and simple design. The limbs designed for the MSP-A-7-1 consist of a rectangular frame and the limbs for MSP-B-8-2 are a rectangular frame with a reinforcing structure (See Figure 43, 44). This reinforcing structure was designed for clearance of the payload deployment mechanism. These limbs will be mounted onto the Solar Array mount which will attach to the front face of the core structure via an array of M5 bolts. The limbs will deploy via a burn wire and spring release system, that is composed of a spring, a thin nylon wire and a high temperature resistant SMD resistor to melt the wire and deploy using the spring force [26]. The nylon wire will be tied between the end of the limb and the core structure with the SMD resistors on

the corresponding limbs. View of the limbs without the solar arrays on them assembled with the solar array deployment mount can be seen below in Figure 45.

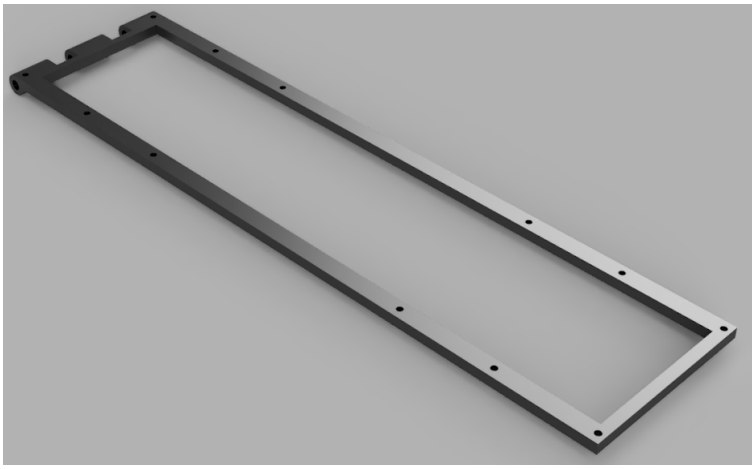

Figure 43. Solar Array mount for MSP-A-7-1

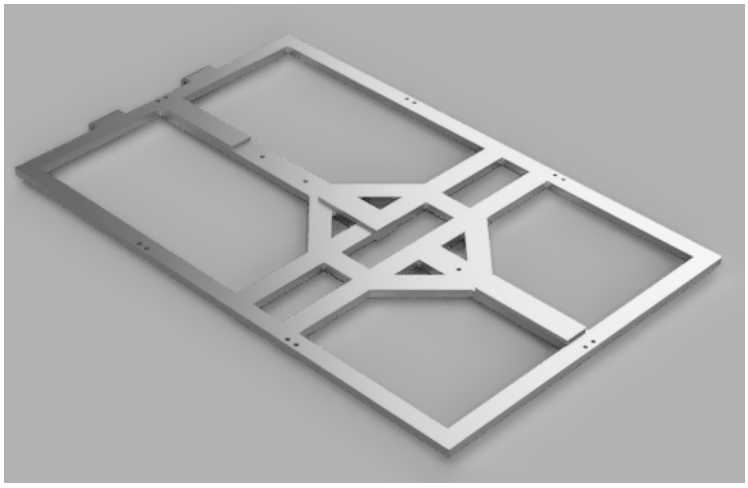

Figure 44. Solar Array mount for MSP-B-8-2

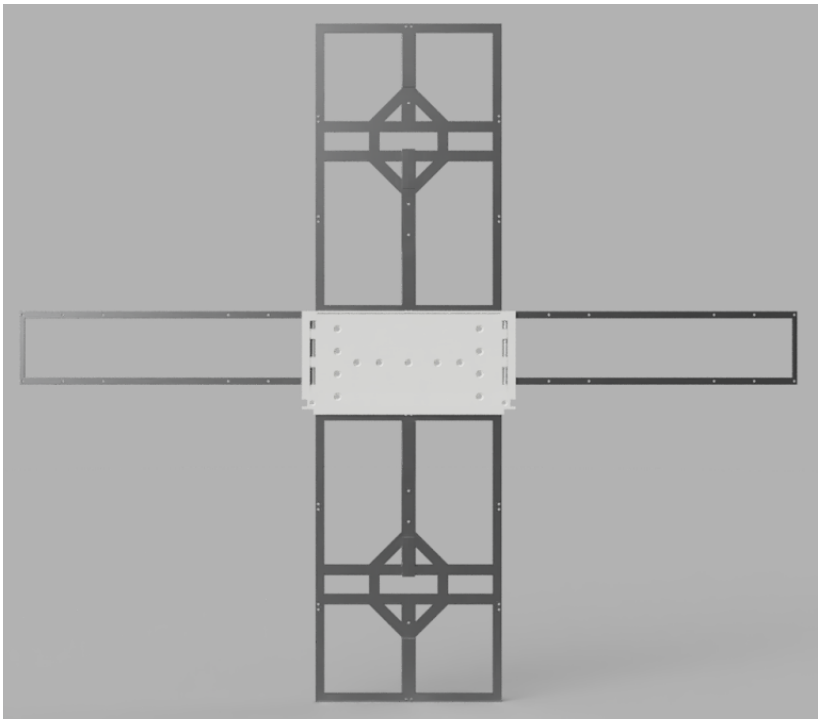

Figure 45. Solar Array deployment mount and limbs

5.2.3 Payload Section

The payload is composed of two moving arms and one printing head, so the payload mount must have suitable mounts for each of these assemblies. The two arms will use the slip ring mounting holes and outer casing mounting points to be bolted into a mounting slot on the payload section (See Figures 5.9 to 5.11). The location of these mounts must be such that there is room on each side of the arms to deploy effectively with the printhead between them. The printhead is mounted to a deployment mechanism mounted to the payload section. This deployment system uses 4 all-thread rods to slowly lower the print head out of the bottom of the cubesat. This mechanism is powered by two Faulhaber 0615 003 S motors and is mounted in between the payload mount and reinforcing brace. There is also a slot cut into the payload section for the camera mounted on the electronics section, see section 5.2.4 for more details.

Figure 46. Deployment system without cover (left) and with cover (right)

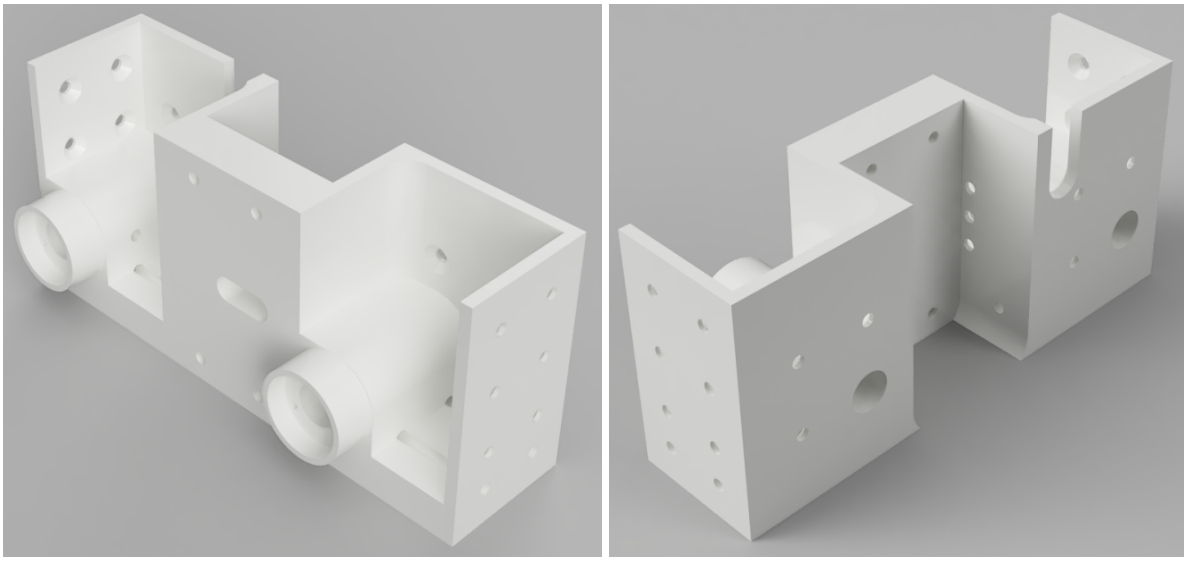

Figure 47. Payload Mount Payload Side (Left) and Electronics Section Side (Right)

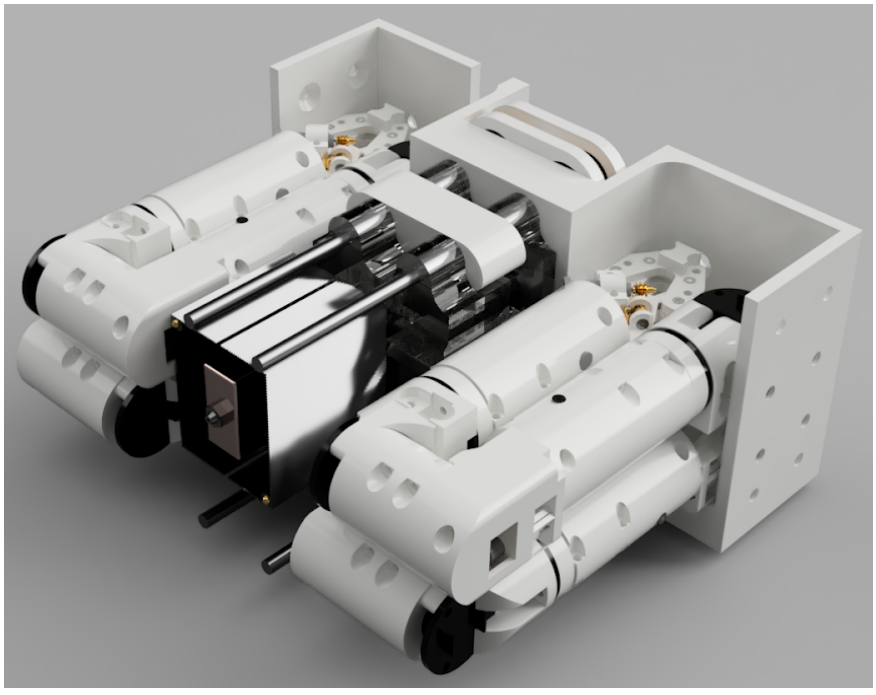

Figure 48. Payload Mount With Payload and Deployment system mounted

5.2.4 Electronics Section

The electronics section was designed to mount all the controlling electronics for the payload, solar panel deployment systems, and mission control systems. With all these expensive and sensitive components in one place the electronics section was also designed to be able to slide into place in the core structure being secured mechanically with M5 bolts. The GSW-600 is mounted directly to the side of the section to minimize the distance to the core structure. The OpenMV Cam H7 is mounted to the rear of the section so the camera has a direct view of the printhead. This direct mounting allows for the structure to be used as a large heatsink for the main cubesat processor. The rest of the electronics are mounted into a horizontal pc104 stack bolted into the side of the electronics section.

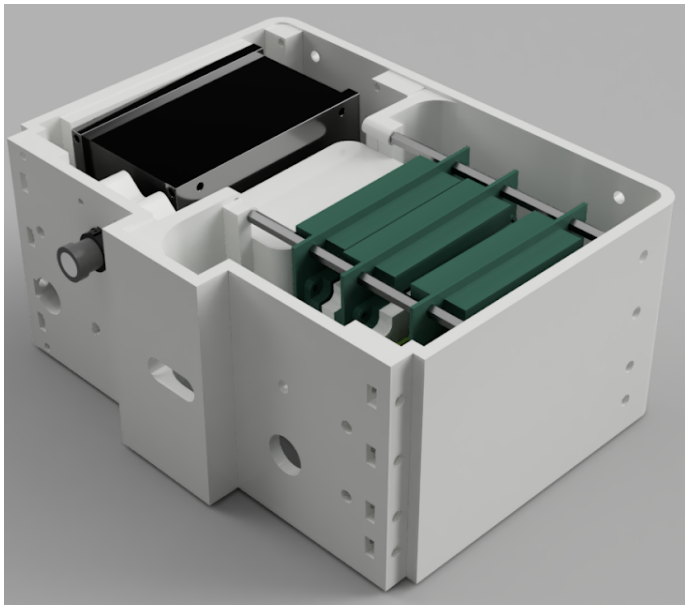

Figure 49. Electronics Bay

5.3 Modeled Assembly

Components were modeled into an assembly assuming clearance and machining tolerances to the nearest 0.2 mm. This assembly meets the total volume requirements dictated by PSC 6U payload specifications. Integration of the structural components with the payload and electronics was important throughout the design process so assembly and prototyping should require only minor modifications. The assembly is held together by M5 bolts and all-thread, with the payload all-thread deployment system rooting the bottom chassis into place. The OCC deployment procedure consists of three major steps:

1. [Ejection from CSD] This stage is when the OCC is ejected from the launch vehicle via the Planetary Systems Corporation Canisterized Satellite Dispenser. (Figure 50)
2. [Solar Array Deployment] After the OCC is ejected and powers on it will orient itself to face the sun with the Z+ face and deploy the solar panels for the initial charging cycle. (Figure 51, 52)
3. [Payload Deployment] Once the system completes its first charge cycle and communicates with ground control the OCC will begin payload deployment. The payload deployment system and the burnwire system holding the bottom of the core structure will activate. This will jettison the bottom of the core structure and move the printhead into operational position. Finally the arms will deploy making the OCC fully operational (Figure 53, 54, 55)

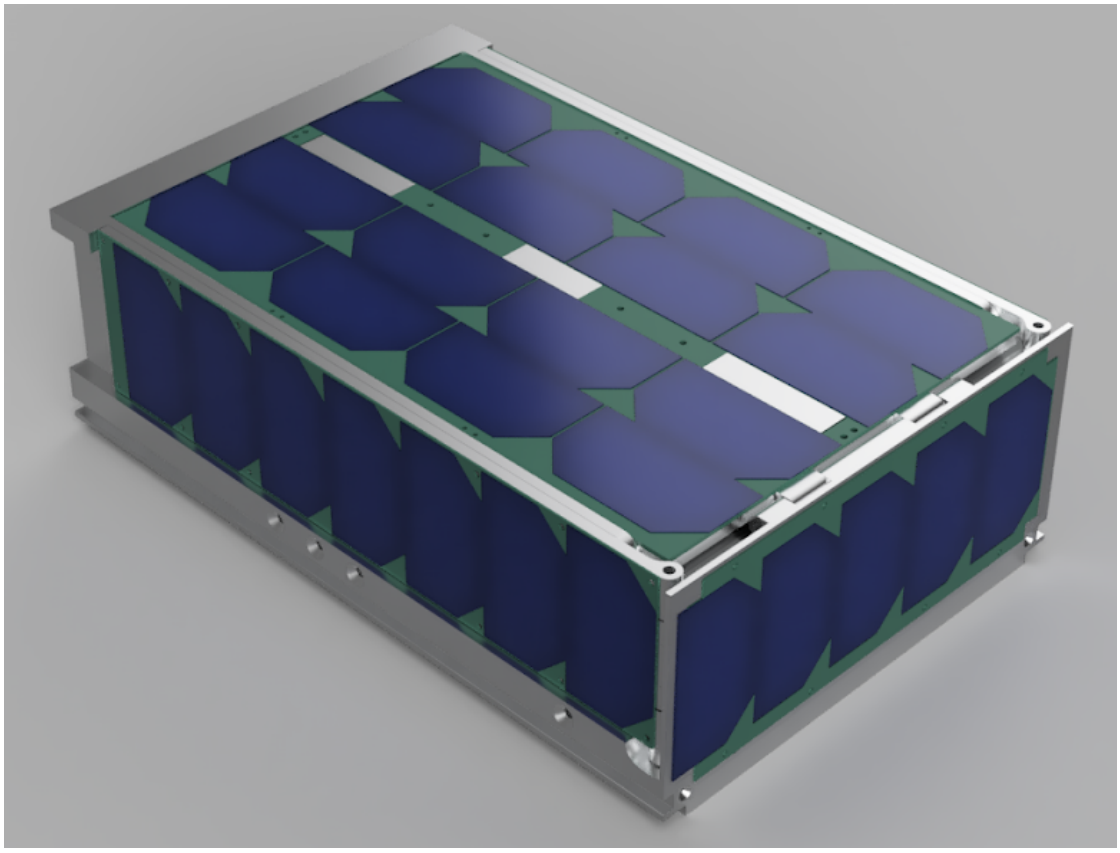

Figure 50. OCC is Ejected from CSD

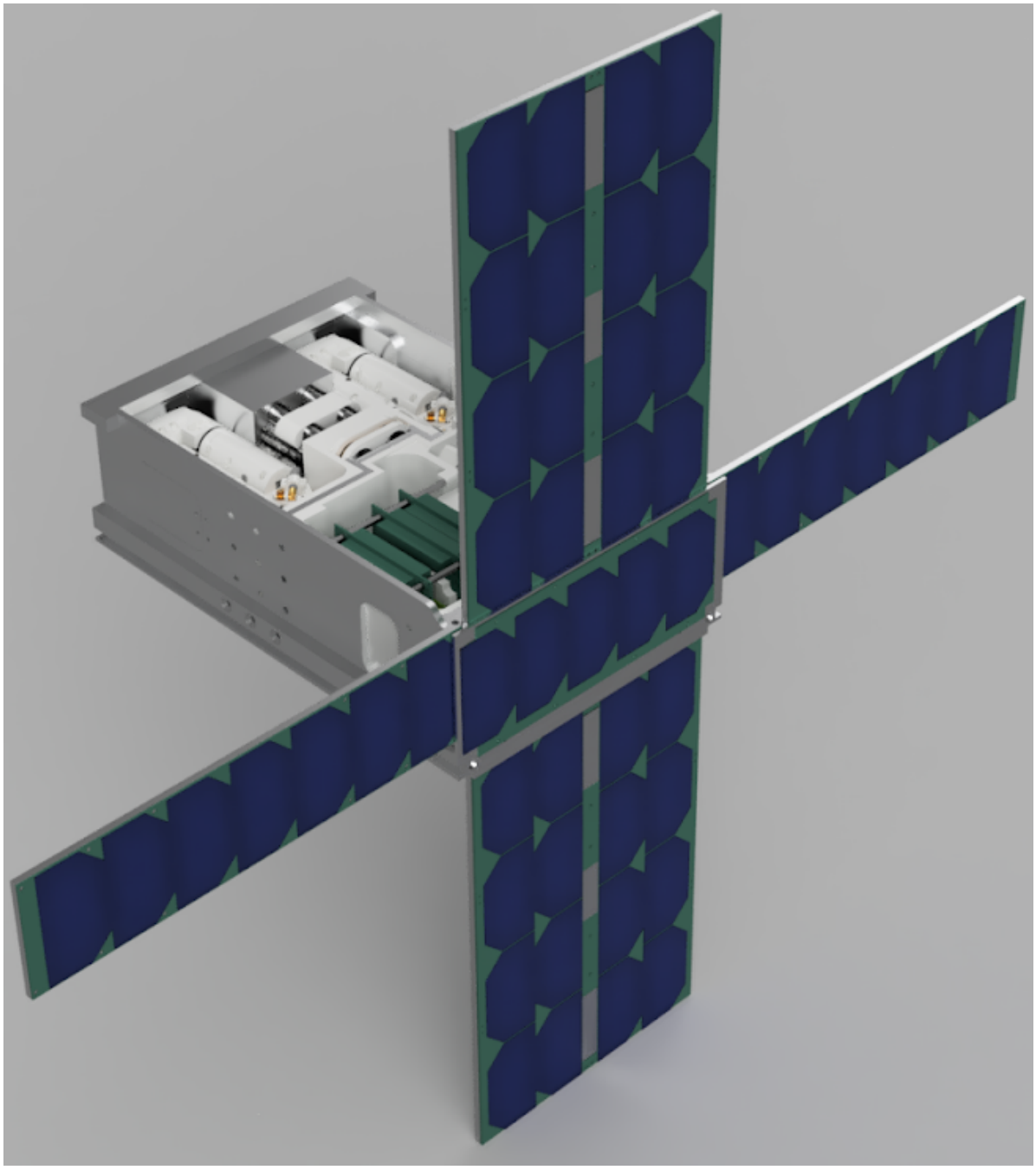

Figure 51. Solar Arrays Deployed

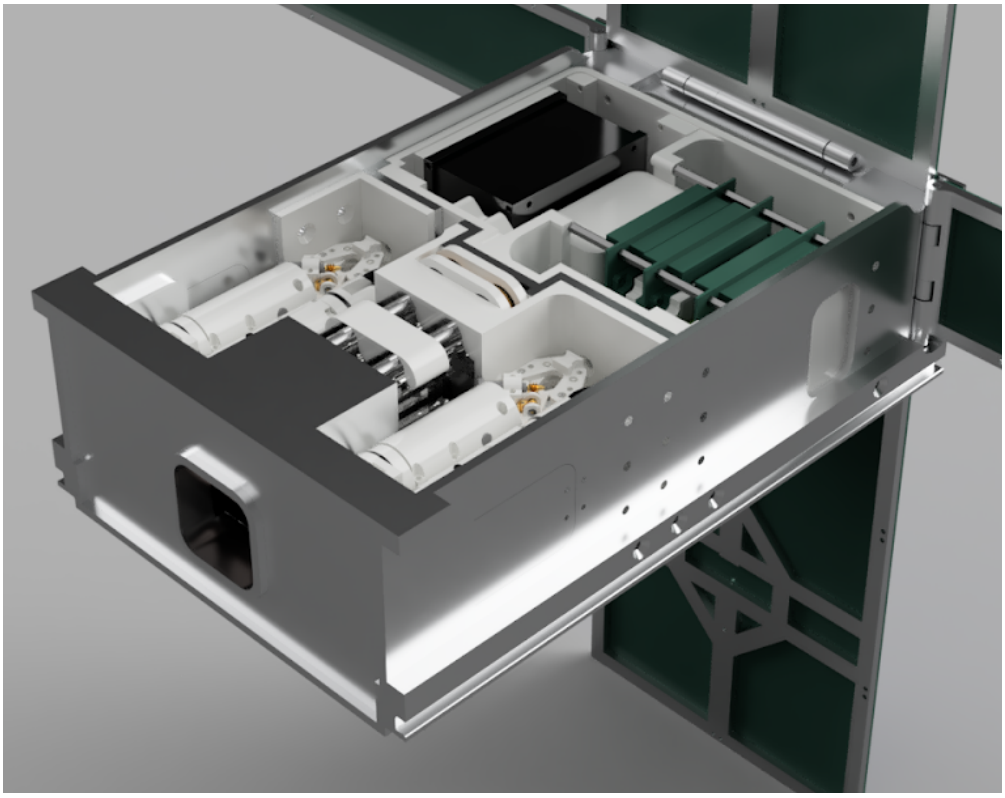

Figure 52. Batteries are have finished charging and Payload deployment begins

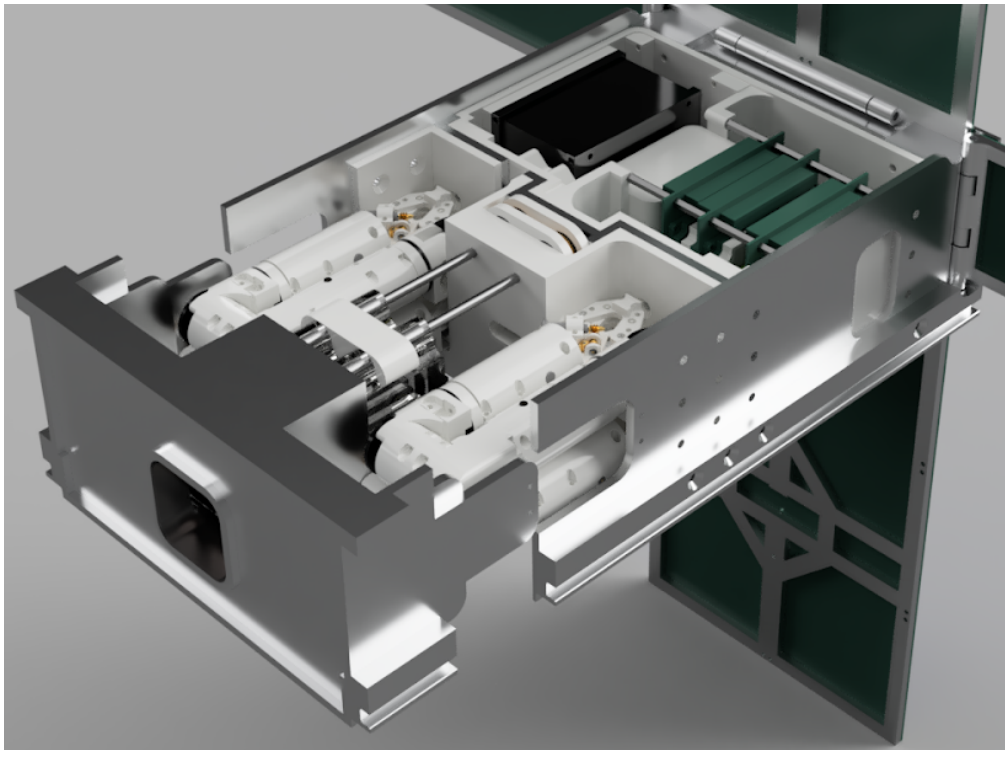

Figure 53. Core Structure bottom burn wire system is activated and All-Thread Payload deployment system fully extends

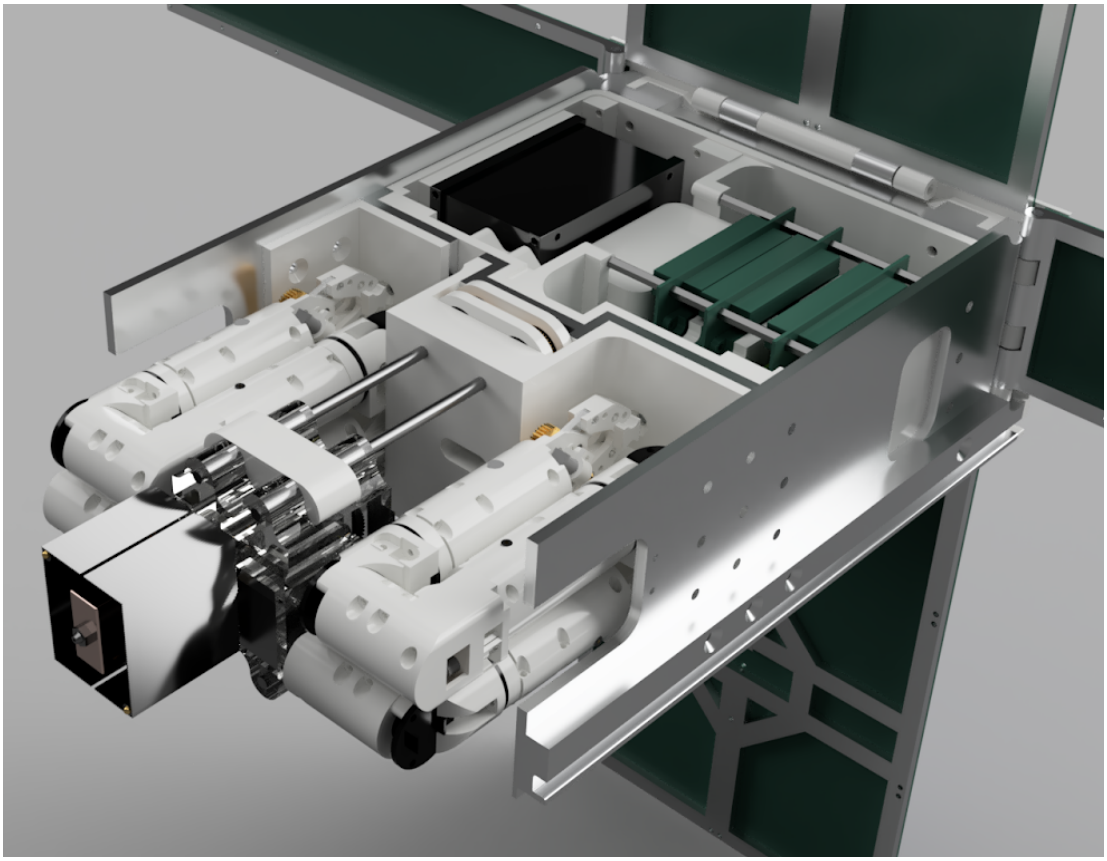

Figure 54. Core Structure bottom is ejected and arms are free to deploy

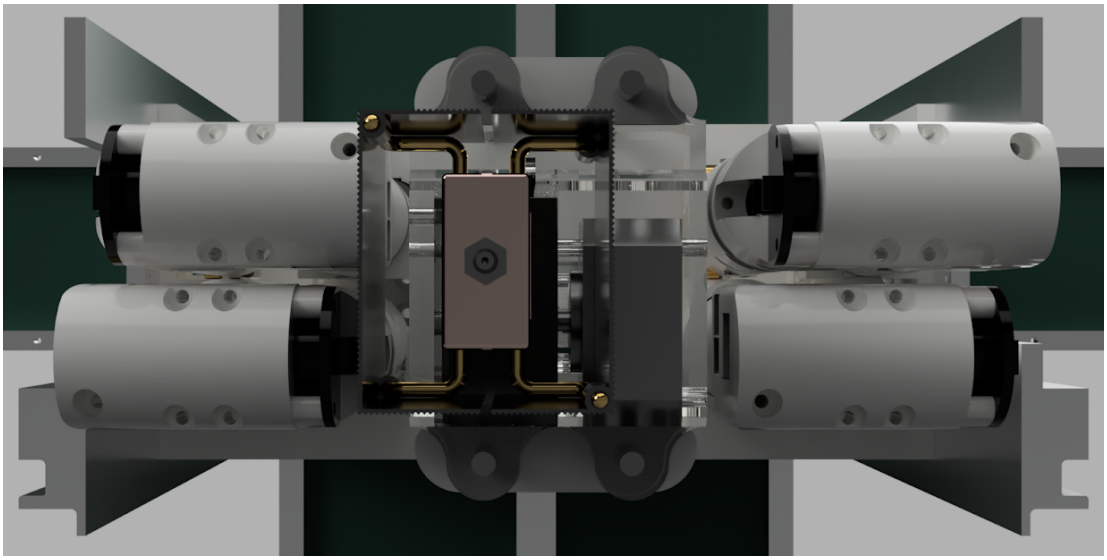

Figure 55. Payload fully deployed and ready to begin printing

This design disconnects the bottom part of the core structure and assumes that it will jettison properly without interfering with operation. No testing or modeling has been done to

ensure this and future design work is required for a fully functional system in this regard. A spring mounted on the core structure right next to the burn wire system was considered but not implemented in any way.

5.4 Comparison to Preliminary Design

Preliminary design power consumption was maintained throughout the design process so this iteration of design was within power budget. Mass budget was over three times the predicted preliminary design mass for the structure alone (See Table 5.19). With the total system mass coming in at 11.56kg according to the modeled Fusion 360 properties calculation. This mass does not include the filament required for the payload to operate, the hardware required for assembly, or the wiring. In the next design iteration, the structure mass must be cut down to meet the 12kg total mass budget while still keeping a functional design.

Component	Mass [g]	Material
Core_Main	1960	Aluminum 7075 Alloy
Core_Brace	372	Aluminum 7075 Alloy
Core_Bottom	1698	Aluminum 7075 Alloy
Array_mount	480	Aluminum 7075 Alloy
A_Panel_1	91	Aluminum 7075 Alloy
A_Panel_2	91	Aluminum 7075 Alloy
B_Panel_1	320	Aluminum 7075 Alloy
B_Panel_2	320	Aluminum 7075 Alloy
Payload_Mount	440	PC/ASA w/ CFR
Elec_Bay	450	PC/ASA w/ CFR
Structure_Sum	6222	Various
Predicted	2000	From Preliminary Design
Over budget	4222	

Table 7. Structural Component Masses

6 Prototyping

6.1 Prototyping Concessions

Due to the expense of assembling a flight ready cubesat, the prototype manufactured for this project is not made with flight ready hardware and will NOT fly. 3D printed PLA

parts were printed on the Creality CR-10 or the Monoprice Mini Select v2 FDM printers, and 3D printed resin parts were printed on the Elegoo Mars SLA photopolymer resin printer. The objective of this prototype is to assess the manufacturing accessibility and feasibility of the components designed in previous chapters.

6.2 Structure

A 3D printed PLA structure will stand in for all machined aluminum 7075 components. This structure was printed from the models seen and discussed in chapter 5, with a minor change to the bottom core structure component. The model had holes cut into it to reduce weight and print mass. The core structure and mounting components can be seen below in figure 56 and 57. Final structure assembly was done after payload assembly, but all components were able to fit and bolt together with minor sanding.

Many of the PLA 3D printed components have warped during printing. This warping is caused by rapid cooling of the filament immediately after extrusion. Over the past weeks the nighttime temperature would routinely drop to 40°F or below making prints warp more frequently. This is difficult to avoid as some prints take upwards of 48 hours of continuous printing to complete. The parts most affected by the warping are thinner longer parts, this can be seen clearly in the solar array panels (See figure 58). This warping problem also affects the structural properties of PLA making it harder but more brittle, as such when removing the support material for the solar panels part of the base shattered. The solar panels were the only structural component to warp so much that they affected the function of the part and as such needed to be mounted loosely in order to still fit on the structure properly. This meant that the spring mechanism was not able to be prototyped or tested, which is acceptable given spring mechanisms are well documented as a solar panel deployment method. We do not expect to face this problem when aluminum parts will be manufactured with CNC machining.

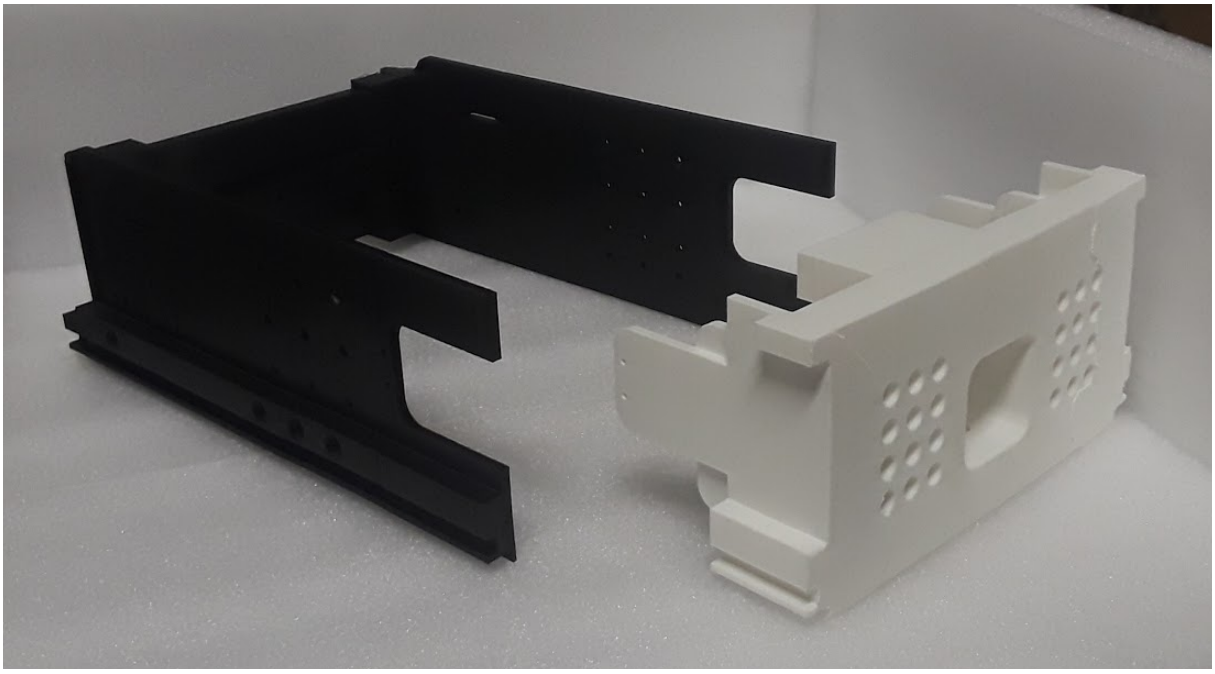

Figure 56. Core Structure without Reinforcing Brace.

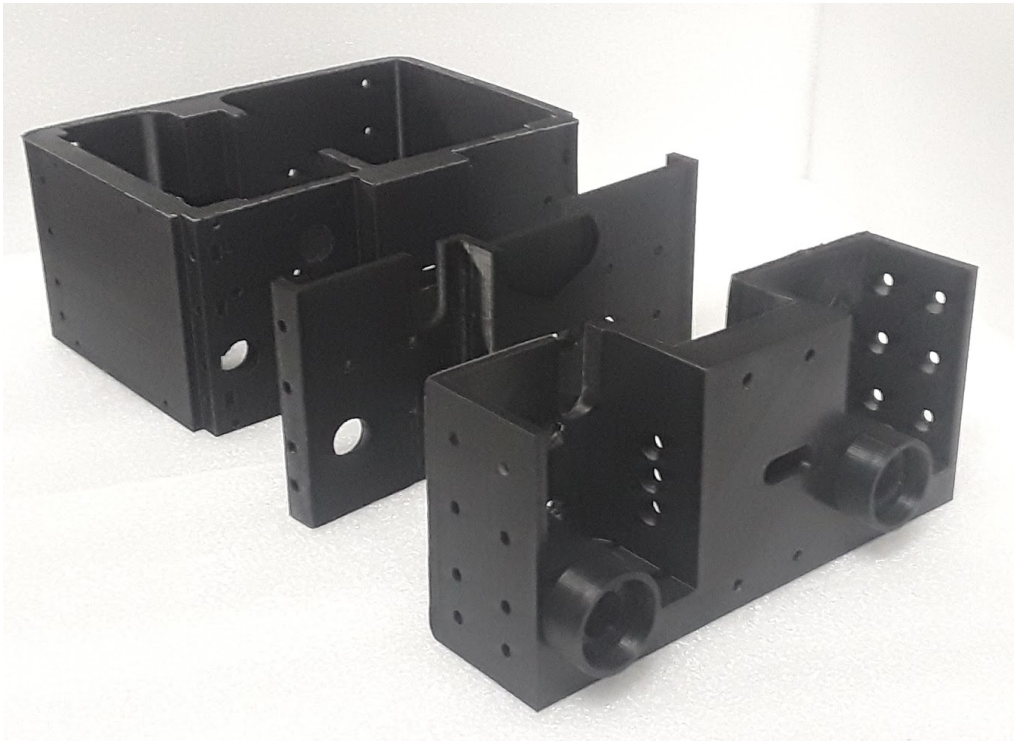

Figure 57. Electronics Bay, Reinforcing Brace, and Payload Mount (Left to Right)

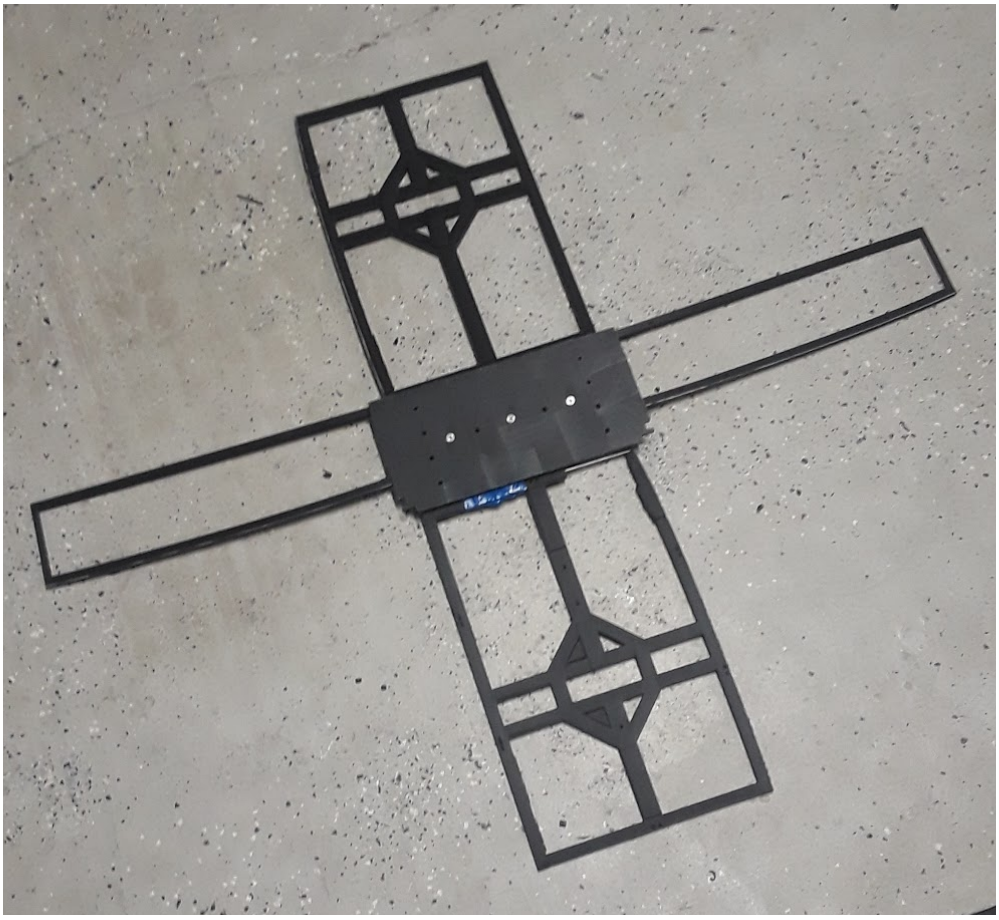

Figure 58. Solar Panel Array

6.3 Payload Assembly

The payload assembly has many concessions made when compared to an actual flight prototype. The main goal for this section was to get an operational arm and operational deployment system with the caveat that these systems would not be 100% representative of a flight prototype system. Unfortunately due to a malfunctioning printer and underspecified motors neither of these were attained. The SLA printer used for manufacturing of the arm components and smaller parts is the only printer that was available for use during this prototyping phase that had the accuracy required for the parts. As such when it began to have initial layer adhesion problems, due to either a damaged LCD screen, damaged protective

film, or repeated resin exposure to low temperatures, a lot of effort was put into returning it to operation. The ARS and TRS prototypes were designed and worked on simultaneously so when a new model for one was printed, work would continue on the other. As such when the motor and printer problems happen, both systems were locked into their most recent design. Due to this abrupt stop in the prototyping process, this section is a log of tests and proposed assembly steps rather than completed design of a functional prototype.

6.3.1 ARS prototype

The designed ARS v2 from chapter 4 was designed with stabilizing bearings, a .5 W 20Krpm motor and brass cast gears. The prototype will not have and bearings, the same motor nor metal gears due to excessive costs. The motors replacing the 0615 series motors are generic 6mm diameter 14mm long micro-quadcopter motors.

ARS prototype v1 was printed with the model of the ARS v2 with no modeling changes, this print was printed horizontally and came out warped. This warping is different from the rapid cooling warping of an FDM style printer, and it is caused by lack of support structures during an SLA print. The next print included support, this also failed due to excessive warping, this is most likely due to the large surface area of the print, so the ARS was oriented vertically without supports. This print came out good, with only minor part inaccuracies, well within the expected deformation due to the SLA printer tolerances. The next components printed were the 50 tooth, 10 tooth, and worm gears. These all came out well on their first prints most likely due to their simplicity. The last core component for the ARS is the slip ring mount that acts as a central rotating shaft onto which bearings are press-fit. For this prototype the modeled slip ring mount was printed as is, with a slip ring adapter printed to adapt the prototype slip rings to the mount for the larger ones called for in

design. The 10 tooth gears were glued to a 1.5mm pin where they were put into the proper slot in the ARS casing. The 50 tooth gear was glued onto the slip ring mount and then this was placed into the casing. The wurm gear was glued onto the motor drive shaft and then the motor was placed into its corresponding slot in the casing. The casing was bolted up and it was ready for testing. This first version of the ARS prototype did not have proper tolerance for the gears and would stall the motor due to excessive friction between the slip ring mount and the casing. To try and fix this without editing the 3D model, a dremel and sandpaper were used to try and remove excess material for better clearance. This process was deemed too time consuming so the model was changed and new parts were printed.

ARS prototype v2 removed material around the gears, and added a protrusion onto the slip ring mount to keep it lined up within the casing due to lack of bearings. These modifications helped operation with the system now being able to be hand turned but there was still too much friction within the casing for motorized operation. Silicone lubricant was applied to the mechanism with another minor reduction to friction but still without consistent motorized operation. Observing the operation of the system showed that the motor would spin briefly then stall or loosen the gears that were mounted and cause them to unmesh. A new wurm gear was designed with a tighter drive shaft hole to try and mitigate loosening of the worm gear, this fixed that problem but the motors kept stalling or loosening the 10 tooth or 50 tooth gears.

To try and ensure a stable 50 tooth gear, the ARS prototype v3 increased the slip ring protrusion to keep everything lined up. This solidified the gears but the motor continued to stall with everything else being meshed perfectly and there being no gear grinding. The motors acquired for prototyping are rated to 47Krpm at less than half the torque of the 0615 series motors used in design. At this point with the mechanics working manually but not

when motorized, it was clear that these motors were not sufficient for a prototype without proper bearings. Around the time this happened the SLA printer began malfunctioning and the prototyping of the small mechanical systems had to come to a close.

Below is a series of steps for assembly of the ARS prototype v3 and their corresponding images:

1. [Prepare Components] Components required for the ARS prot v3 are: Slip Ring Mount, Casing 1 (contains motor slot), Casing 2, 50 tooth gear, 2x 10 tooth gear 1x 18mmx1.5mm OD steel pin, 2x m2 washers, 4x M2x12mm bolts, 4x M2 nuts, worm gear, 6mm motor. (See figure 59)
2. [Assemble geared components] Glue the worm gear to the motor driveshaft to prepare the motor. Glue the 50 tooth gear to the slip ring mount to prepare the main shaft, then slide the slip ring into the slip ring mount, this should be press fit. Glue a 10 tooth pin approximately 1.5mm from one end of the 1.5mm shaft, wait to dry, then put both washers on, then glue the other 10 tooth gear onto the shaft. (See Figure 60)
3. [Insert Components] Place the geared shaft, slip ring mount, and motor into their locations on Casing 1. Then apply silicone lubricant to the slip ring mount and gears. (See Figure 61)
4. [Close Casing] Place the other side of the casing onto the assembly and insert the screws. (See Figure 62)

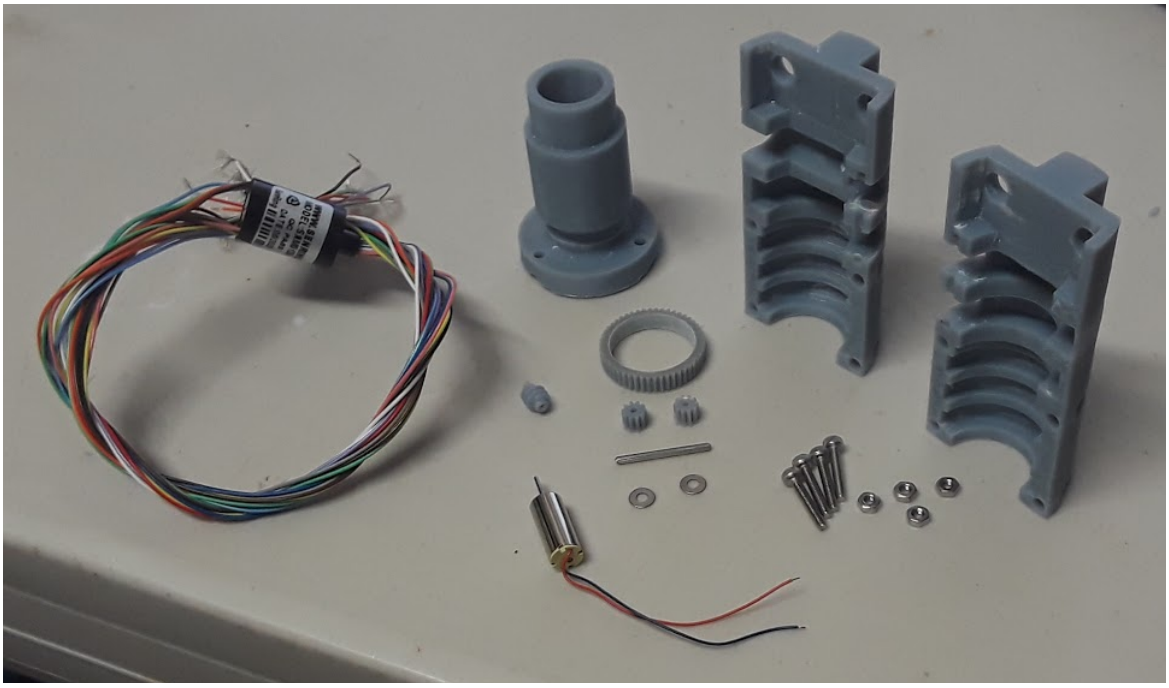

Figure 59. ARS prototype components

Figure 60. Motor, slip ring mount and geared shaft.

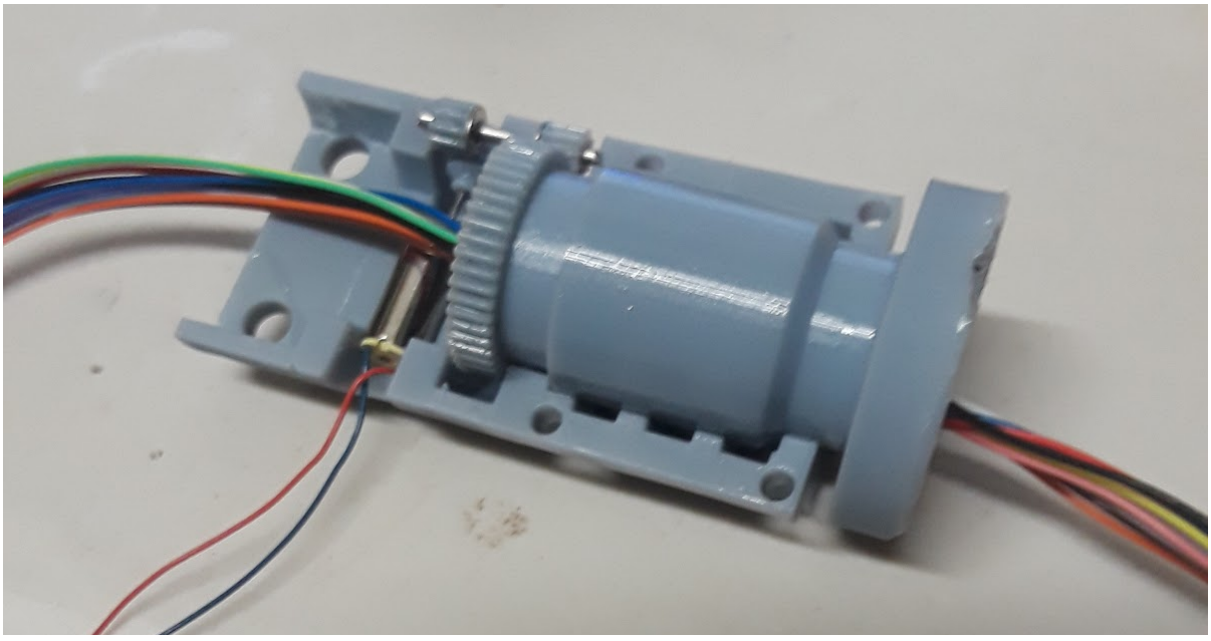

Figure 61. ARS prot v3 with internal components in their locations

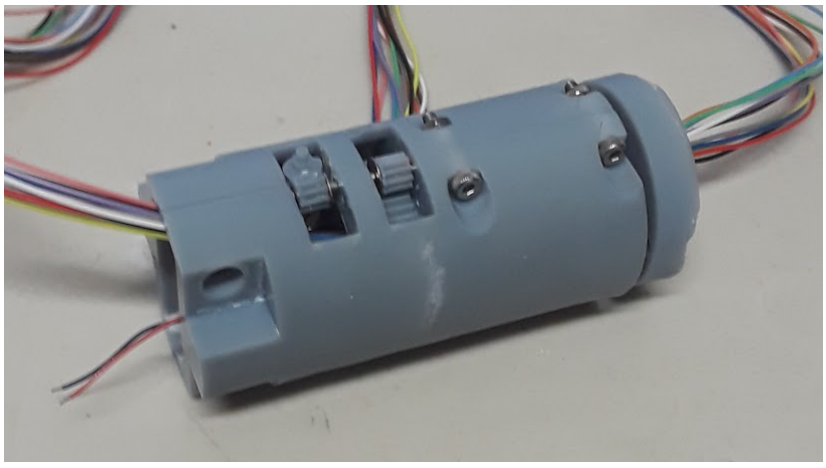

Figure 62. ARS prot v3

Alternatively the first ARS needs to be mounted to the prototype mount before construction, once it is bolted into place construction is the same as before, see Figures 63 through 65.

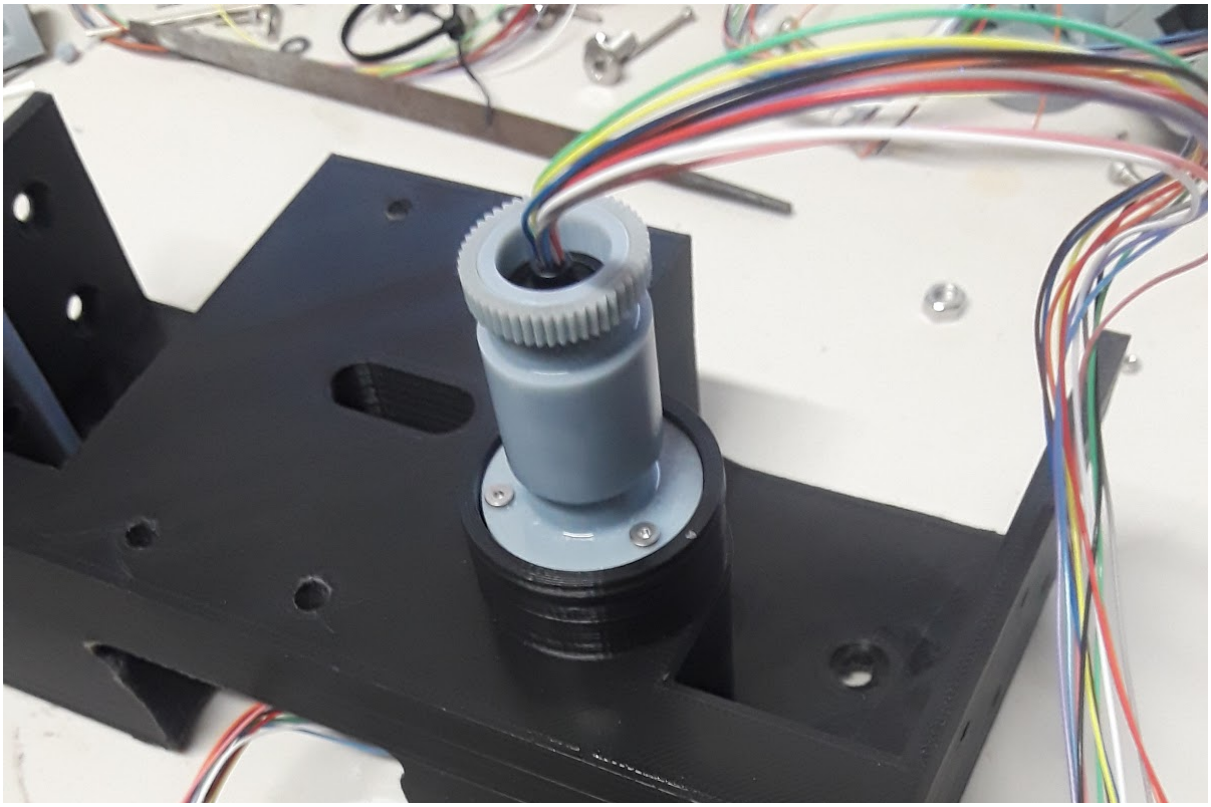

Figure 63. Slip ring mount bolted onto the payload mount

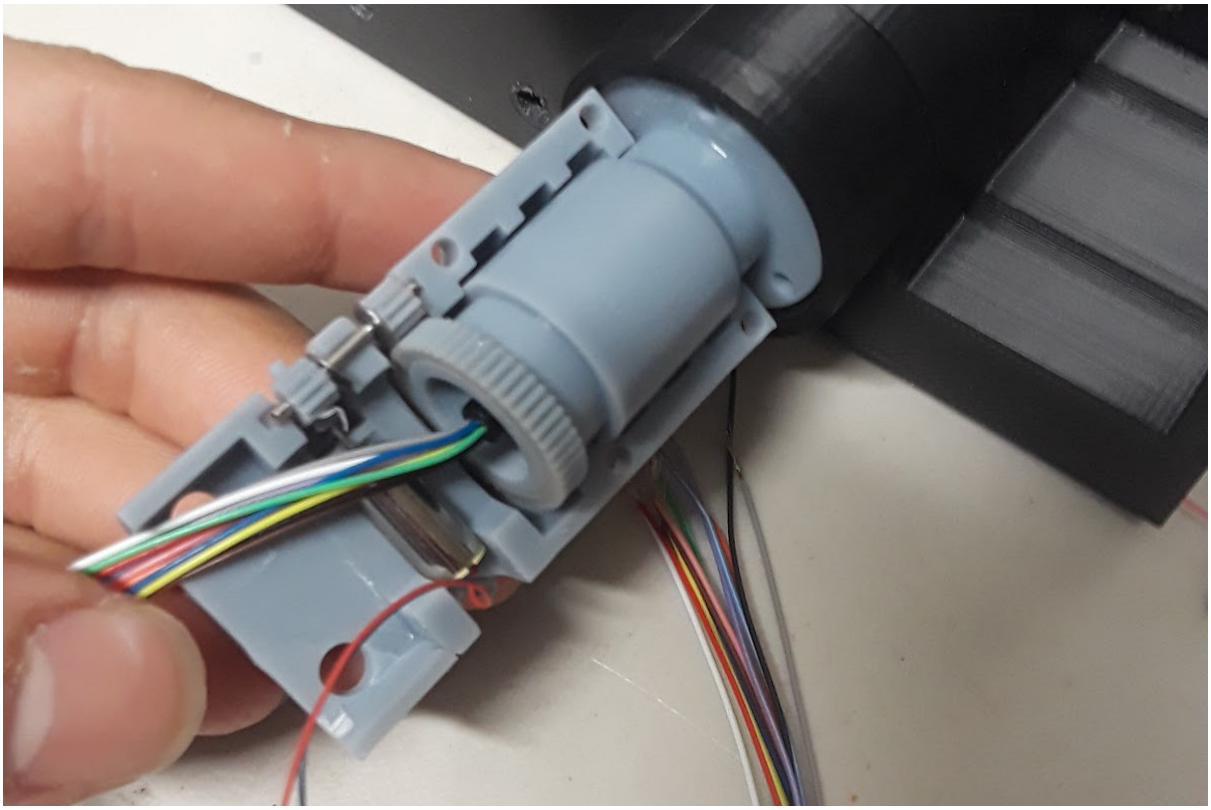

Figure 64. Assembling internal components for ARS prot v3

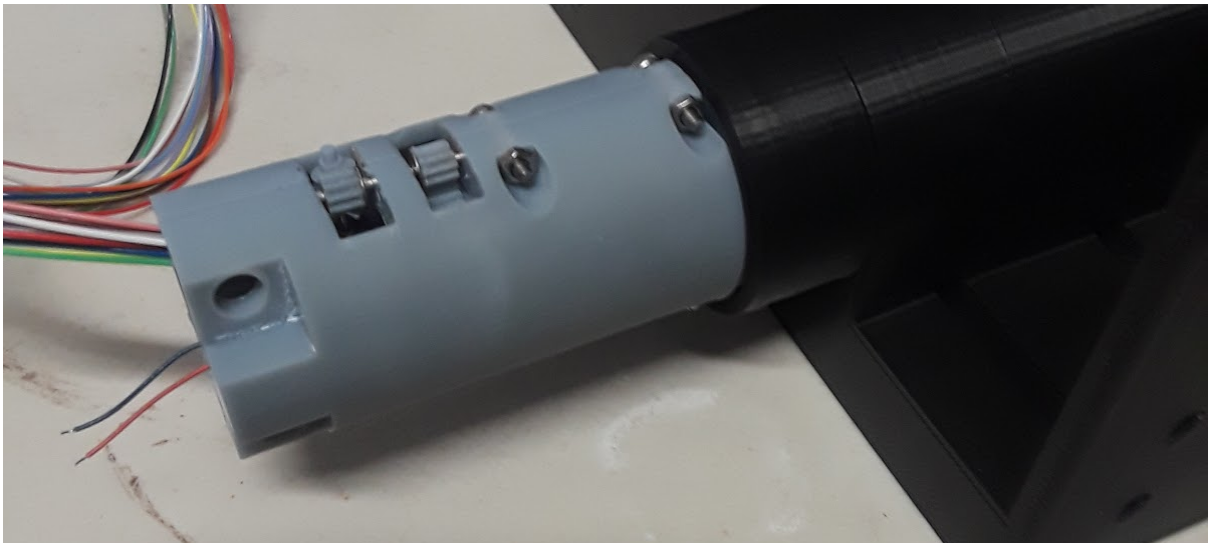

Figure 65. ARS prot v3 mounted onto payload mount

6.3.2 TRS

TRS prototype v1 started similar to ARS prototype with the same concessions made in regards to parts and the same initial model being taken directly from the TRS V3 CAD. The TRS prototype v1 did not have enough clearance on the rotating section to rotate freely and had a mechanically weak slip ring mount that broke in testing This mount would be replaced by a slip ring adapter that would serve a similar function as that of the ARS slip ring adapter. There was minor warping in the first few prints but it did not affect structural stability or functional interfacing between the parts. The external mount and the TRS casing_2 were difficult to secure together because of the lack of printing accuracy in the aligned channels and pre-tapped holes. To mitigate this problem the parts were sanded and glued together. The wiring that needed to pass through them did not have sufficient clearance so a hole was cut, this hole would be modeled into the next print.

TRS prot v2 varied from the initial with respect to the wiring whole and modification of casings one and two, these were changed to fit the adapter modifications due to the lack of

bearings. Without the bearings, there was nothing securing the gear driveshaft so notches were made into the bearing mounts in the casing for M2 nuts to hold the driveshaft in place. TRS prot v3 changed the length of the slip ring mount to help with the large friction generated between the flat face of the slip ring mount and the casings. The increased length allowed the 50 tooth gear to be printed onto the mount directly and made for better mounting of the mount holder. At this point silicon lubricant was applied to the system and it benefited greatly from it, however the same problems with the ARS prototype movement were present in the TRS prototype. The motor would either loosen the gearing or stall, with some instances of gears breaking due to uneven curing and becoming brittle.

TRS prot v4 decreased the volume of the interface between the ARS and the TRS external mount, as the previous version would not mesh without significant dremel work and minor chipping. The TRS prot v4 was a partial failed print as the slip ring mount lost print bed adhesion partially through the print. This is where the 3D printer stopped producing usable prints, and as such the prototyping ended.

Below is the instructions and accompanying pictures for assembly of the TRS prototype v3:

1. [Prepare Components] Resin Components required: Slip Ring Mount (geared), Mount Holder, Casing_2, Casing_1, External mount, mount adapter, 2x 10 tooth gears, and a worm gear. Hardware: 24mmx15mm “U” pin, 3x M2x16mm flathead bolts, 4x M2x12mm bolts, 1x M2x20 bolt, 17mmx1.5mm OD steel pin. 3x M2 washers, 11x M2 nuts. Electronics required: 6mm diameter motor and slip ring. (See Figure 66)
2. [Assemble Geared Elements] Glue the 10 tooth gears onto the 1.5mm steel rod with 2mm of clearance on each end. Glue the M2 nut into the slot on the casing_1

component (See Figure 67). Place a washer onto each end of the geared steel rod and place an M2 nut on one end, then slide into place on casing_1 (See Figure 68). Press fit the slip ring into the slip ring mount. Super Glue worm gear onto motor, and the external mount to casing_1.

3. [Insert Components] Place the flat head M2 bolts into the slip ring mount, then place the slip ring mount into casing 2 and apply lubricant (See Figure 69). Screw M2 nut onto M2x20 bolt about 15mm and place M2 nut into casing 2 slot to serve as a retaining nut (See Figure 70)
4. [Close Casing and attach mount] Place Casing_2 onto Casing_1 making sure to have the retaining nut stay secure and bolt together using the 4x M2x12 bolts, the M2x20 w/nut and the M2 nuts (See figure 71). Bolt on the mount holder attachment (See Figure 72)
5. [Prepare ARS] Attach the adapter to an ARS module, then slot in using the mount holder side and secure using the “U” pin (See Figure 73).

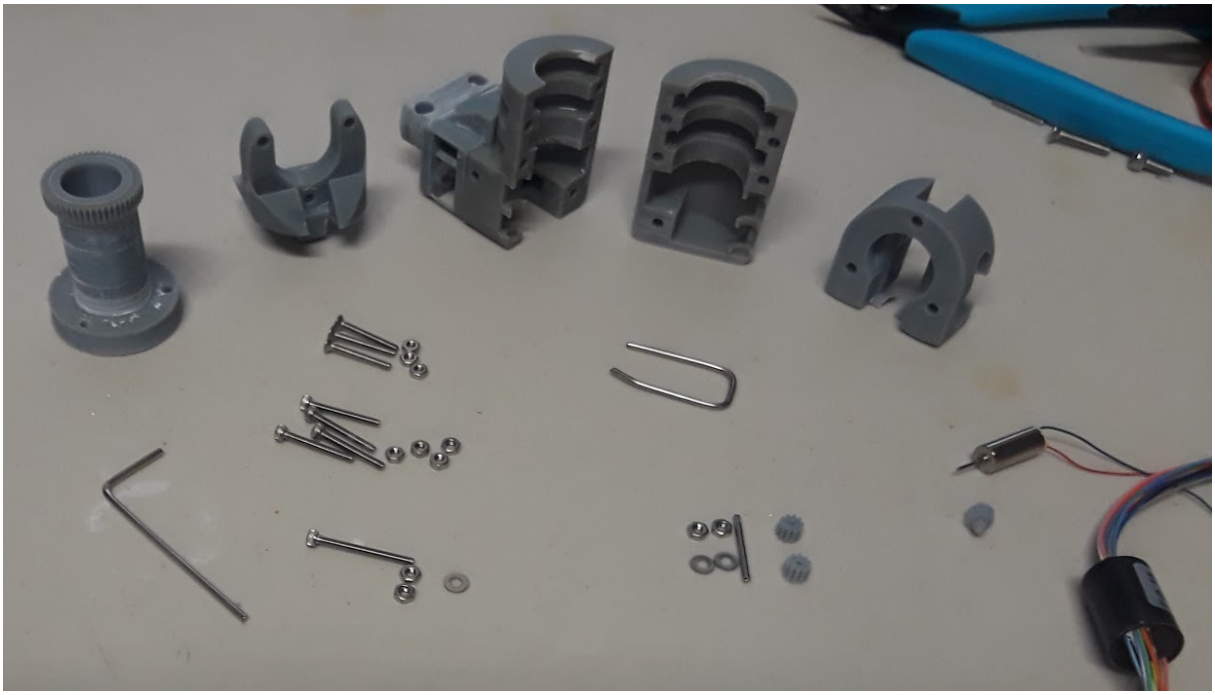

Figure 66. Resin Components: left to right, slip ring mount w/ 50 tooth gear, mount holder, casing_2 with external mount attached, casing_1, and adapter. with all internal components.

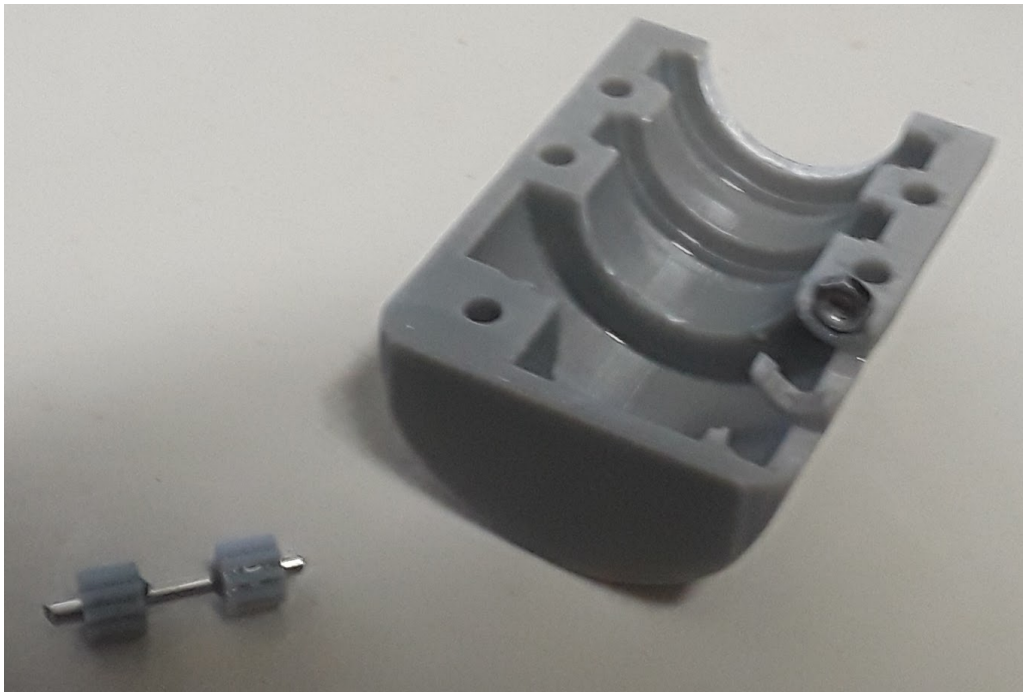

Figure 67. Steel rod with gears (left) and Casing_1 with nut installed (right)

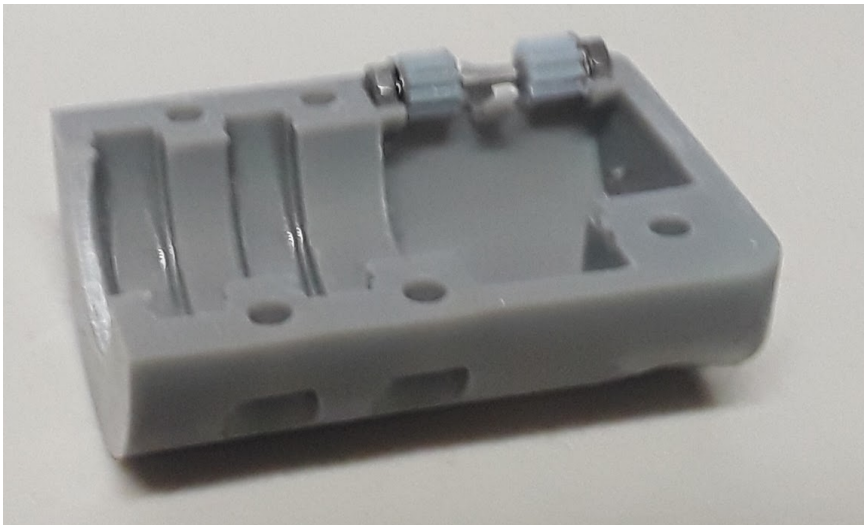

Figure 68. Casing_1 with geared rod washers and holding nuts in place

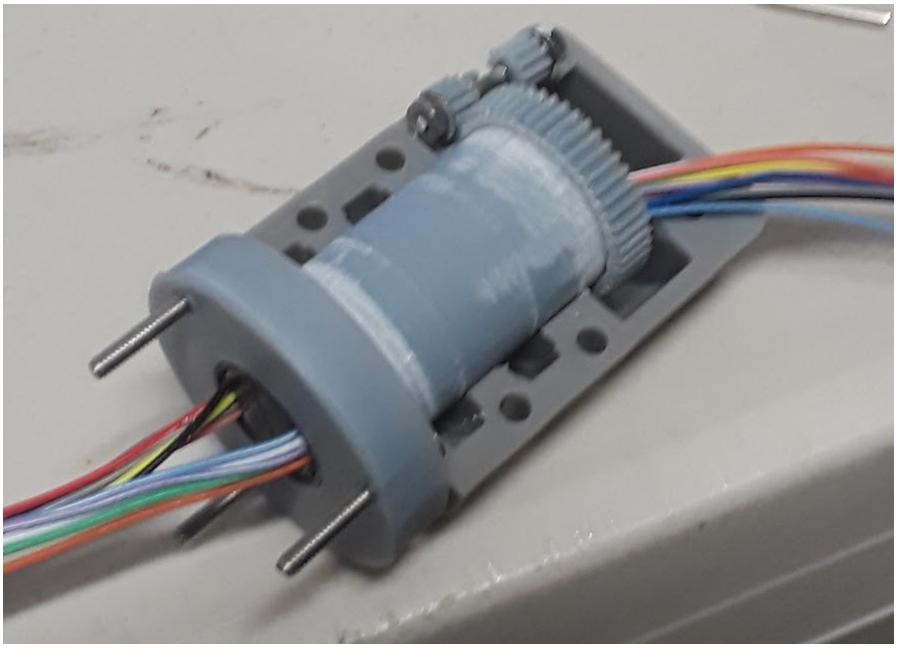

Figure 69. Casing_1 with slip ring mount and geared rod in place

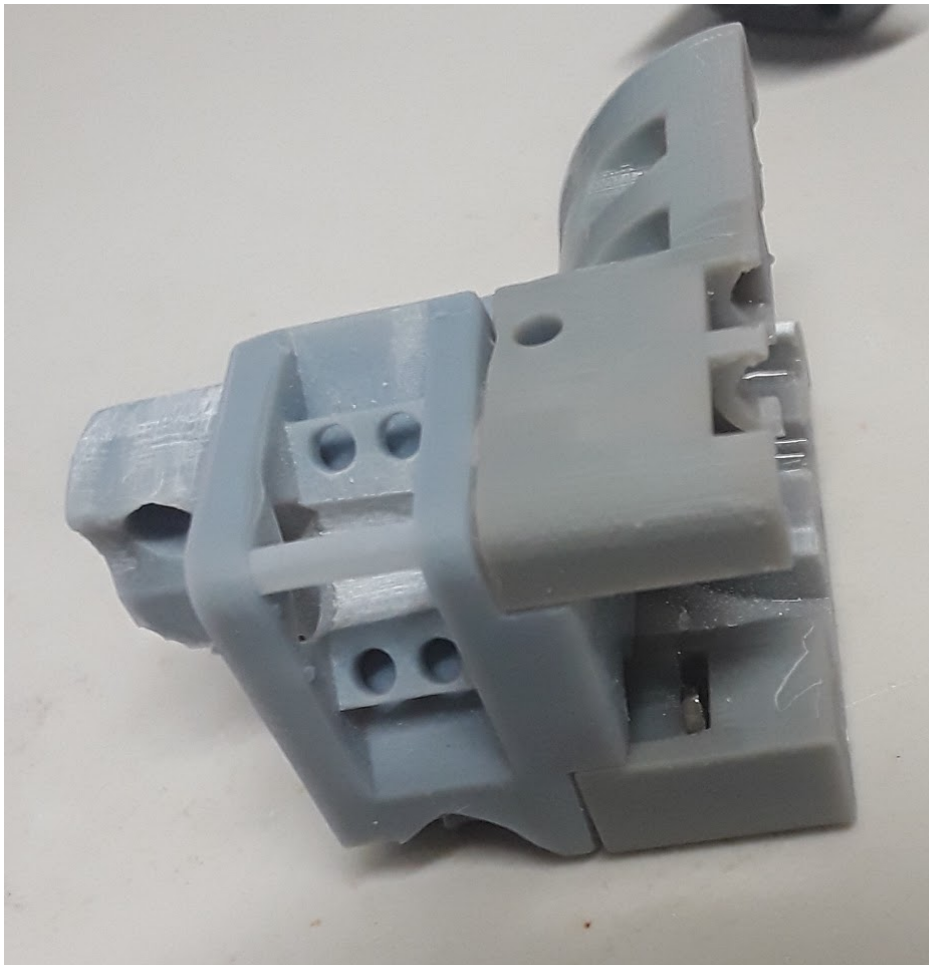

Figure 70. M2 Nut in slot in Casing_2

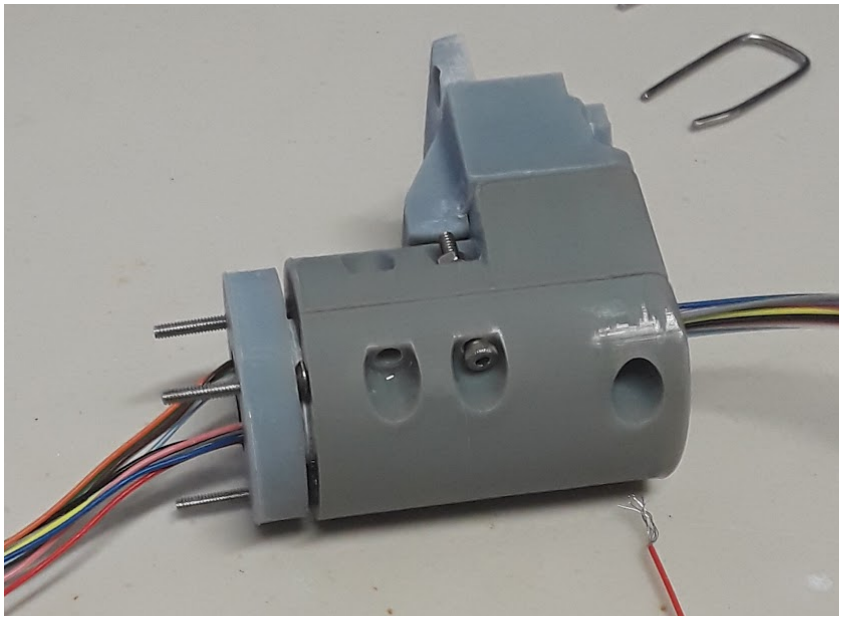

Figure 71. Casing closed (note this image only shows 2 of the bolts inserted)

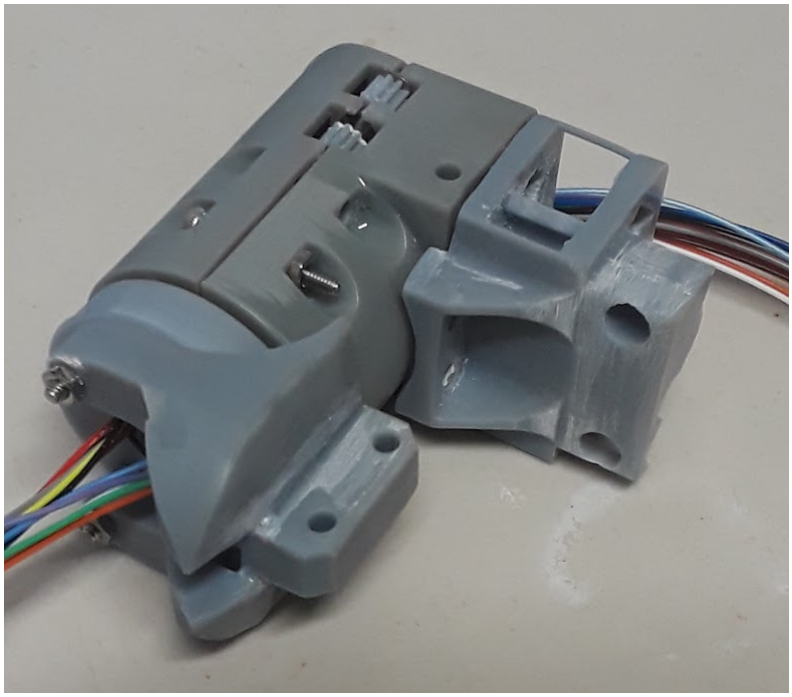

Figure 72. Mount holder installed onto TRS prot

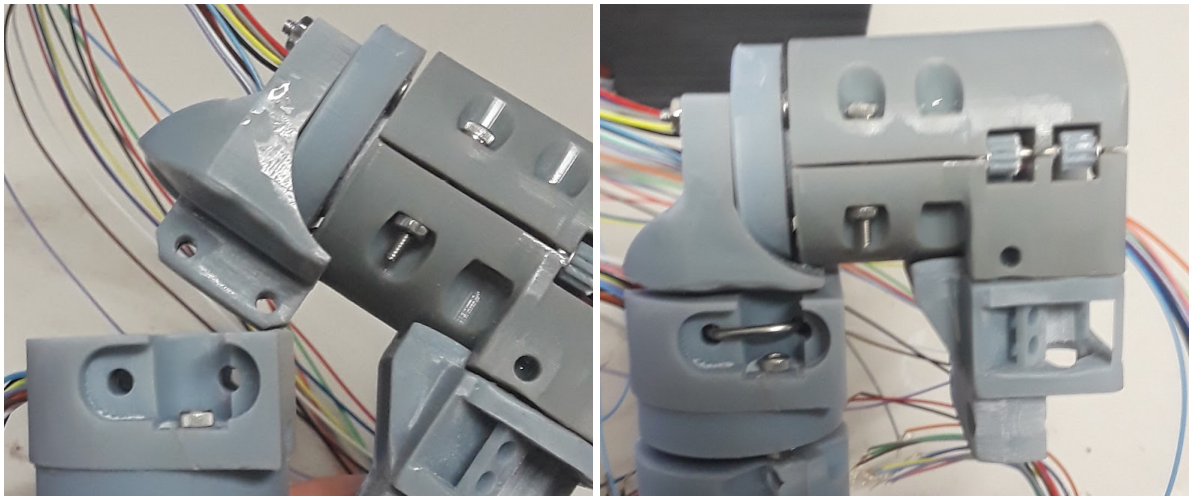

Figure 73. TRS prot about to be inserted to the ARS via adapter (left) and
TRS attached to ARS via adapter with retaining pin inserted (right)

Alternatively, the TRS will attach to the other side of an ARS module using just M4 bolts

(see Figure 74)

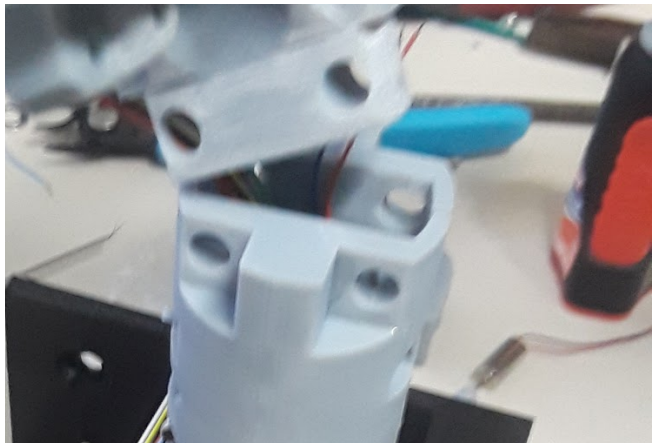

Figure 74. TRS about to attach to the ARS via the alternative mount.

6.3.3 Payload Deployment System Prototype

The payload deployment system went together very easily with only minor sanding needed (see Figure 75). The gears of the payload deployment system operate correctly however the motors are again not powerful enough to drive the system even when lubricated. To ensure operation a bolt was added to each side of the system so that it could be turned manually while still using the mechanism. This was an effective alternative to motorized operation when the back panel was not attached as it blocked access to the rear of the deployment system. However due to the lack of uniform force on a 2 crank system, during one disassembly the brittle resin components are vulnerable to excess loads that could cause a fracture (See Figure 76).

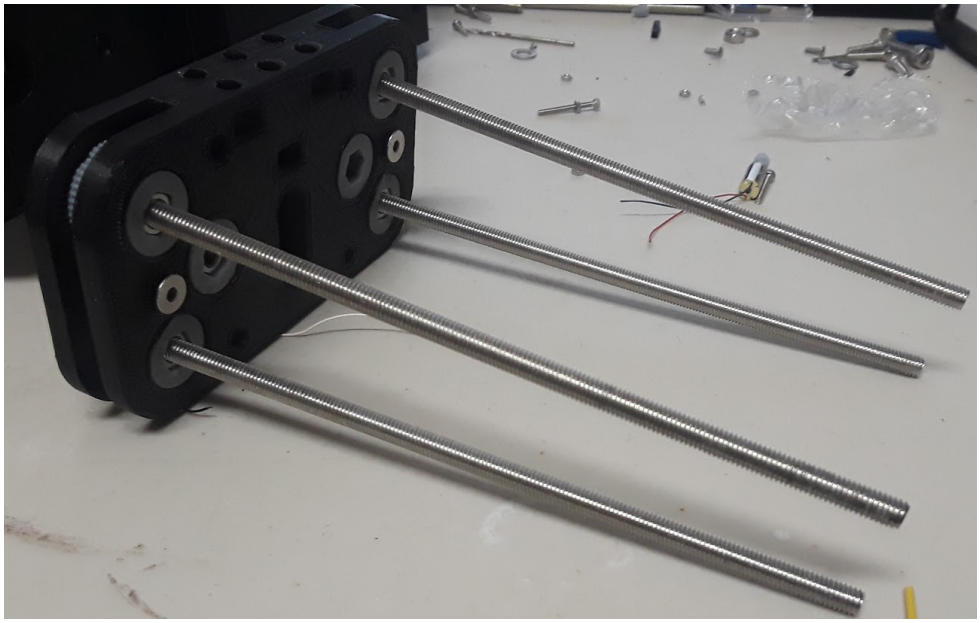

Figure 75. Payload deployment system assembled

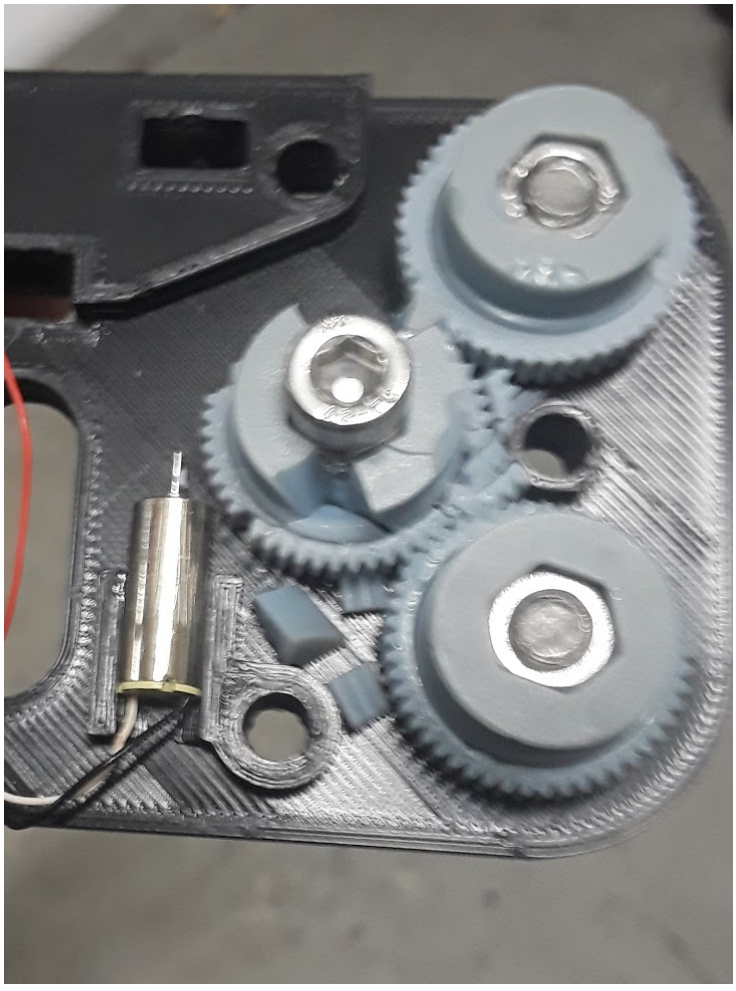

Figure 76. Payload Deployment System with Fractured Gear

6.4 Prototyping Results

The final prototype is a scale model of the Orbital Construction cubesat with a mechanically similar stand-in arm and payload system. The model is currently an informative showpiece for visual scaling purposes and technical accessibility testing. Assembling and constructing of the arm structure has allowed for further iteration into the design of the arm segment. Using additive manufacturing for structural and mechanical components showed the strengths and weaknesses of each technology. For structural components the FDM printer worked very quickly and reliably, reinforcing the core motivation for this project in that structural systems made using FDM technology are quick to produce and effective. For a lot of the more complicated components that the FDM printer could not produce, like the arms and gears, the limitations of the materials currently used in consumer ready SLA photopolymer are apparent due to its susceptibility to mechanical failure. This and the SLA printers continuing malfunction, the choice of FDM as the better and more robust printing system for in orbit operation is again reinforced. The claw component was never able to be prototyped, but more work still needs to be done on the rest of the arm system so this is not much of a setback for future projects. The internal wiring for the arm was able to keep all 12 channels throughout the length of the arm showing potential for future work to be able to integrate the full 24 channel system. Below are some images of the final prototype.

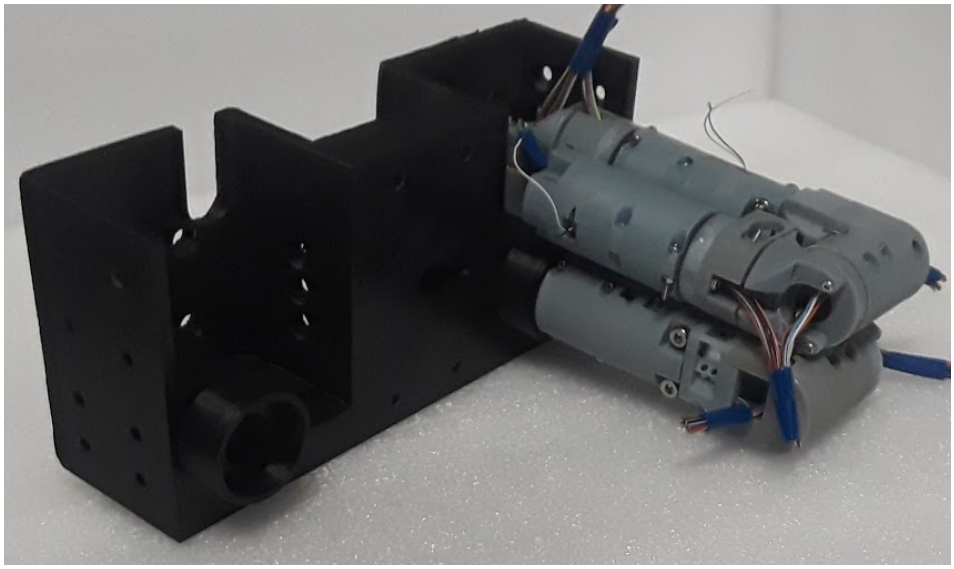

Figure 77. Payload mount with single arm installed

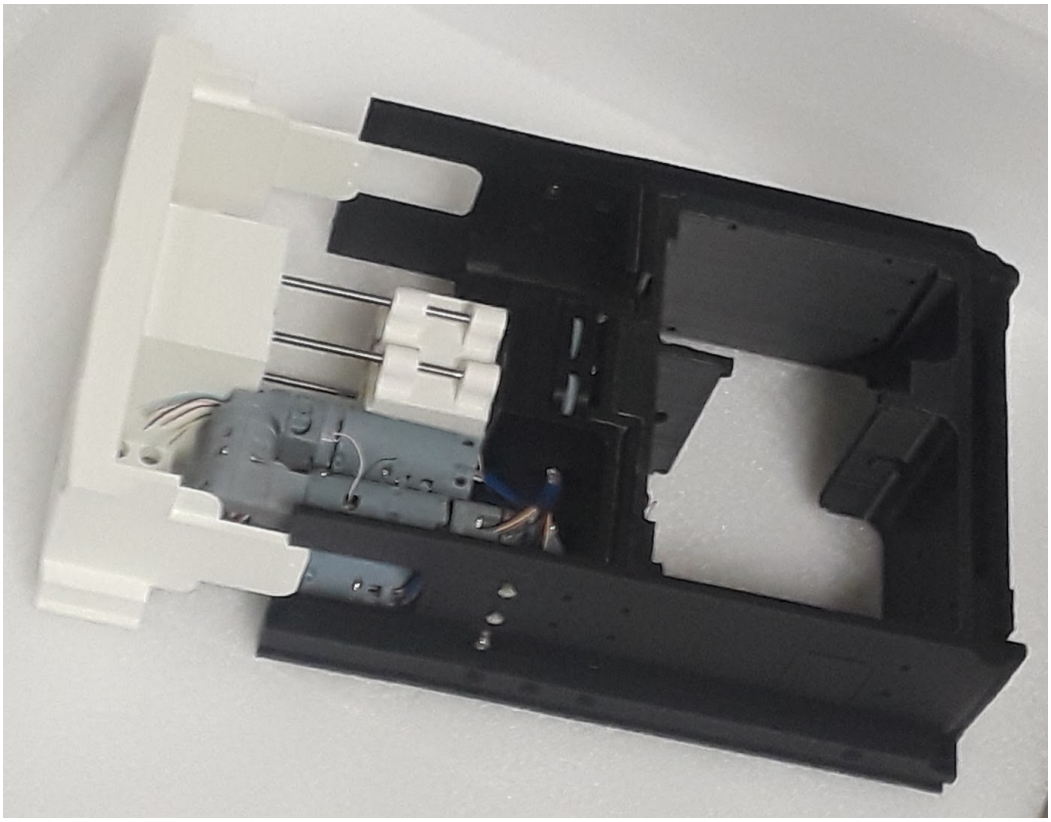

Figure 78. OCC prototype with payload retracted without solar array mount

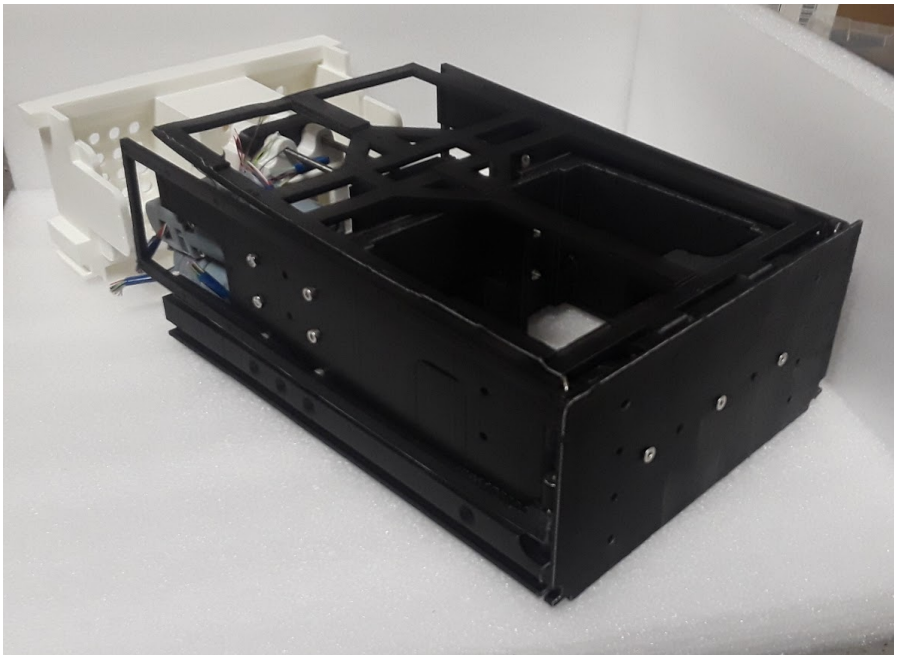

Figure 79. OCC Prototype with payload deployed

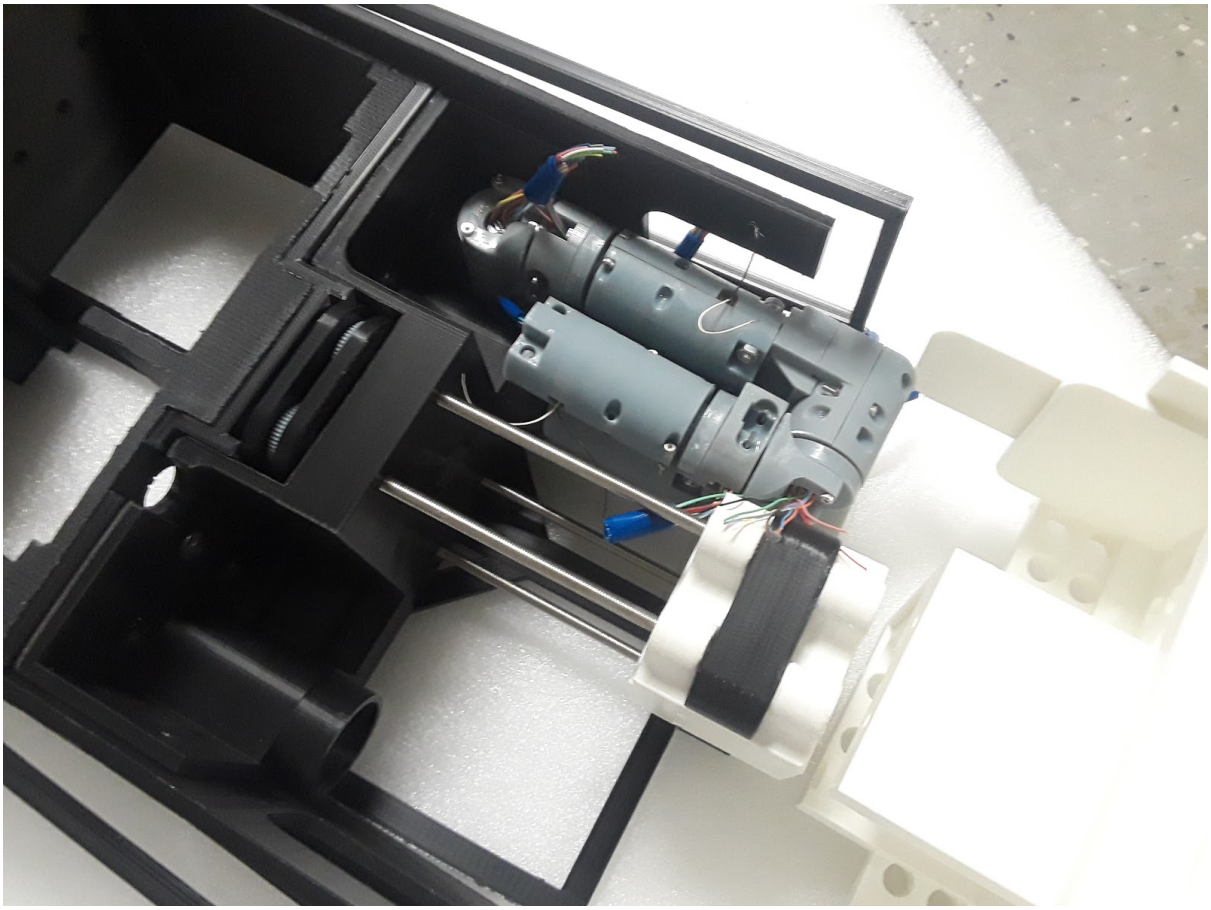

Figure 80. OCC Prototype with payload deployed from above

7 Conclusion

7.1 Design Iterations

This section will discuss designs that were thought of and explored to some extent but were left out due to changes in design later in the project.

7.1.1 Printhead Arm

A system of four revolute joints revolving about the Z-axis was designed in order to ensure constant orientation of the nozzle as well as adequate mobility and precision. Three limb segments and a rotating section mounted to the top of the printing head will enable this 4 joint system. The three limbs are identical with an integrated Portescap 08GS61 motor and 250:1 gearbox (See Figure 81). The gearbox is designed into the limb with the use of 2mm rods and 2-3mm bearings, two worm gears and three spur gear make the 250:1 transition. The use of worm gears here is important as it allows for the motor to transfer power to the system but not vice versa, allowing for little to no power requirements to maintain position. The 08GS61 motor was selected for its low power of operation at .5 W maximum power draw, for prototyping this motor works well however a brushless motor with similar performance will need to be integrated instead due to the requirements of LEO operating environment. This system was dropped for an armless printing head to decrease the possible points of failure and meet the internal structure volume requirements.

Figure 81 Unused printing head arm

7.1.2 Grabbing Claw Alternative

Suction grabbers are extremely effective grabbers in the atmosphere so alternative attachment options to claws might be an option. Given that the proposed filament for in-orbit

printing would have tungsten microparticles embedded, it could be possible to embed a more ferrous microparticle in order to use a magnetic grabber. With this magnetic arm letting go would be easier and there would be very little need for proper orientation of the magnetic head. This could allow for a simpler arm with multiple parallel revolute joints and a linear actuator instead of a 6-axis arm. This idea was dropped due to power concerts of the electromagnet as well as insufficient ferrous properties in the final material proposed for the 3D printing filament.

7.2 Future Work

The next step in development for the Orbital Construction Cubesat is to further develop the structural design with a full vibrational simulation conducted on the structure and analysis to ensure structural stability during launch. A high fidelity thermal analysis with use of MLI and radiators to balance the temperature from internal and external sources must also be conducted on the system. The structure could also benefit from having the tab be on another supporting structure to try and lower manufacturing difficulty. An operating program must be developed using the camera module and data from the arms to assign a relative XYZ coordinate to the printhead allowing for Gcode files to print on the cubesat. The control system and communications systems for this machine will also need to be developed. Also filament of PC/ASA with carbon fibre core and embedded tungsten microparticles must be manufactured and tested for structural characteristics and UV resistance as well as printability in microgravity and in vacuum.

7.3 Final Thoughts

The design process showed that it is technically possible to condense a traditional FDM system into the power and size requirements of a 6U cubesat and the prototype showed that it was mechanically possible to fit the arm and printing head system into the payload section. The cubesat platform is fantastic for projects such as this that use low cost commercially available components to test a novel technology. Such as the printhead, with only minor modifications to the physical characteristics of a low cost off the shelf component and no modifications to its functionality, the part is considered ready for testing. This prototype is remarkably strong and is a reassuring factor that this project will continue in future work.

References:

1. Kulu, E., Nanosats Database Available: https://www.nanosats.eu/. [Accessed 2020]
2. “A Basic Guide to Nanosatellites,” Alén Space Available: https://alen.space/basic-guide-nanosatellites/. [Accessed 2020]
3. Litkenhous, S., “In-Space Manufacturing,” NASA May, 22 2019 Available: https://www.nasa.gov/oem/inspacemanufacturing. [Accessed 2020]
4. “The 7 categories of Additive Manufacturing: Additive Manufacturing Research Group: Loughborough University,” The 7 categories of Additive Manufacturing | Additive Manufacturing Research Group | Loughborough University, 2012 Available: https://www.lboro.ac.uk/research/amrg/about/the7categoriesofadditivemanufacturing/. [Accessed 2020]
5. Gebhardt, A., and Hötter Jan-Steffen, Additive manufacturing 3D printing for prototyping and manufacturing, Munich: Hanser Publishers, 2016.
6. Asif, M., Ramezani, M., Sun, X., Wang, L., Xu, X., Giffney, T., Travas-Sejdic, J. adranka, and Aw, K., “A New 3D Printing Technique Using Extrusion of Photopolymer,” ResearchGate, January 2017 Available: https://www.researchgate.net/publication/317577575_A_New_3D_Printing_Technique_Using_Extrusion_of_Photopolymer.
7. Hu, Q., Duan, Y., Zhang, H., Liu, D., Yan, B., and Peng, F., “Manufacturing and 3D printing of continuous carbon fiber prepreg filament,” Journal of Materials Science, vol. 53, Sep. 2017, pp. 1887–1898.
8. Bettini, P., Alitta, G., Sala, G., and Landro, L. D., “Fused Deposition Technique for Continuous Fiber Reinforced Thermoplastic,” Journal of Materials Engineering and Performance, vol. 26, Dec. 2016, pp. 843–848.
9. Santos, R. M., Botelho, G. L., and Machado, A. V., “Artificial and natural weathering of ABS,” Journal of Applied Polymer Science, Jan. 2010.
10. Rohde, S., Cantrell, J., Jerez, A., Kroese, C., Damiani, D., Gurnani, R., Disandro, L., Anton, J., Young, A., Steinbach, D., and Ifju, P., “Experimental Characterization of the Shear Properties of 3D–Printed ABS and Polycarbonate Parts,” Experimental Mechanics, vol. 58, Oct. 2017, pp. 871–884.
11. Ram, A., Zilber, O., and Kenig, S., “Life expectation of polycarbonate,” Polymer Engineering and Science, vol. 25, 1985, pp. 535–540.
12. “3DXMAX® PC/ASA,” 3DXTech Available: https://www.3dxtech.com/engineering-grade-filaments/3dxmax-pc-asa/. [Accessed 2020]
13. Shemelya, C. M., Rivera, A., Perez, A. T., Rocha, C., Liang, M., Yu, X., Kief, C., Alexander, D., Stegeman, J., Xin, H., Wicker, R. B., Macdonald, E., and Roberson, D. A., “Mechanical, Electromagnetic, and X-ray Shielding Characterization of a 3D Printable Tungsten–Polycarbonate Polymer Matrix Composite for Space-Based Applications,” Journal of Electronic Materials, vol. 44, Mar. 2015, pp. 2598–2607.

14. “Properties Table,” All-In-One 3D Printing Software Available: https://www.simplify3d.com/support/materials-guide/properties-table/. [Accessed 2020]
15. “Payload Specification for 3U, 6U, 12U and 27U,” Planetary Systems Corp. August 4, 2016 Available: http://www.planetarysystemscorp.com/web/wp-content/uploads/2016/08/2002367D-Payload-Spec-for-3U-6U-12U-27U.pdf
16. Dinh, Dai, "Thermal Modeling of Nanosat" 2012 Master's Theses. 4193.
17. “NanoPower MSP Datasheet,” GOMSpace, March 28, 2019 Available: https://gomspace.com/UserFiles/Subsystems/datasheet/gs-ds-nanopower-msp-12.pdf
18. “NanoPower BP4 Datasheet,” GOMSpace, October 10, 2018 Available: https://gomspace.com/UserFiles/Subsystems/datasheet/gs-ds-nanopower-bp4-27.pdf
19. CubeSpace, “CubeWheel,” *CubeSpace* Available: https://www.cubespace.co.za/products/adcs-components/cubewheel/. [Accessed 2020]
20. “NanoMind A3200 Datasheet,” GOMSpace, December 10, 2018 Available: https://gomspace.com/UserFiles/Subsystems/datasheet/gs-ds-nanomind-a3200_1006901.pdf
21. “NanoCom AX100 Datasheet,” GOMSpace, November 29, 2019 Available: https://gomspace.com/UserFiles/Subsystems/datasheet/gs-ds-nanocom-ax100.pdf
22. “NanoCom ANT-6F UHF Datasheet,” GOMSpace, June 24 2019 Available: https://gomspace.com/UserFiles/Subsystems/datasheet/gs-ds-nanocom-ant6f-uhf-21.pdf
23. “Volcano Nozzles,” *E3D Online* Available: https://e3d-online.com/collections/nozzles/products/volcano-nozzles. [Accessed 2020]
24. *PCM* Available: http://config.watlow.com/CPQ/Configurator/Config.aspx?InstanceID=CPQ81. [Accessed 2020]
25. “NanoPower BPX Datasheet,” GOMSpace, May 8, 2018 Available: https://gomspace.com/UserFiles/Subsystems/datasheet/gs-ds-nanopower-bpx-3-18.pdf
26. Park, T.-Y., Chae, B.-G., and Oh, H.-U., “Development of 6 U CubeSat's Deployable Solar Panel with Burn Wire Triggering Holding and Release Mechanism,” *International Journal of Aerospace Engineering* 2019 Available: https://doi.org/10.1155/2019/7346436.
27. “AFT BULKHEAD CARRIER AUXILIARY PAYLOAD USER’S GUIDE” May 2014 Available: https://www.ulalaunch.com/docs/default-source/rockets/abc_users_guide_2014.pdf.

```
T0 = 300;       % Temperature in kelvin of filament before heating
Tm = 540;       % Temperature in kelvin for polycarbonate/ASA filament to melt
dT = Tm-T0;     % Total temperature change required
Cp_PC = 1.25e3; % Specific heat capacity in kJ/kg*K of Polycarbonate
Cp_ASA = 1.3e3; % Specific heat capacity in kJ/kg*K of ASA
Cp_cf = 2.02e3; % Specific heat capacity in kJ/kg*K of Carbon Fibre
Cp_tp = 1.3e3;     % Estimated specific heat of PC/ASA mix in kj/kg*K
rho_PCASA = 1140;     % Density of PC/ASA composite in kg/m^3
rho_cf = 1760;  % Density of carbon fibre in kg/m^3
V = .001;       % Print speed in m/s
D = 1.5e-3;    % Diameter of filament in m
D_cf = (2*(.04/pi)^.5)*10^-3;         % Diameter of carbon fibre core in m from .04mm^2 ar
ea of T300-1000 filament
A_tp = pi*(D/2)^2;  % Area of CCF filament
A_cf = pi*(D_cf/2)^2;  % Area of carbon fibre in CCF filament
A_r = A_cf/A_tp;    % Area ratio of carbon fibre to total
rho = rho_PCASA*(1-A_r)+rho_cf*A_r; % average density
m_m_tp = rho_PCASA*(A_tp)*(1-A_r);    % mass per meter of in kg/m
m_m_cf = rho_cf*A_cf;       % mass per meter in kg/m
m_R = m_m_cf/m_m_tp; % mass ratio of carbon fibre to thermo plastic
m_m_sum = m_m_tp+m_m_cf;
A = 1.1e-3*.6e-3;   % area of layer after extrusion (1.1mm layer width and .6mm layer heig
ht)
mdot = rho*V*A;     % estimated mass flow rate
Cp = m_R*Cp_cf+(1-m_R)*Cp_tp;
Q_req = dT*Cp*mdot+mdot*134*(1-m_R); % estimated constant heat required for increasing tem
p from 300K to 540K + 134kJ/kg melting heat required
horzcat(num2str(Q_req),' Joules')
```

```
ans =

    '0.24244 Joules'
```

Published with MATLAB® R2018b

Solar Panels				Dimensions:						
Side	Product Name	Cells	Mass (g)	Z (mm)	Y (mm)	X (mm)	Power min	Power Max	Voltage [V]	Current [A]
A1	MSP-A-7-1	7	190	326.5	1.5	82.6	7.9450	8.4	16.1	0.5
A2	MSP-A-7-1	7	190	326.5	1.5	82.6	7.9450	8.4	16.1	0.5
B1	MSP-B-8-2	16	438	326.5	209.0	2.5	18.1600	19.2	18.4	1
B2	MSP-B-8-2	16	438	326.5	209.0	2.5	18.1600	19.2	18.4	1
C	MSP-C-5-1	5	132	1.5	221.5	97.5	5.6750	6	11.5	0.5
D	n/a	n/a	n/a	n/a	n/a	n/a	n/a	n/a		
Total		51	1388				57.8850	61.2		
Battery	Product Name	Cells	Mass (g)	Z (mm)	Y (mm)	X (mm)	V Range	V nominal	Capacity [Wh]	Capacity [Ah]
	BPX 4S-2P	8	500	92.2	85.5	40.5	12-16.8	14.8	77	5.2

Component										
	option	type	name							
Hot End	1	comercial	V6 All-Metal HotEnd							https://e3d-online.com/collections/hotends/products/v6-all-metal-hotend
	2	custom	modified V6 All-Metal HotEnd							
	option	type	diameter	length	min watt	max watt	cat #	mass	material	link
Cartridge Heater	1	comercial	1/4 in. (6.35mm)	1" (25.4mm)	10	25	SC25-1			https://www.hotwatt.com/webdav/files/Product-Documents/Cartridge-j https://www.watlow.com/Products/Heaters/Cartridge-Insertion-Heaters?adgroupid=182270848 1&gclid=Cj0KCQjw6uT4BRD5ARIsADwJQ1-qNUUDV0qiYJnU4oyz38F55Wtt5saxmmf0tjhOw1qP9rh9B-Lj14aAvJG
	2	comercial	6mm	40mm	10	30	MS6-40			https://www.hotwatt.com/webdav/files/Product-Documents/Cartridge-and-Immersion.pdf
	3	custom	1/8 in. (3.175mm)	1"	3	37	cust		304 stainless ste	http://config.watlow.com/CPQ/Configurator/Config.aspx?InstanceID=CPQ81&AppID=App80_Prod&HeaderID=CMSf5b7dcf9-fa36-40d6-8af8-09c286c7be39&ConfigurationID=CMSf5b7dcf9-fa36-40d6-8af8-09c286c7be39&PageTitle=1%2F8%22%20FIREROD%C2%AE%20Cartridg
	option	type	name	max temp	diameter	length	power			link
Temperature sensor	1	cartridge	PT100	500 deg C	3mm	15mm	.25w Max			https://e3d-online.com/products/pt100-temperature-sensor
	option	type	name	type	rated filament Ø					link
Extruder	1	comercial	Titan	direct drive	1.75mm					https://e3d-online.com/products/titan-extruder#
	optioon	type	name	type	power draw (w)					
Extruder Motor	1	comercial	17HS08-1004S	Stepper	3.5					https://www.oyostepper.com/images/upload/File/17HS08-1004S.pdf
	option	type	description	material	Cp kJ/kg*K	thermal conductivity				
Nozzle	1	comercial	v6 nozzle X	AISI Type H13 Hot Work Tool Steel	0.46	24.4 w/m*K				https://e3d-online.com/collections/nozzles/products/v6-nozzles
	2	custom	1.5mm diameter modification to v6 nozzle X	AISI Type H13 Hot Work Tool Steel	0.46	24.4 w/m*K				
	3	comercial	volcano nozzle X	AISI Type H13 Hot Work Tool Steel	0.46	24.4 w/m*K				https://e3d-online.dozuki.com/Document/QbiVvVR3XEvUkNDR/Volcano_Nozzle.pdf
	4	custom	1.5mm diameter mod to volcano nozzle X	AISI Type H13 Hot Work Tool Steel	0.46	24.4 w/m*K				

			Voltage [V]			Current [A]			Power Draw [W]										
Subsystem	Component	Name/Product #	Min	Nom	Max	Min	Nom	Max	Min	Nom	Max	Mass [g]	Datasheet	Product	V_cc target	CAD	Required #	Times Redundant	Total #	In CAD?
GNC	Controller	NanoMind A3200	3.2	3.3	3.4		0.05	0.27		0.17	0.9	24	https://gom	https://go	3.3V		1	0	1	1
	Reaction Wheels	NanoTorque GSW-600	4.9	5	5.1		0.06	0.5		0.3	2.55	940	https://gom	https://go	5V		1	0	1	
	GPS	NovAtel GPS		3.3			<.4	0.4			1.32	31	https://gom	https://go	3.3V		1	0	1	1
	Component Dock	NanoDock DMC-3	4.3		6	N/A	N/A	N/A	N/A	N/A	N/A	51	https://gom	https://go	5V		1	0	1	1
Comms	Tranciever	NanoCom AX100	3.3	3.3	3.4	0.045	0.055	0.12		4	4	24.5	https://gom	https://go	3.3V		1	0	1	1
	Antena	NanoCom ANT430	N/A	N/A	N/A	N/A	N/A	N/A	N/A	N/A	N/A	30	https://gom	https://go	N/A		1	0	1	
Power	Battery	NanoPower BPX										500	https://gom	https://go	Solar Panels		1	0	1	
	Panels to Battery	ACU-200										54	https://gom	https://go	See Comment		1	1	2	2
	Battery to System	PDU-200										57	https://gom	https://go	See Comment		3	1	6	6
	Power Dock	P-60 Dock										80	https://gom	https://go	See Comment		1	1	2	2
Payload	Arm Motors	0615 003 S	3	3	3	0.03		0.14	0.09		0.42	2	https://www	https://ww	3V		18	0	18	n/a
	Motor Encoder	PA2-50		3.3			0.008			0.028		1	https://www	https://ww	3V		18	0	18	n/a
	Motor Driver	MCDC 3002 P	8	8	30	0.04	2	3	0.32	1.26	3.969	7	https://www	https://ww	8V		18	0	18	18
	Camera/Cpu	OpenMV Cam H7	3.3	3.3	3.3	0.11	0.16	0.17	0.36	0.53	0.56	19	Various	https://op	3.3V	https:	1	0	1	
	Heater	Custom	3.3	5	8	0.75	2	10	0	6	30	3.32								
	Extruder Motor	17HS08-1004S		3.6		0	1	2		3.6	7.2	150								

Energy Disipation	Area (m^2)	Area (m^2)	Area (m^2)	Area (m^2)	Emissivities			Solar constant	From Earth	Albedo	Sum	Radiator surface area (m2)		
Max	Cubesat Body	Solar Panels Deployed	Arms extended	sum	Solar Panel Collect	Polished Gold	Aluminum (Chassis)	1414W/m^2	241 W/m^2	0.3 @ 1414 @/m^2				
X	0.042456	0	+10%	0.042456	0.75	0.025	0.1	45.024588	0.2557974	1.80098352	47.08136892	0.1421941479	sigma	0.000000056703
Y	0.087474	0	+10%	0.087474	0.75	0.025	0.1	92.766177	0.52703085	3.71064708	97.00385493	0.2929689772	epsilon	0.95
Z	0.027724	0.25986	+10%	0.287584	0.75	0.025	0.1	304.982832	1.7326936	12.19931328	318.9148389	0.9631798058	T	280

Energy Disipation	Area (m^2)	Area (m^2)	Area (m^2)	Area (m^2)	Emissivities			Solar constant	From Earth	Albedo	Sum	Radiator surface area (m2)		
Min	Cubesat Body	Solar Panels Deployed	Arms extended	sum	Solar Panel Collect	Polished Gold	Aluminum (Chassis)	1414W/m^2	241 W/m^2	0.25 @ 1414 @/m^2				
X	0.042456	0	+10%	0.042456	0.75	0.025	0.1	0	0.233508	0	0.233508	0.000705235889	sigma	0.000000056703
Y	0.087474	0	+10%	0.087474	0.75	0.025	0.1	0	0.481107	0	0.481107	0.001453029117	epsilon	0.95
Z	0.027724	0.25986	+10%	0.287584	0.75	0.025	0.1	0	1.581712	0	1.581712	0.004777052903	T	280

Energy Disipation	Max	X	Y	Z		Energy Disip	Min	X	Y	Z
Area (m^2)	Cubesat Body	0.042456	0.087474	0.027724		Area (m^2)	Cubesat Body	0.042456	0.087474	0.027724
Area (m^2)	Solar Panels D	0	0	0.25986		Area (m^2)	Solar Panels Deploye	0	0	0.25986
Area (m^2)	Arms extended	+10%	+10%	+10%		Area (m^2)	Arms extended	+10%	+10%	+10%
Area (m^2)	sum	0.042456	0.087474	0.287584		Area (m^2)	sum	0.042456	0.087474	0.287584
Emissivities	Solar Panel Co	0.75	0.75	0.75		Emissivities	Solar Panel Collect	0.75	0.75	0.75
	Polished Gold	0.025	0.025	0.025			Polished Gold	0.025	0.025	0.025
	Aluminum (Cha	0.1	0.1	0.1			Aluminum (Chassis)	0.1	0.1	0.1
Solar constant	1414W/m^2	45.024588	92.766177	304.982832		Solar constant	1414W/m^2	0	0	0
From Earth	241 W/m^2	0.2557974	0.52703085	1.7326936		From Earth	241 W/m^2	0.233508	0.481107	1.581712
Albedo	0.3 @ 1414 @/	1.80098352	3.71064708	12.1993132		Albedo	0.25 @ 1414 @/m^2	0	0	0
Sum		47.08136892	97.00385493	318.914838		Sum		0.233508	0.481107	1.581712
Radiator surface area (m2)		0.1421941479	0.2929689772	0.96317980		Radiator surface area (m2)		0.00070523588	0.001453029	0.004777052903

		sigma	epsilon	T				sigma	epsilon	T
		0.00000005670373	0.95	280				0.0000000567(	0.95	280

Power in [W]	55	
orbit time [min]	128	
orbit time [hour]	2.133333333	
% in sunlight	59	
time in sun [min]	75.52	
time in sun [hour]	1.258666667	
Power generated [Wh]	69.22666667	
Battery required [Wh]	28.38293333	
Total system power	32.45	
charge dedicated power	22.55	
sanity check	0.8746666667	2.133333333

V1						
Subsystem	Mass [kg]		V - A	Power [W]		
Structure	2	~1800g from cad example +10%		n/a		
Power	1.388	Solar Panels		55		
	0.27	NanoPower BP4		22.55		
GNC	0.45	3x CubeWheel Medium		6.9	21.26%	
	0.009	Raspberry Pi zero	5.1v @ 120mA	0.612	1.89%	
	0.003	raspery camera module v2	5.1v @ 250mA	1.275	3.93%	
	0.024	NanoMind A3200		0.9	2.77%	
Communications	0.0245	NanoCom AX100	3.4V @ 1.2A	4.08	12.57%	
	0.09	NanoCom Ant-6f UHF		2	6.16%	
payload	7.7415	tbd		16.683	51.41%	
check	12			32.45		
V2						
Subsystem	Mass [kg]		V - A	Power [W]		
Structure	2	~1800g from cad example +10%		n/a		
Power	1.388	Solar Panels		55		
	0.27	NanoPower BP4		22.55		
GNC	0.45	3x CubeWheel Medium		6.9	21.26%	
	0.003	Teensy 4.0 Development Board	3.3v @ 100mA	0.33	1.02%	
	0.001	BF3710 720p camera		0.14	0.43%	
	0.024	NanoMind A3200		0.9	2.77%	
Communications	0.0245	NanoCom AX100	3.4V @ 1.2A	4.08	12.57%	
	0.09	NanoCom Ant-6f UHF		2	6.16%	
payload	7.7495	tbd		18.1	55.78%	
check	12			32.45		
V2						
Subsystem	Mass [kg]		V - A	Power [W]		

Structure	2	~1800g from cad example +10%		n/a		
Power	1.388	Solar Panels		55		
	0.5	NanoPower BPX		22.55		
GNC	0.94	NanoTorque GSW-600	5.1v @ 500mA	2.55	7.86%	
	0.003	Teensy 4.0 Development Board	3.3v @ 100mA	0.33	1.02%	
	0.001	BF3710 720p camera		0.14	0.43%	
	0.024	NanoMind A3200		0.9	2.77%	
Communications	0.0245	NanoCom AX100	3.4V @ 1.2A	4.08	12.57%	
	0.09	NanoCom Ant-6f UHF		2	6.16%	
payload	7.0295	tbd		22.45	69.18%	
check	12			32.45		

Printer Head						
	Sections	Component	Mass [g]	power est. [W]	power max [W]	description
	Hot End	Heating Cartridge	3.32	6	30	2x 3W custom heaters that provide heat to the system
		Heat Block	95.281	n/a	n/a	Transfers heat from cartridge to nozzle
		Temperature sensor	4.6	0.2	0.25	Detects Temperature of Heat Block ~ Nozzle temp
		Radiator	19.514	n/a	n/a	2x radiator panels
		Heat pipes	14.576	n/a	n/a	
		Heat Break	2.985	n/a	n/a	
	Nozzle	Nozzle	4.148	n/a	n/a	Tip through which filament is extruded
	Extruder	assembly	26.7	n/a	n/a	
		motor: 17HS08-1004	150	3.6	3.6	
	adapter		9.685			
Printer Arm						
	Motors	3x 08GS61	11.4	1.5		
	arms		161.676	n/a		
	mount	1x 08GS61	96.296	0.5		
	Sum		600.181	11.8		
	Budgeted amount		4000	10.6		
	remaining		3399.819	-1.2		
Moving Arms						
	Motors	Series 0615 ... S				
	encoders	PA2-50				
Printer Head						
	Sections	Component	Mass [g]	power est. [W]	power max [W]	description
	Hot End	Heating Cartridge	3.32	6	30	2x 3W custom heaters that provide heat to the system
		Heat Block	95.281	n/a	n/a	Transfers heat from cartridge to nozzle
		Temperature sensor	4.6	0.2	0.25	Detects Temperature of Heat Block ~ Nozzle temp
		Radiator	19.514	n/a	n/a	2x radiator panels
		Heat pipes	14.576	n/a	n/a	
		Heat Break	2.985	n/a	n/a	
	Nozzle	Nozzle	4.148	n/a	n/a	Tip through which filament is extruded
	Extruder	assembly	26.7	n/a	n/a	
		motor: 17HS08-1004	150	3.6	3.6	
	adapter		9.685			
Printer Arm	mount		147.26	0		
	Sum		478.069	9.8		
	Budgeted		4000	10.6		
	remaininc		3521.931	0.8		

Printer Head						
	Sections	Component	Mass [g]	Power Est. [W]	Power Max [W]	Description
	Hot End	Heating Cartridg	3.32	6	30	2X 3W Custom Heaters That Provide Heat To The System
		Heat Block	95.281	N/A	N/A	Transfers Heat From Cartridge To Nozzle
		Temperature Ser	4.6	0.2	0.25	Detects Temperature Of Heat Block ~ Nozzle Temp
		Radiator	19.514	N/A	N/A	2X Radiator Panels
		Heat Pipes	14.576	N/A	N/A	
		Heat Break	2.985	N/A	N/A	
	Nozzle	Nozzle	4.148	N/A	N/A	Tip Through Which Filament Is Extruded
	Extruder	Assembly	26.7	N/A	N/A	
		Motor: 17Hs08-1	150	3.6	3.6	
	Adapter		9.685			
Printer Arm						
	Motors	3X 08Gs61	11.4	1.5		
	Arms		161.676	N/A		
	Mount	1X 08Gs61	96.296	0.5		
	Sum		600.181	11.8		
	Budgeted Amour		4000	10.6		
	Remaining		3399.819	-1.2		
Moving Arms						
	Motors	Series 0615 ... S				
	Encoders	Pa2-50				
Printer Head						
	Sections	Component	Mass [G]	Power Est. [W]	Power Max [W]	Description
	Hot End	Heating Cartridg	3.32	6	30	2X 3W Custom H
		Heat Block	95.281	N/A	N/A	Transfers Heat F
		Temperature Ser	4.6	0.2	0.25	Detects Tempera
		Radiator	19.514	N/A	N/A	2X Radiator Pan
		Heat Pipes	14.576	N/A	N/A	
		Heat Break	2.985	N/A	N/A	
	Nozzle	Nozzle	4.148	N/A	N/A	Tip Through Whi
	Extruder	Assembly	26.7	N/A	N/A	
		Motor: 17Hs08-1	150	3.6	3.6	
	Adapter		9.685			
Printer Arm	Mount		147.26	0		
	Sum		478.069	9.8		
	Budgeted Amour		4000	10.6		
	Remaining		3521.931	0.8		

Component	Mass [g]	Material	
Core_Main	1960	Aluminum 7075 Alloy	
Core_Brace	372	Aluminum 7075 Alloy	
Core_Bottom	1698	Aluminum 7075 Alloy	
Array_mount	480	Aluminum 7075 Alloy	
A_Panel_1	91	Aluminum 7075 Alloy	
A_Panel_2	91	Aluminum 7075 Alloy	
B_Panel_1	320	Aluminum 7075 Alloy	
B_Panel_2	320	Aluminum 7075 Alloy	
Payload_Mount	440	PC/ASA w/ CFR	
Elec_Bay	450	PC/ASA w/ CFR	
Structure_Sum	6222	Various	
Predicted	2000	From Preliminary Design	
Over budget	4222		